SCUOLA DI ALTA FORMAZIONE
DOTTORATO IN BIOTECNOLOGIE PER L'UOMO

PhD Program in
Biotechnologies for Human Health

Physicochemical and biological characterization of magnetic nanoparticles for biomedical applications

Candidate: Enrico Catalano

Tutor: Prof.ssa Lia Rimondini

PhD coordinator: Prof. Claudio Santoro

2014-2015

Cycle XXVII

Table of contents

Preface

Nanomaterials are defined as the production of matter with at least one dimension ranging between 1 and 100 nanometers. Due to the very small size and the resulting high surface/volume ratio, nanomaterials have physical-chemical properties that differ from those of macroscopic materials. Nowdays nanomaterials are often applied in many industrial fields including electronics, optics, textile and many others till to biomedicine [1].

The use of nanoparticles (NPs) in medicine has expanded recently, especially in diagnostic [2]. Actually nanoparticles could be designed as contrast agents or nanocarriers able to bind, specifically transport biomolecules and accumulate to the site to treat.

Chapter 1 Introduction

1. Different types of nanoparticles

Different types of NPs are most used in the medical field. The nanoparticles can be classified into two main groups: organic and inorganic nanoparticles.

1.1 Organic nanoparticles

Organic nanoparticles can be defined as particles composed of organic compounds, mainly lipids or polymers [3]. They are often designed as liposomes, conjugated polymers, micelles, polymeric NPs, dendrimers, or carbon nanotubes. Sometimes they are derived from virus capsides. They are used as colloids to carry drugs or genes, to coat materials or as templates in various manufacturing processes [3]. The most common nanoparticles of organic origin used as drug delivering carriers are liposomes, micelles and polymer conjugates.

1.1.1 Liposomes

Liposomes are lipid vesicles of spherical shape, consisting of a double membrane structure composed of amphiphilic lipid molecules, with an average diameter between 50 and 500 nm [4].

Their structure is characterized by an external phospholipid bilayer and an aqueous phase core which contain hydrophilic substances [4].

1.1.2 Micelles

Micelles are nanoparticles formed by supramolecular self-assembly of surfactants and lipids [5]. The assembly principle of micelles formation is the hydrophobicity of the amphiphilic molecules in water, generating colloidal aggregates of these molecules. In general, micelles are colloidal particles formed by detergents and soaps [6]. Micelle formation needs to be started to have a minimum concentration of surfactant. In the initial formation phase, micelles show spherical shapes and their dimensions increase with the addition of more amount of surfactant [7].

1.1.3 Polymer conjugates

Polymer conjugates are hydrophilic hybrid structures consisting of polymer chains covalently bound to a drug or a protein. Polymer conjugates correspond to drug molecules or bioactive molecules that can be linked to a macromolecule through a spacer molecule, which can incorporate a breaking point to allow the release of the drug at the target site [8]. A high percentage of the applications of polymer conjugates are in the therapeutic and nanomedical field [9].

1.1.4 Dendrimers

Dendrimers are repetitively highly branched, star-shaped monodispersed macromolecules with nanometer-scale dimensions that emanate radially from a central core [10]. Dendrimers are defined by three components: a central core, an interior dendritic structure (the branches), and an exterior surface with functional surface groups [10]. In the biomedical area, dendrimers had been used for in vitro diagnosis, as contrast agents in magnetic resonance imaging when conjugated with other molecules, as drug delivery systems, in gene therapy as vectors to transfer genes through the cell membrane, and in regenerative medicine [11-16].

1.1.5 Polymeric Nanoparticles

Polymeric nanoparticles are by far the most studied organic particles. Polymeric NPs, also known as polymeric nanospheres, are usually defined as submicron-sized solid polymer particles with matrix type structure, in which a cargo can be encapsulated within the polymer matrix or absorbed in the surface [17]. Polythiophenes, polyfluorenes, poly(p-phenylenevinylene)s, and poly(p-phenyleneethynylene)s derivatives are polymeric NPs that can be used for electro-optical and photoluminescence applications [18, 19].

1.2 Inorganic nanoparticles

This category include nanoparticles with different chemical origin whose composition are not based only on C, O N, and H chemistry. The nanoparticles of metallic origin are excellent candidates both in the diagnostic field, as contrast agents in MRI (Magnetic resonance imaging), and therapeutically, such as for drug delivery.

1.2.1 Gold nanoparticles

Gold nanoparticles (GNPs) are inorganic NPs that could be used as a promising tool for different biological applications thanks to their size- and shape-dependent physical properties. GNPs are pretty inert, mostly biocompatible, and almost easy to be functionalized and synthesized [20, 21]. GNPs are used due to their unique optical-electronics properties in high technology applications such as organic photovoltaics, sensory probes, therapeutic agents, drug delivery, electronic conductors and catalysis. The optical and electronic properties of gold nanoparticles are tunable by changing the size, shape, surface chemistry, or aggregation state [22]. In fact, the size of spherical gold nanoparticles (AuNPs) influences their ability to enhance the response of optical sensors based on surface plasmon resonance (SPR) [23]. Thus, GNPs are a very promising candidate for biological imaging techniques.

1.2.2 Quantum dots

Quantum dots (QDs) are colloidal nanometre-sized crystals of semiconductor materials that are small enough to exhibit quantum mechanical properties [24]. The electronic properties of QDs are intermediate between those of bulk semiconductors and discrete molecules [25]. Smaller quantum dots (2 nm) present blue fluorescence emission (380-440 nm), while larger particles (5 nm) have red

fluorescence emission (605-630 nm) [26]. QDs have many advantages in respect with the most common organic dye molecules. QDs are robust and stable light emitters thanks to their inorganic makeup and are not so susceptible to photobleaching than organic dye molecules. This photostability makes very useful in observing cells for a long period of time [26, 27]. Different surface modifications of QDs were achieved to visualize labelling of whole cells and tissue sections [28, 29]. Quantum dots can be employed such as delivery and reporter systems in transfection therapies in vivo.

1.2.3 Magnetic nanomaterials

Magnetic materials include various materials and are classified according to their chemical origin, crystallographic configuration and magnetic properties. Magnetic nanoparticles (MNPs), consisting of magnetic elements (iron, cobalt, nickel oxides), are of great interest, particularly in biomedicine fields. The use of iron oxide nanoparticles in biomedical research is progressively gaining a lot of importance, with the purpose to develop new types of functionalized and biocompatible magnetic nanoparticles. Different types of iron-oxide nanoparticles can be produced, such as hematite (α-Fe_2O_3), maghemite (γ-Fe_2O_3) and magnetite (Fe_3O_4), among which the latter could be very interesting for different biomedical applications [30].

Susceptibility to magnetic fields is a criterion to classify magnetic materials into diamagnetic materials which have a weak repulsion from an external magnetic field corresponding to a negative susceptibility, paramagnetic materials showing small and positive susceptibility, and ferromagnetic materials which have a large and positive susceptibility to magnetic fields [31].

Superparamagnetism of iron oxide particles is a prerequisite to MNP use, as well as an underlying reason for its limitations. Superparamagnetism gives the possibility to magnetize the nanoparticles by an external magnetic field. This property is highly useful especially in biomedicine [32]. The limit volume to have superparamagnetic nanoparticles at a certain temperature is related to the magnetocrystalline anisotropy. Iron-oxide nanoparticles have superparamagnetic properties although they have larger dimensions compared to any other magnetic metal [32]. Magnetic nanoparticles have the unique ability that can be directed under the influence of an external magnetic field. Each magnetic particle can be considered similar to a single magnetic domain that shows superparamagnetic behavior when its size is below 10-20 nm and when the temperature is

above the so-called blocking temperature [33]. An important property of iron-oxide nanoparticles is the loss of their magnetization when the magnetic field is switched off.

1.2.4 Cobal ferrite

Cobalt ferrite nanoparticles are used in hyperthermia treatment, since in nanosized state, cobalt magnetic moment relaxes much slower than in magnetite or maghemite nanoparticles with similar size [34, 35]. Cobalt ferrite ($CoFe_2O_4$) is a hard magnetic material with multiple properties: large magnetic anisotropy, high coercivity, high Curie temperature, large magnetostrictive coefficient, moderate saturation magnetization with good mechanical hardness and chemical stability [36, 37]. Moreover the saturation magnetization of cobalt ferrite is almost the same as magnetite but its crystalline anisotropy is one order of magnitude larger, making it suitable for hyperthermia treatment [38].

1.2.5 Manganese ferrite

The $MnFe_2O_4$ has a structure with excellent properties such as high resistivity, high saturation magnetization, high initial permeability compared to the other ferrites [39]. The magnetic susceptibility of $MnFe_2O_4$ nanoparticles is higher respect to other ferrite nanoparticles such as Fe_3O_4, $CoFe_2O_4$ and $NiFe_2O_4$ [40]. $MnFe_2O_4$ nanoparticles could be used as novel MRI contrast agents [41]. $MnFe_2O_4$ MNPs have a greater biocompatibility and a strong phase contrast for magnetic resonance imaging in comparison with Fe_3O_4, γ-Fe_2O_3, $CoFe_2O_4$, and $NiFe_2O_4$ MNPs. Thus, $MnFe_2O_4$ MNPs can provide the multiple functionalities of imaging, hyperthermia and triggered drug release [42].

1.2.6 Zinc doped ferrites

Zinc oxide is commonly used as additive in ferrites. It can improve the properties and drive the medical applications of ferrite-based nanoparticles [43, 44]. Zinc oxide increases the saturation of magnetization in small amounts [45].

1.3 Methods of production of iron-oxide nanoparticles

The most common synthesis strategies for the preparation of iron-oxide nanoparticles are:

1) Wet chemical preparation methods, such as sol-gel synthesis, oxidation method, chemical co-precipitation, hydrothermal reactions, flow injection synthesis, electrochemical method, aerosol/vaporphase method, sonochemical decomposition reactions, supercritical fluid method, and synthesis using nanoreactors [46-48].

2) Physical methods, such as gas-phase deposition and electron beam lithography. These methods, however, do not allow to control the particle sizes down to the nanometer scale [49, 50].

3) Microbial methods, these methods allow efficient and effective control on the composition and the particle geometry of the resulting material [51]. Diverse microorganisms belonging to prokaryotes are able to synthesize iron-oxide nanoparticles, e.g. Clostridium acetobutylicum [52, 53]. The synthesis of nanoparticles may be intracellular or extracellular. The size and shape of the nanoparticles vary with the organism employed and conditions employed during the synthesis which included pH, temperature and substrate concentration [52].

1.4 Biomedical applications of magnetic nanoparticles

Magnetic nanoparticles can be used for a variety of biomedical applications: 1) Transport and pharmacological release of drugs on specific sites, drug targeting; 2) Gene delivery systems; 3) Hyperthermia; 4) Tissue engineering and repair; 5) Diagnosis by Magnetic resonance imaging (MRI); 6) MRI-guided therapeutic cell replacement; 7) Theranostics; 8) Biochemical separations; 9) Immunoassay platforms; 10) Bioanalysis; 11) Magnetofection for target cancer gene therapy [54-57].

Magnetic nanoparticles could play a key-role in the treatment of tumors, using two different approaches: 1) targeted drug delivery in the cancer site and 2) cancer magnetic induction hyperthermia in which an alternating magnetic field is used to heat up magnetic nanomaterials and hereby destroy targeted cancer cells [58-60].

In this regard, iron-oxide nanoparticles with magnetic properties are one of the most suitable devices to achieve biomedical applications listed above.

1.5 Cytocompatibility of nanoparticles

The safety of nanoparticles (NPs) in biomedical applications is a controversial issue. In the last years, the interest in nanotoxicology has increased and more studies regarding the cytotoxic properties of NPs have emerged [61-65]. The assessment of NP safety is related to a great variety of factors: (1) types of NPs, (2) stabilizing coating agents, (3) physicochemical parameters of the NPs, (4) incubation conditions (time and concentration), (5) type of cells used, (6) type of assay used [61-68]. Surface coatings and particle size play a key-role for NPs-induced toxic effects, as they influence cellular responses, intensity of effects, and potential mechanisms of toxicity [65]. Numerous studies have demonstrated different toxic effects associated with exposure to nanomaterials, including mitochondrial damage, oxidative stress, chromosomal and oxidative DNA damage and altered cell cycle regulation [69-73]. Contact of the NPs with the cells may further affect the morphology, cytoskeleton, proliferation, differentiation, migration, and survival [64].

1.6 Drug targeting

The design of nanocarriers for drug delivery with selectivity to disease and anatomical sites has a great potential. For instance nanoparticle-conjugated drug and gene delivery systems could be used to treat neurological diseases using MNP-conjugated drugs to cross the blood-brain barrier [74, 75]. Nanotechnology for drug delivery can be used to achieve (1) site-specific delivery of drugs in tissue and organs; (2) improved delivery of poorly water-soluble drugs; (3) transcytosis of drugs across tight epithelial and endothelial barriers; (4) co-delivery of two or more drugs for combination therapy; (5) theranostic application of drug delivery by combining therapeutic agents with imaging modalities [76, 77]. The basic principles of magnetic targeting of MNP-conjugated drugs have been investigated experimentally. The surface hydrophilicity of MNPs plays a key-role for drug delivery. Targeted therapy using MNPs assembled with drugs was already tested in clinical trials as a cancer therapy [60]. Various studies investigated the biodistribution of MNPs through intravenous injection directed by an external magnetic field to concentrate MNPs at a specific target site; this procedure has been well tolerated in cancer patients [59, 60].

1.6.1 Passive and Active Drug Targeting

There are two kinds of targeted drug delivery of nanocarriers: 1) active targeted drug delivery, that overcome the limitations of passive targeting by conjugation with affinity ligands (antibodies, peptides, aptamers, etc.) that recognize and bind to specific receptors on the target cell surface [78]; and 2) passive targeted drug delivery, such as the enhanced permeability and retention effect (EPR-effect) that allows migration of molecules up to 50-100 nm in diameter into the target site [79]. In fact drug carriers are expected to stay in the blood for long time, accumulate in pathological sites with affected and leaky vasculature (tumors, inflammations, and infarcted areas) via the enhanced permeability and retention (EPR) effect, and facilitate targeted delivery of specific ligand-modified drugs and drug carriers into poorly accessible areas [80]. The active drug targeting increases the selectivity of the delivery of drugs [79]. Passive and active drug targeting with nanocarriers to disease or tumor site reduce toxic side-effects, increase efficacy, and enhance delivery of poorly soluble or sensitive therapeutic molecules [79].

1.7 Biosensor technologies

A widespread application of MNPs is cell sorting, sometime streptavidin-coated magnetic beads for phenotypic selection of different cell types, including stem cells [81], lymphocytes, neuronal cells, etc [82, 83]. MNPs linked to monoclonal antibodies, could be used to purify blood from infective agents [84]. Moreover, MNP-based magnetic bioseparation could be applied for biosensor technologies (e.g detection of protein analytes using specific MNP-conjugated antibodies) [85].

1.8 Hyperthermia

Hyperthermia is a very promising therapy for cancer that concentrates a localized heating above 43 °C for about 30 min in the site of tumors [86]. Hyperthermia initiates a series of subcellular events in the tumor site, inducing various forms of damage including apoptosis, leading to subsequent cell death [87, 88]. Moreover, hyperthermia induce other effects in the tumor site such as enhancement of tumor blood flow, activation of immunological responses and oxygenation via greater vascular perfusion and permeability, and a shift toward anaerobic metabolism, all leading to an altered extracellular microenvironment [89]. MNPs are able to induce heat in the specific site of tumor under the influence of alternating magnetic fields due to energy reductions in the traversing of the

magnetic hysteresis loop [32]. Induction of heat is related to the magnetization properties of different types of MNPs and magnetic field parameters [30]. The functionalization of MNPs with silica coatings and other reactive chemical groups could improve the selectivity to tumors [90]. In fact, selectivity of magnetic nanoparticles uptake by tumors during hyperthermia therapy could be improved using MNPs conjugated with antibodies which target tumor-specific antigens or modified receptors [91].

1.9 Magnetofection

Another application of MNPs could be magnetofection to transfect permissive and non-permissive cells using MNPs associated to DNA vectors under external magnetic field influence [92]. In fact with this strategy a great increase in transfection performance for both non-viral and viral vectors was demonstrated [93].

1.10 Tissue Engineering

Tissue engineering may have a great benefit by application of magnetic nanomaterials. In fact tissue engineering is useful to overcome the organ transplantation crisis, and thus create artificial organs and tissues [94]. To realize this objective similar architectures of *in vivo* organs should be replicated *in vitro*, in which the cells are allocated precisely. For this purpose, three-dimensional constructs (scaffolds or hydrogels) functioning similarly as under *in vivo* conditions should be firstly built up [95]. To allocate precisely cells into the three dimensional constructs magnetic force-based tissue engineering technique could be useful to provide magneto-responsive features to the cells and to achieve an efficient cell seeding and a controlled tissue assembly and complex tissue formation [96, 97]. The inclusion of magnetic particles has no significant effect on the porosity, stability and wetting properties of the composite scaffolds, making them compatible for cellular support and cultivation [97].

1.11 PhD thesis overview

The overall goal of this PhD project was the biological characterization by in vivo and in vitro testing of magnetic nanoparticles that can be used for various applications. In recent years, considerable efforts have been spent to develop magnetic nanoparticles (MNPs) and improve their applicability in several areas [76]. Nanoparticles could open a new arena in the field of biomedicine. In fact, magnetite/maghemite nanoparticles combinations have already been approved for clinical use as MRI contrast agents [98]. Precise control over the synthesis conditions and surface functionalization of MNPs is crucial for their final physicochemical properties, colloidal stability, and biological behaviour/fate [60]. The aim of this work was to understand which of the synthesized magnetic nanoparticles could be more suitable to be used as a carrier or platform for various applications in different scientific fields.

During this PhD program two different kinds of magnetic nanoparticles were developed: naked iron-oxide nanoparticles and silica or silica-based coated nanoparticles (core shell-type nanoparticles). The materials were synthesized at Politecnico di Torino - Laboratory of the Applied Science and Technology Department directed by Prof. Enrica Vernè. During this project three sequential syntheses of magnetic nanoparticles were developed. The concentration of the stock solutions of MNPs changed in the different syntheses of nanoparticles. The technology allowed to produce and gradually improve dispersibility, colloidal stability and biocompatibility of MNPs. Cytocompatibility assessment was performed using both direct and not-direct contact cytotoxicity evaluation with murine endothelial cells (MS1) both in static and dynamic conditions. ROS detection and apoptosis evaluation were also carried out to investigate influence of MNPs on these aspects. Murine endothelial cells were used for two reasons: 1) Endothelial cells are the first cell barrier that come in contact with MNPs intravenously injected; and 2) MS1 cells are involved in the stage of production and expansion of lentiviral vectors (transfection). In fact, MNPs could be used for applications of cancer gene therapy. Due to the formation of cluster of nanoparticles in static conditions, cytocompatibility of MNPs was also evaluated in dynamic conditions of cell culture. In fact, cells were seeded on polycaprolactone strips and cultivated under a continuous medium flow bioreactor to simulate blood stream. Then, *in vivo* biocompatibility and biodistribution of MNPs for 7 days in mice was investigated after intravenous administration of MNPs via tail vein. Two doses of 2 and 20 mg/kg MNPs were separately given to the mice via tail vein injections. Hematological parameters, changes in serum and tissue iron levels were analyzed after 1 week of MNPs to mice. Experiment term of 7 days was chosen for biodistribution of MNPs. Tissue iron levels were

analyzed by ICP-AES and histological Perl's Prussian Blue Staining. MNPs biodistribution evaluation was important to investigate the nanotoxicological effects of magnetic nanoparticles within tissues and organs. During the different cytocompatibility evaluation two concentrations of MNPs were standardized: 2 and 20 mg/kg body weight. In particular the concentration of 2 mg/kg body weight was found to be biocompatible and then suitable to be used as it is or as a nanocarrier for intravenous administration of drugs.

Chapter 2

Characterization of Mag and Mag-SiO_2 nanoparticles synthesized via co-precipitation method

2.1 Aim

The purpose of this part was to compare and optimize the development, production and cytocompatibility of iron oxide (Fe_3O_4) nanoparticles respect to the silica coated iron-oxide nanoparticles (SiO_2-Fe_3O_4). A modified chemical co-precipitation method was used to prepare naked iron-oxide nanoparticles (Fe_3O_4), while silica coating was based on wet chemistry (Stöber method) and condensation of silica precursor tetraethyl orthosilicate (TEOS). The silica shell not only serves to protect nanoparticles from agglomeration but also assists further modifications so increasing their versatility and surface functionalization properties. Moreover it is durable in acid, and useful for the conjugation with biomolecules and for drug delivery.

Silica is known to be one of the most suitable coating layer for superparamagnetic MNPs due to its chemical stability, biocompatibility [99] and versatility for surface modification. Moreover, it helps to convert hydrophobic NPs into hydrophilic water-soluble particles [100]. In addition, silica coating may provide flexibility in the construction of well-defined core-shell nanostructures.

2.2 Materials and methods

2.2.1 Synthesis of nanoparticles

Two different types of magnetic iron-oxide nanoparticles (MNPs) were synthesized: pure magnetite (Mag) and silica-coated magnetite (Mag-SiO_2) (Table 1). Magnetite nanoparticles were synthesized by co-precipitation method [101]: aqueous solutions 0,1 M of $FeCl_2$ and $FeCl_3$ were mixed to obtain

a stoichiometric ratio of Fe^{2+}/Fe^{3+} of 1:2; subsequently NH_4OH was added drop by drop under stirring, up to reach a pH value of about 10. The solution was placed in an ultrasound bath for 20 min. After 24 hours magnetite nanoparticles were washed with bi-distilled water and redispersed always in water.

The Mag-SiO_2 nanoparticles were synthesized following the Stöber method [102]: 0,33 ml of tetraethyl orthosilicate (TEOS), 3 ml of water and 3 ml of ethanol were added to 40 ml of magnetite suspension, the pH of the solution was adjusted at 10 and the suspension was placed in orbital shaker at room temperature for 3 hours at 150 rpm. Then the Mag-SiO_2 nanoparticles were washed with bi-distilled water and redispersed in water. All chemicals were purchased from Sigma Aldrich.

The starting concentrations of MNPs were 4.9 mg mL^{-1} for Mag and 1.4 mg mL^{-1} for Mag-SiO_2. Before use, the magnetic nanoparticles (Mag and Mag-SiO_2) were sterilized by ultra-violet radiation for 60 minutes.

2.2.2 Nanoparticle characterization

Mag and Mag-SiO_2 nanoparticles were characterized by means of transmission electron microscopy (TEM, Philips CM12, working at 120 kV operating voltage with a LaB6 filament), field emission scanning electron microscopy (FESEM - SUPRATM 40, Zeiss), scanning transmission electron microscopy (STEM-FESEM MERLIN Zeiss.) and energy dispersive spectroscopy (Edax PV9800). Selected area electron diffraction (SAED) patterns were obtained for each sample to observe the morphology and structure.

FESEM micrographs of magnetic nanoparticles were captured using a SUPRATM 40, Zeiss field emission microscope (JEOL, Japan) operated at an excitation voltage of 10 kV. The elemental compositional study was investigated through energy dispersive spectroscopy (EDS) by using EDAX PV 9900 instrument coupled with STEM-FESEM.

A droplet of an aqueous dispersion of nanoparticles was placed on a copper grid for FESEM, TEM and STEM-FESEM sample preparation, allowed to dry, and examined under electron microscopy previously cited.

SAMPLE	MATERIAL	MEDIUM	Concentration of stock solution	pH approx	Notes
Mag	Magnetite nanoparticles	PBS	4.9 mg/ml	7.70	Not stable in solution
Mag-SiO_2	SiO_2 coated magnetite nanoparticles	PBS	1,4 mg/ml	7.22	Not stable in solution

Table 1. Main characteristics of Mag and Mag-SiO_2 NPs.

2.2.3 Cell cultures

Endothelial cell lines derived from mouse cells (MS1 - ATCC - CRL 2460) were used to evaluate cytocompatibility of nanoparticles. MS1 cells were cultivated in Dulbecco's Modified Eagle Medium (DMEM, Sigma Aldrich) additioned with 2 mM L-glutamine, 10% FBS and 1% antibiotics/antimycotics (penicillin/streptomycin/gentamycin, Gibco). Cells were cultured at confluence in a humidified 5% CO_2 atmosphere at 37°C. Afterwards murine endothelial cells were detached using 0.05% trypsin/EDTA solution (Sigma Aldrich) for five minutes.

2.2.4 Not direct contact cytotoxicity evaluation

Not direct contact cytotoxicity evaluation of MNPs was done using leaching solutions. These latter were obtained by adding MNPs to DMEM in a sterile closed tube at the concentration of 0.1 g/mL. Leaching conditions were 37°C for 24 and 72 hours according to ISO standard 10993-12: 1996. Then the specimens were centrifuged at 2500 rpm for 5 minutes and the supernatant was removed by suction and filtered through a microporous filter (0.22 µm) to provide the final eluating solutions. Afterwards, eluates were supplemented with 10% FBS and used to cultivate MS1 cells. Cells were seeded in a defined number ($4x10^3$/well) into 96 wells plates (Cell Star, PBI International, Milan, Italy) and cultivated for three experimental time-points: 24, 48 and 72 hours at 37°C, in humidified 5% CO_2 atmosphere. DMEM without any supplementation was used as a control. At each experimental time cells viability was evaluated by the (3-(4,5-Dimethylthiazol-2-yl)-2,5-diphenyltetrazolium bromide colorimetric assay (MTT, Sigma). Briefly, 100 µl of MTT solution (3mg/ml in PBS) were added to each sample and incubated 4 hours in the dark at 37° C; afterwards, formazan crystals were solved with 100 µl of dimethyl sulphoxyhde (DMSO, Sigma) and 50 µl were collected and centrifuged to remove any debris. Surnatant optical density (o.d.) was

evaluated at 570 nm using a spectrophotometer (Spectra Count, Packard Bell, Meriden, CT, USA). The optical density of control sample was considered as 100% viability. Cell viability was calculated as follow: (indirect contact eluate o.d. / control o.d.)*100. Experiments were performed using four replicates at each experimental time. Furthermore, cells morphology was visually investigated at each experimental time by light microscopy (Leica AF 6500, Leica Microsystems) at 20x magnification.

2.2.5 Direct static contact cytotoxicity evaluation

Direct static contact cytotoxicity evaluation of MNPs was done according to ISO standard 10993-5: 2009. The cells were seeded in 24-well plates (1.6×10^4 cells per well) in DMEM medium and cultured for 24 h at 37°C in 5% CO_2 atmosphere-controlled incubator. After 24 hours the medium was substituted with a new one obtained by adding MNPs to DMEM to obtain the following concentrations: 10 μg/ml, 20 μg/ml, 40 μg/ml and 80 μg/ml (w/v).

MS1 endothelial cells cultivated onto polystyrene wells in presence of DMEM additioned with 2 mM L-glutamine, 10% FBS and 1% antibiotics/antimycotics were used as control. Afterwards, cell viability was evaluated after 24, 48 and 72 hours using MTT assay, as above described for the indirect cytocompatibility assay. The viability of controls were considered as 100% viability.

In addition, Trypan blue (TB) exclusion test of cell viability was used to assess the plasma membrane damage. The TB dye passes via the cell membrane of dead cells and thus stains the cells blue. The percentage of dead cells compared to control was determined. Briefly, the cells were seeded onto 24-well plates at a density of 1.6×10^4 cells and cultivated as above described for 24h. After further 24-h, 48-h and 72-h exposure to DMEM additioned with MNPs at the concentrations of 10 μg/ml, 20 μg/ml, 40 μg/ml, 80 μg/ml, the culture medium with nanoparticles was removed and the cells were detached from the plate surface using trypsin/EDTA solution (0.25% trypsin and 0.02% EDTA). Then, DMEM containing 10% FBS (1 ml) was added to each well in order to inactivate trypsin. The cells were stained with TB by mixing equal volumes of the cell suspension and 0.4% TB solution. The experiments were done in triplicate and repeated four time.

2.2.6 Cells morphology evaluation by fluorescent microscopy

Cells morphology after 24, 48 and 72 h in contact with MNPs at the concentrations above described was investigated by fluorescent microscopy (Leica AF 6500, Leica Microsystems, Basel, Switzerland). For the immunofluorescent (IF) staining the following procedure was used: cells were fixed with 4%

paraformaldehyde in PBS for 20 minutes at room temperature and then washed 3 times with PBS. Phalloidin (rhodamine B tetramethyl isothiocynate, 1/2000 in PBS, AbCam, Cambridge, UK) solution was added for 45 minutes at room temperature (RT) in order to investigate cells cytoskeleton; afterwards, the specimens were washed for further 3 times with PBS and co-stained with 4',6-diamidino-2-phenylindole (DAPI, Sigma-Aldrich) to dye nuclei. Fluorescence images were acquired with a fluorescent microscope (Leica AF 1500, Leica Instruments).

2.2.7 Reactive oxygen species (ROS) in cells

The production of ROS in cells was measured using CellROX Oxidative Stress Reagents (Life Technologies) as an oxidation-sensitive probe. CellROX Oxidative Stress Reagents are fluorogenic probes designed to reliably measure reactive oxygen species (ROS) in live cells. CellROX Green Reagent is a DNA dye, and upon oxidation, it binds to DNA; thus, its signal is localized primarily in the nucleus and mitochondria. Briefly, 2.5 mM CellROX Green Reagent stock solution was diluted 500-fold with cell culture medium without serum or other additives to prepare a 5 µM working solution. MS1 cells were seeded in 12-well plates (7.5×10^4 cells per well). After exposure to Mag and Mag-SiO_2 NPs at the concentrations of 10, 20, 40 and 80 µg/ml for 24 h, the cells were washed with PBS and incubated in 1 mL of CellROX Green Reagent at a final concentration of 5 µM at 37°C in the dark for 30 min. Experimental time-point (24 h) of ROS production induced by MNPs was chosen according to literature [103, 104]. Menadione (25 µM) was used as a positive control. Then, MS1 cells were analyzed with Flow cytometry (BD FACSCalibur) at an excitation wavelength of 485 nm for CellROX Green Reagent. Statistical data were obtained from the dot plots using CellQuest software (BD Biosciences).

2.2.8 Statistical analyses

All statistical analyses were performed using IBM Statistical Package for Social Sciences v. 20 software (SPSS - IBM). Data were expressed as means ± standard deviations. The results were analyzed using one way analysis of variance (ANOVA) followed by Scheffe's test, and P values less than 0.05 were considered to be statistically significant.

2.3 Results

2.3.1 Nanoparticles: characterization

In Figure 1, TEM images and SAED patterns of Mag and Mag-SiO_2 nanoparticles are reported. It can be observed that both nanoparticles were spherical and the mean diameter was roughly 10-15 nm. Diffraction patterns matched for magnetite [105]. In the case of Mag-SiO_2 samples broad halos can be observed together with the diffraction signals characteristics of magnetite (that resulted a little attenuated), and can be attributed to the amorphous coating.

In Figure 2, FESEM, TEM and STEM images of Mag-SiO_2 sample are reported. FESEM confirms the spherical shape of particles with a diameter of about 10-15 nm. TEM and STEM observation showed the presence of a dense core (magnetite) covered by a less dense shell (silica) with a thickness of 1-2 nm. EDS analyses (spectra not reported for brevity) confirm the presence of iron (Fe) and oxygen (O) in the Mag sample and the appearance of the Si signal for Mag-SiO_2 one.

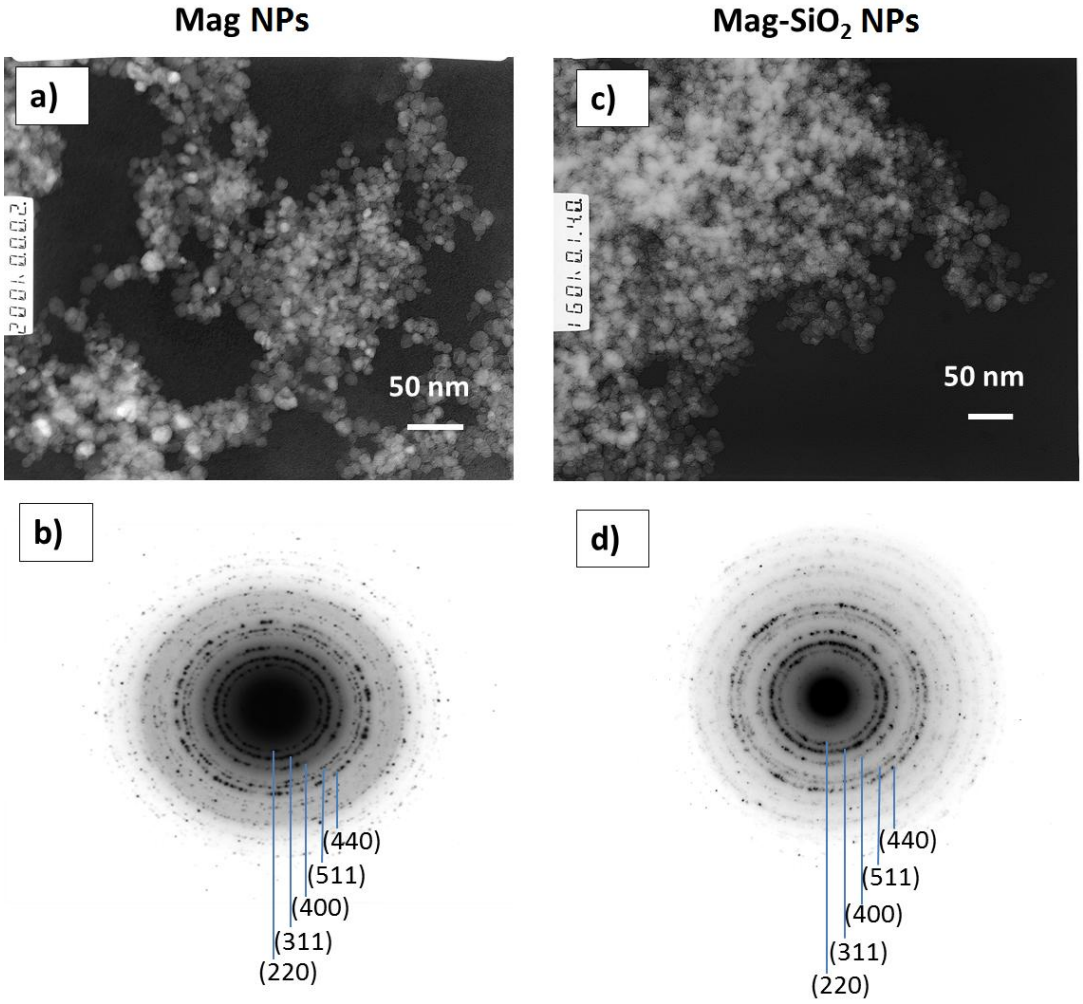

Figure 1: TEM Images and SAED patterns of Mag and Mag-SiO_2 samples. a) TEM image of Mag, b) SAED pattern of Mag, c) TEM image of Mag-SiO_2, d) SAED pattern of Mag-SiO_2. The numbers in SAED patterns refer to the distances of crystal planes of Mag and Mag-SiO_2 NPs according to a defined crystallographic direction.

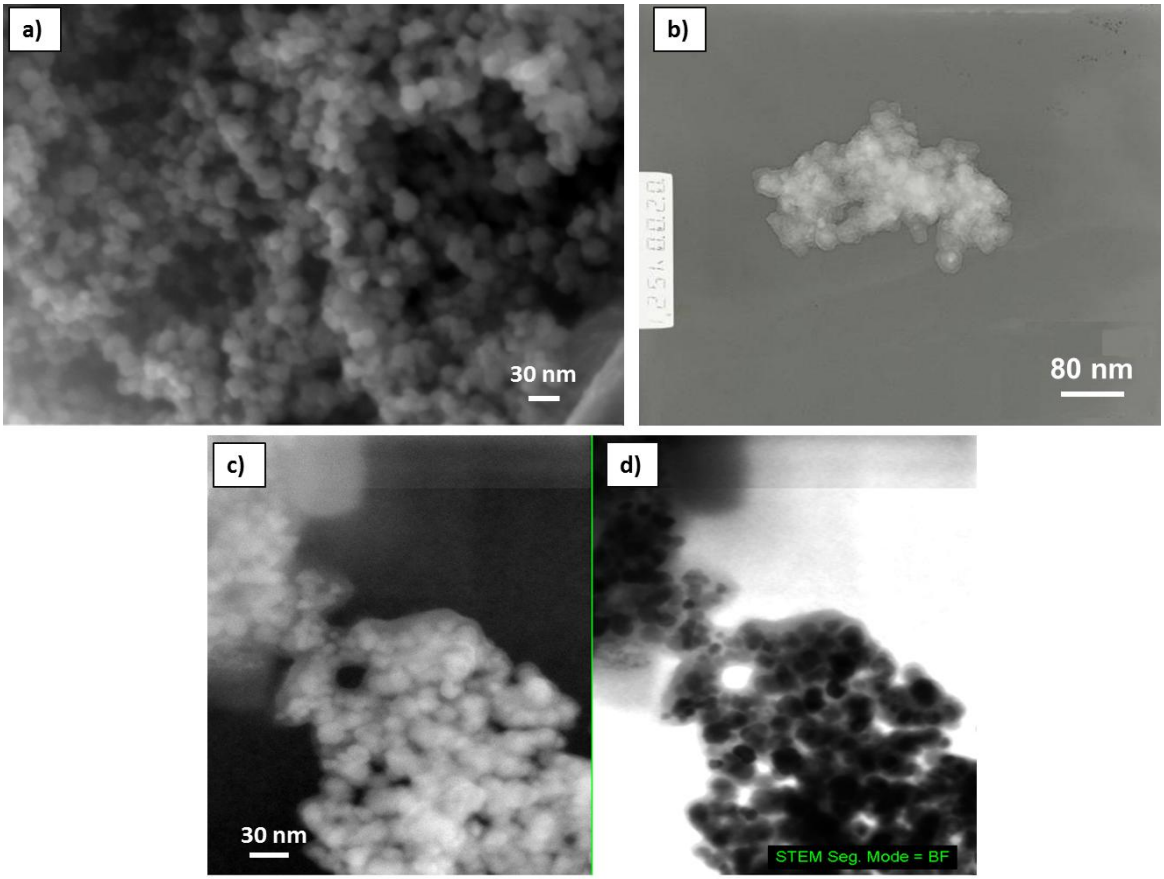

Figure 2: FESEM (a), TEM (b) and STEM (c - dark field mode, d - bright field mode) images of Mag-SiO_2 NPs.

2.3.2 Not direct contact cytotoxicity

MTT assay demonstrated that the eluate solutions obtained by soaking magnetic nanoparticles in DMEM culture medium for 24 h showed a cell viability in a range of 66-73% and of 77-92% for Mag and Mag-SiO_2 nanoparticles respectively (Fig. 3).

In a similar way the eluate solutions obtained by soaking MNPs in DMEM for 72 h showed cell viability in a range of 65-72% and of 78-92% for Mag and Mag-SiO_2 nanoparticles respectively (Fig. 3).

Trypan blue assay showed that the leaching solutions obtained from Mag nanoparticles in both soaking conditions showed higher cell mortality in a range of 28-35% ($p < 0.05$) after three experimental time-points compared to that observed for Mag-SiO_2 NPs in a range of 8-23%.

Trypan blue assay validated the results obtained with MTT assay (Tables 2 and 3). The differences were statistically significant ($p < 0.05$) at 24, 48 and 72 h time-point evaluations. No morphological alterations by microscopic observation were observed when cells cultivated with test media were compared with control ones (Figure 3).

Not direct contact cytotoxicity (37°C for 24 h) Percentage of TB positive MS1 cells			
Samples	24 h	48 h	72 h
Mag	26.4 ± 1.2*	28.7 ± 1.3*	31.1 ± 0.9*
Mag-SiO_2	7.6 ± 0.7	16.5 ± 0.9**	22.4 ± 1.2**

Table 2. Trypan blue exclusion test. MS1 cell mortality after not direct contact with MNPs (37°C for 24 h). Data are shown as the mean ± standard deviation (n = 4). *P < 0.05 compared with control and Mag-SiO_2 nanoparticles. **P < 0.05 compared with control.

Not direct contact cytotoxicity (37°C for 72 h) Percentage of TB positive MS1 cells			
Samples	24 h	48 h	72 h
Mag	27.6 ± 1.1*	29.1 ± 1.4*	32.5 ± 1.6*
Mag-SiO_2	7.9 ± 1.0	18.8 ± 1.1**	21.9 ± 1.3**

Table 3. Trypan blue exclusion test. MS1 cell mortality after not direct contact with MNPs (37°C for 72 h). Data are shown as the mean ± standard deviation (n = 4).*P < 0.05 compared with control and Mag-SiO_2 nanoparticles. **P < 0.05 compared with control.

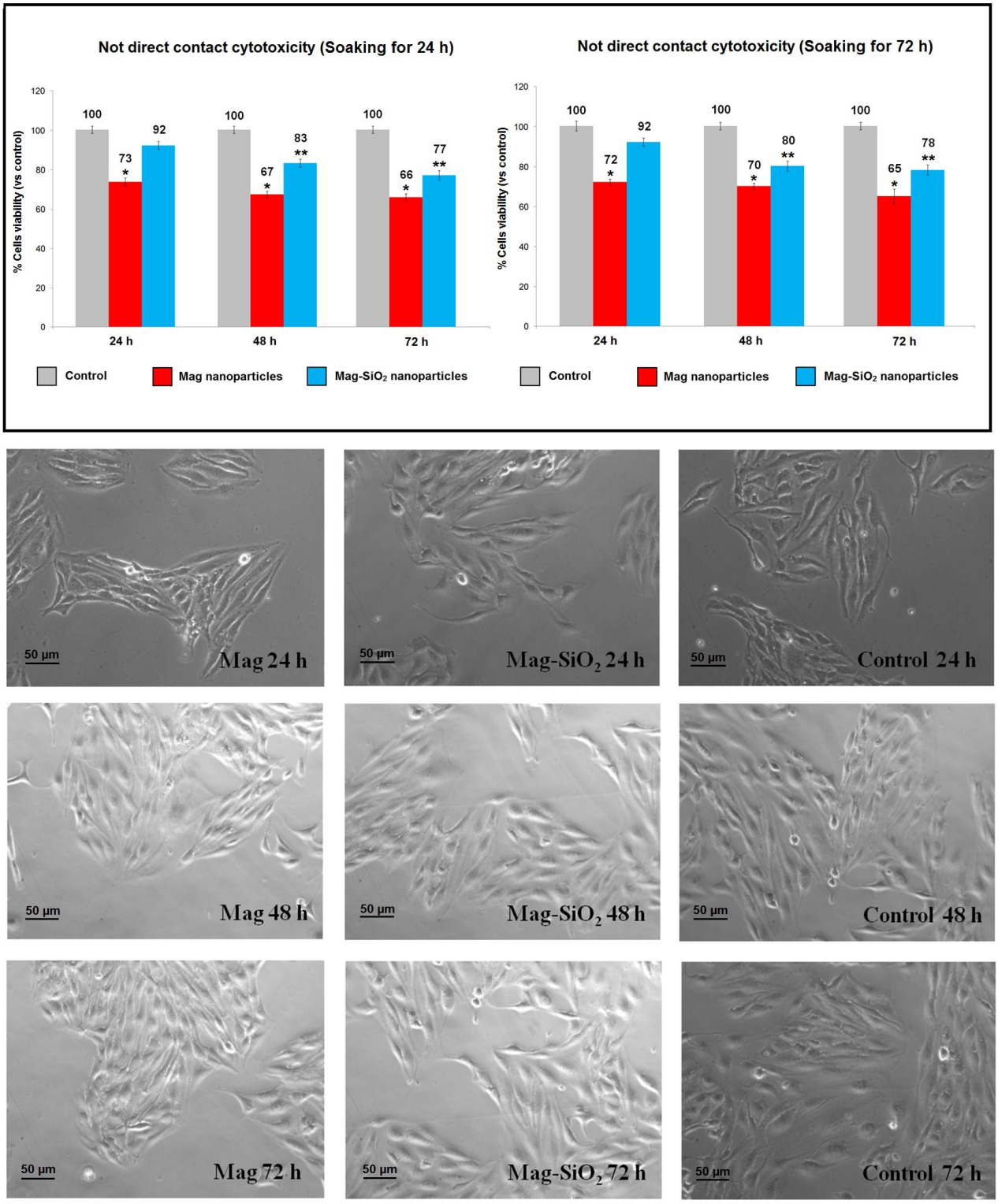

Figure 3. Not direct contact cytotoxicity evaluation of MNPs using murine endothelial cells (MS1 cells) and different eluates (24 and 72 h of soaking); MTT assay and optical microscopic images. Magnification: 20x, bar scale = 50 µm. Data are shown as the mean ± standard deviation (n = 4). *P < 0.05 compared with control and Mag-SiO_2 NPs. **P < 0.05 compared with control.

2.3.3 Direct contact cytotoxicity

MS1 endothelial cells showed cell viability similar to that of control when put in direct contact with MNPs at the concentration of 10 µg/ml. Viability slightly decreased by increasing the concentrations of MNPs (20-80 µg/ml) for both Mag and Mag-SiO_2 nanoparticles (Fig. 4). The same trend was observed at all experimental time-points: 24, 48 and 72 hours (Fig. 5 and 6).

Cell viability after contact with Mag-SiO_2 NPs was in a range of 81-97% and not significantly differed when compared with Mag NPs (viability range between 86 and 98%) for concentrations ranging from 10 to 80 µg/ml (Figures 4-6). Trypan blue assay validated the results obtained with MTT assay (Tables 4-6).

No morphological alterations were observed between cells in direct contact with MNPs and control using IF staining (Fig. 7-9) and microscopic observation (Fig. 10-12).

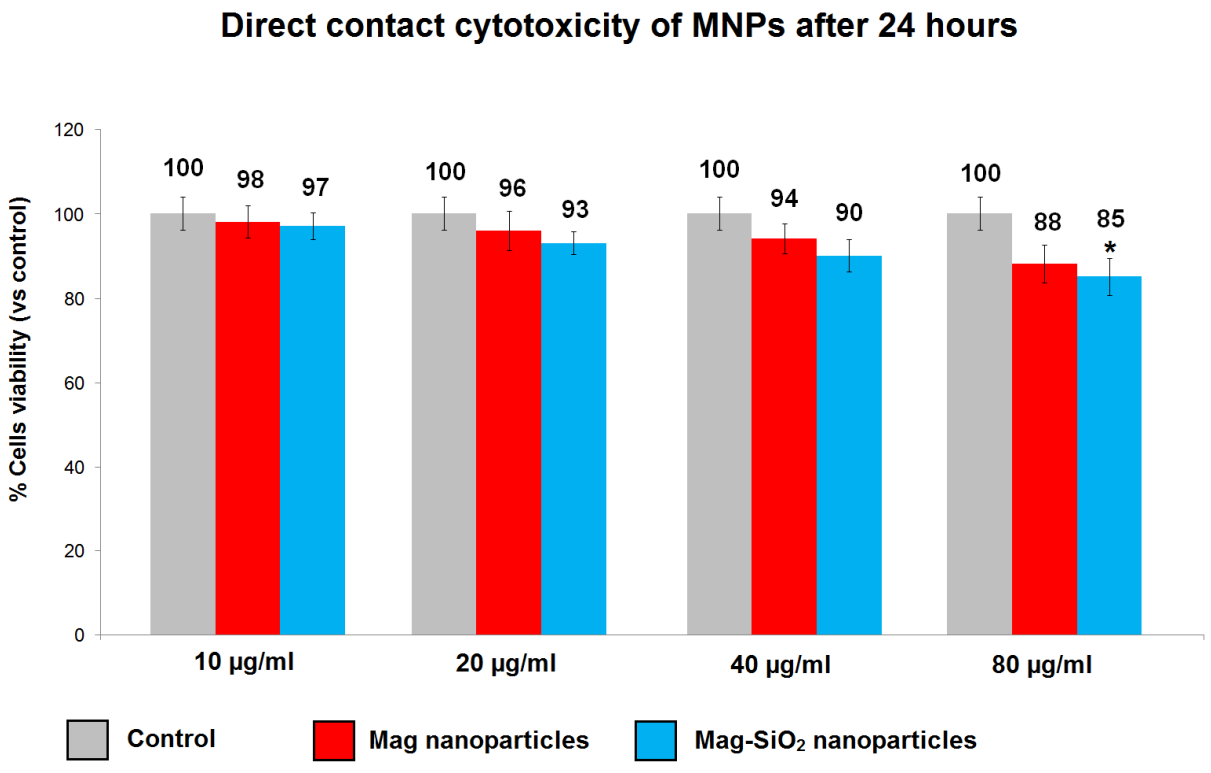

Figure 4. Cytocompatibility assessment of MS1 cells after 24 hours in contact with different concentration of MNPs. Data are shown as the mean ± standard deviation (n = 4). *P < 0.05 compared with control.

Percentage of TB positive MS1 cells after 24 hours of contact with MNPs

Samples	10 µg/ml	20 µg/ml	40 µg/ml	80 µg/ml
Mag	1.7 ± 0.9	4.2 ± 1.5	5.8 ± 0.7	12.6 ± 1.2*
Mag-SiO_2	2.9 ± 1.0	6.4 ± 1.2	9.6 ± 0.8*	14.7 ± 1.4*

Table 4. Trypan blue exclusion test. MS1 cell mortality after direct contact of 24 hours with MNPs. Data are shown as the mean ± standard deviation (n = 4). *P < 0.05 compared with control.

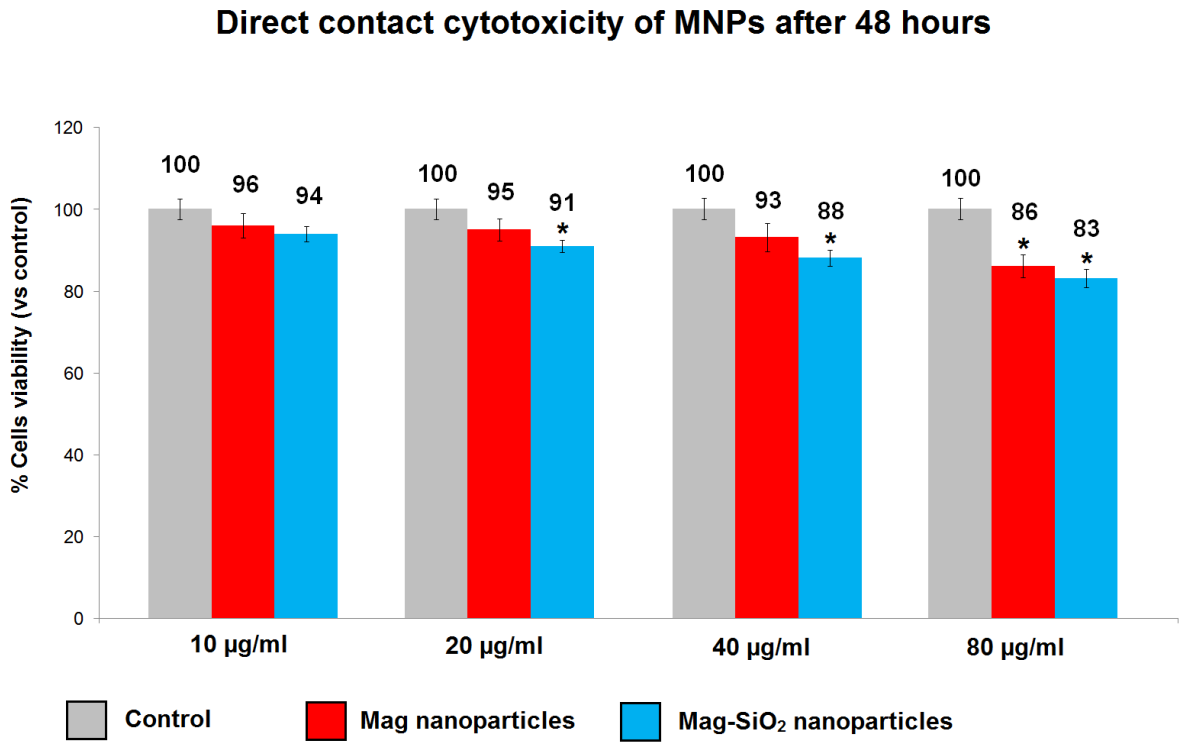

Figure 5. Cytocompatibility assessment of MS1 cells after 48 hours in contact with different concentration of MNPs. Data are shown as the mean ± standard deviation (n = 4). *P < 0.05 compared with control.

Percentage of TB positive MS1 cells after 48 hours of contact with MNPs

Samples	10 µg/ml	20 µg/ml	40 µg/ml	80 µg/ml
Mag	4.0 ± 0.7	4.8 ± 0.9	6.4 ± 1.2	13.3 ± 1.4*
Mag-SiO_2	5.9 ± 0.9	8.5 ± 1.4*	11.4 ± 1.5*	16.9 ± 0.8*

Table 5. Trypan blue exclusion test. MS1 cell mortality after direct contact of 48 hours with MNPs. Data are shown as the mean ± standard deviation (n = 4). *P < 0.05 compared with control.

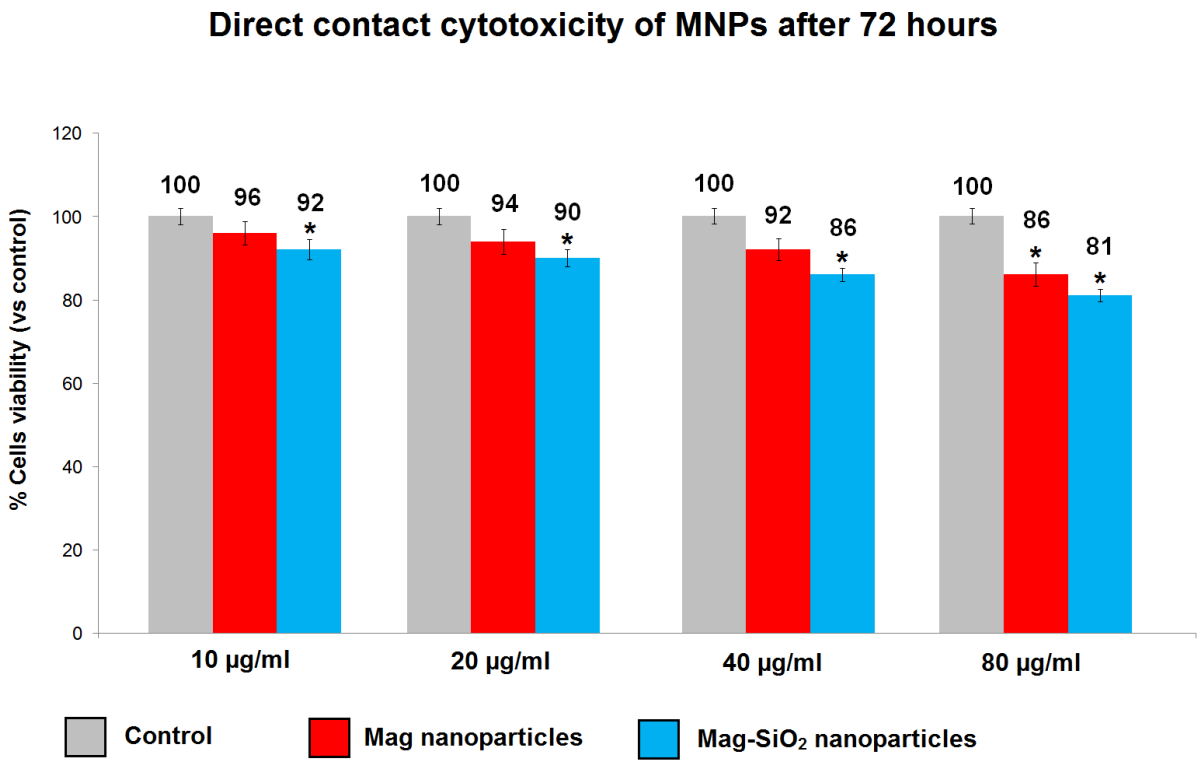

Figure 6. Cytocompatibility assessment of MS1 cells after 72 hours in contact with different concentration of MNPs. Data are shown as the mean ± standard deviation (n = 4). *P < 0.05 compared with control.

Percentage of TB positive MS1 cells after 72 hours of contact with MNPs

Samples	10 µg/ml	20 µg/ml	40 µg/ml	80 µg/ml
Mag	4.3 ± 1.4	6.2 ± 1.3	7.9 ± 1.0	14.3 ± 1.1*
Mag-SiO_2	7.9 ± 1.8	8.9 ± 0.6*	13.6 ± 1.3*	18.4 ± 1.4*

Table 6. Trypan blue exclusion test. MS1 cell mortality after direct contact of 72 hours with MNPs. Data are shown as the mean ± standard deviation (n = 4). *P < 0.05 compared with control.

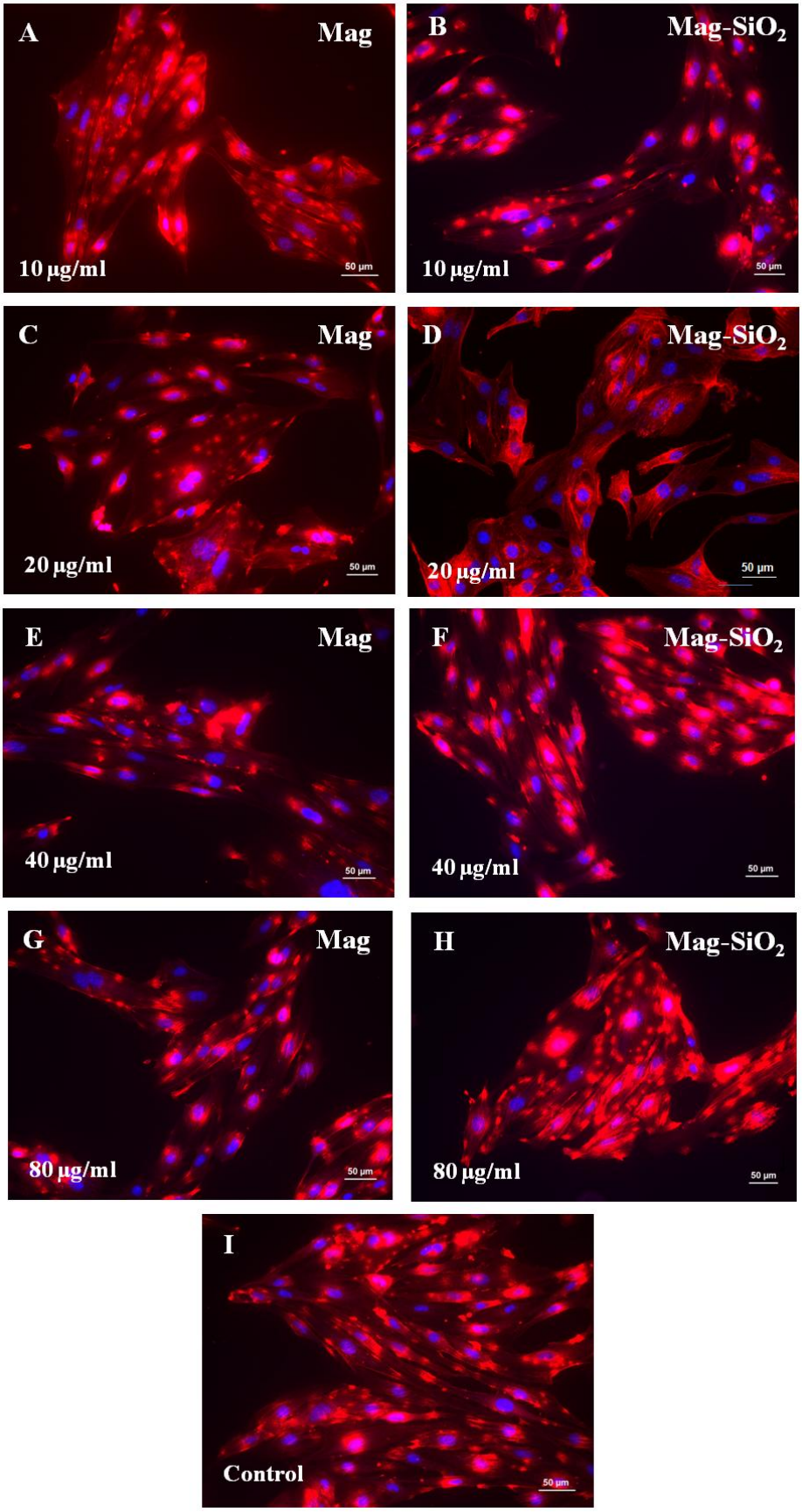

Figure 7. Cells seeded for 24 h in contact with nanoparticles (10-80 µg/ml). IF staining with DAPI (blue) and phalloidin (red). Magnification: 20x, bar scale = 50 µm.

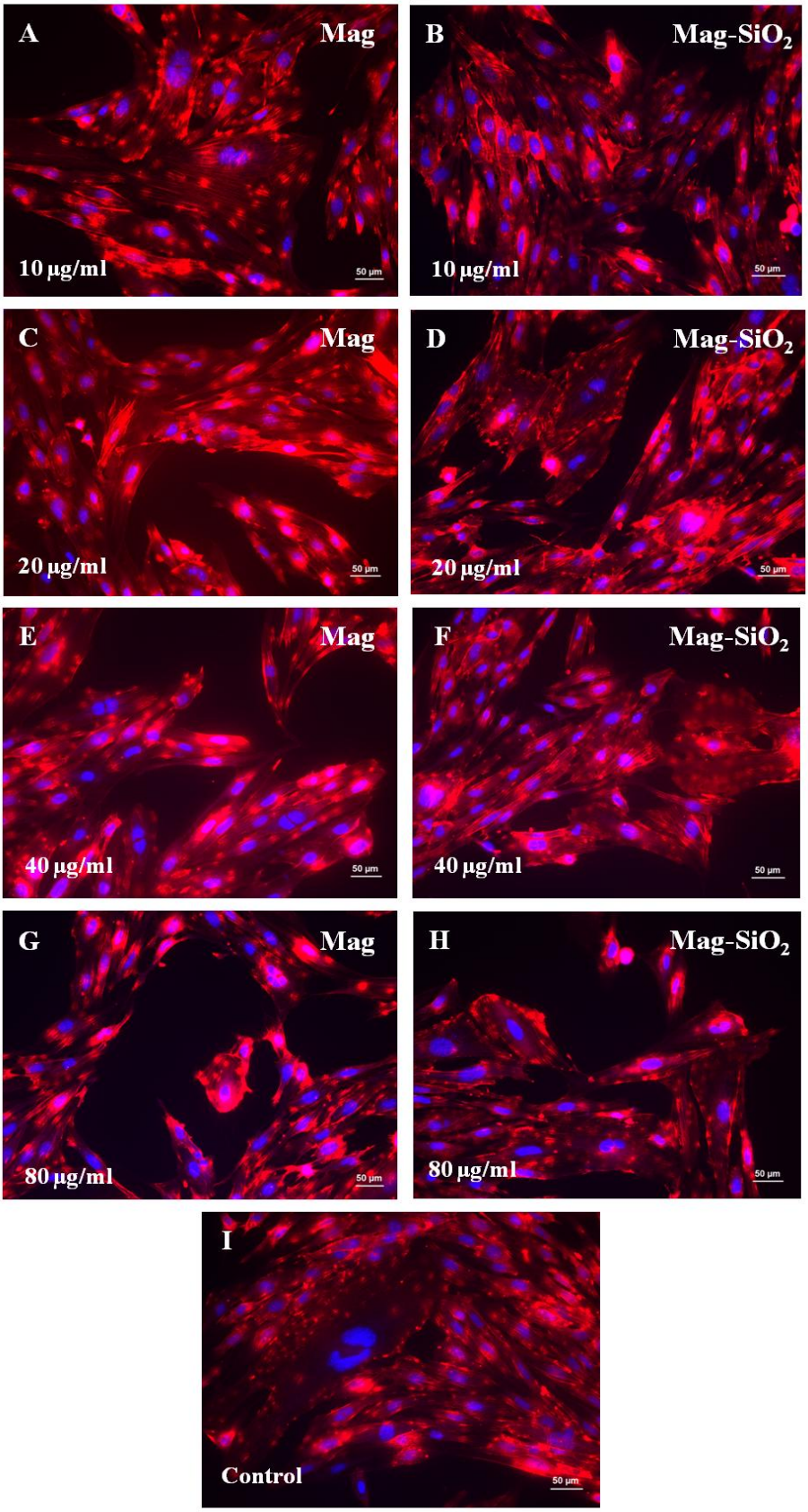

Figure 8. Cells seeded for 48 h in contact with nanoparticles (10-80 µg/ml). IF staining with DAPI (blue) and phalloidin (red). Magnification: 20x, bar scale = 50 µm.

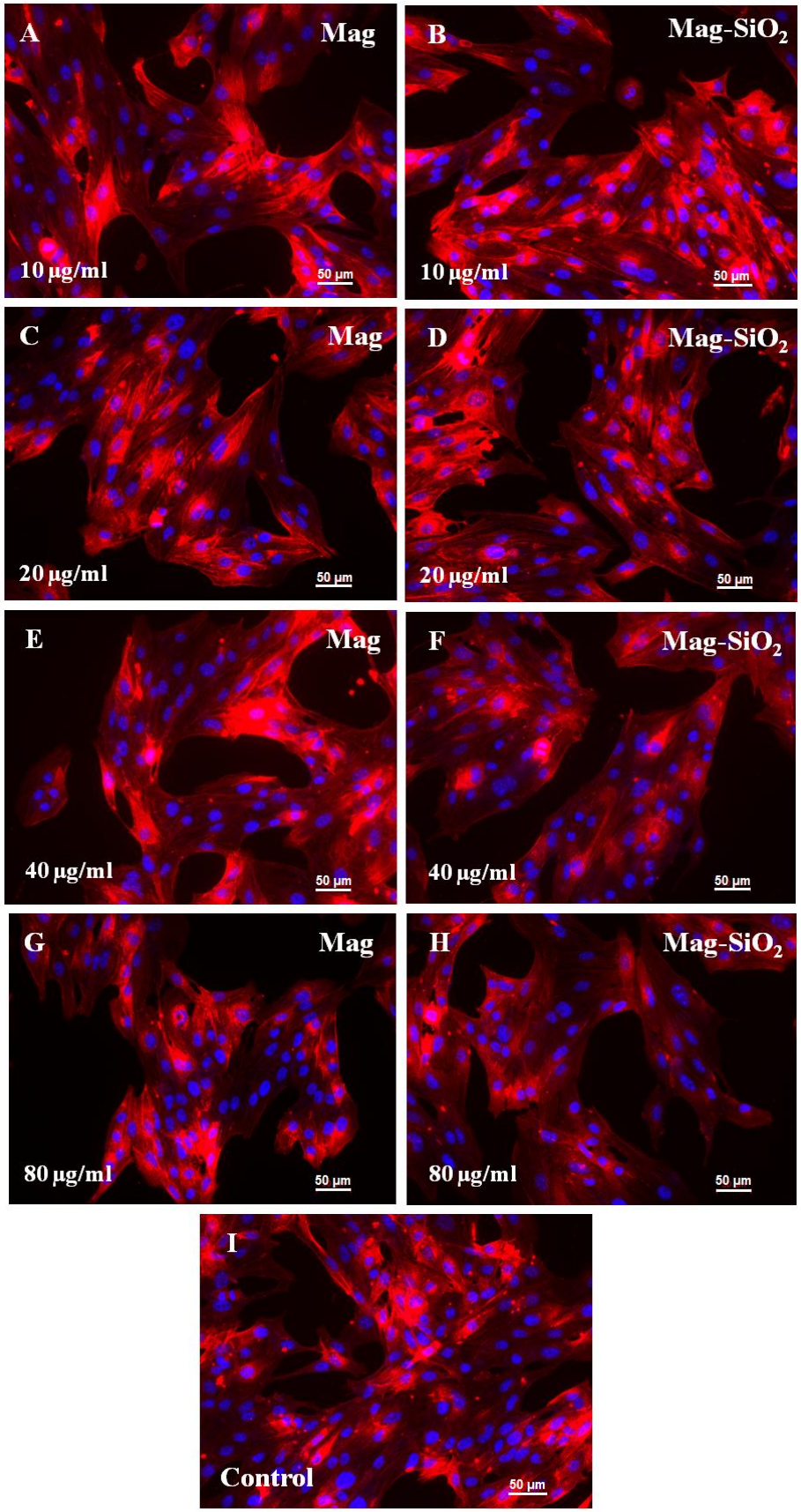

Figure 9. Cells seeded for 72 h in contact with nanoparticles (10-80 µg/ml). IF staining with DAPI (blue) and phalloidin (red). Magnification: 20x, bar scale = 50 µm.

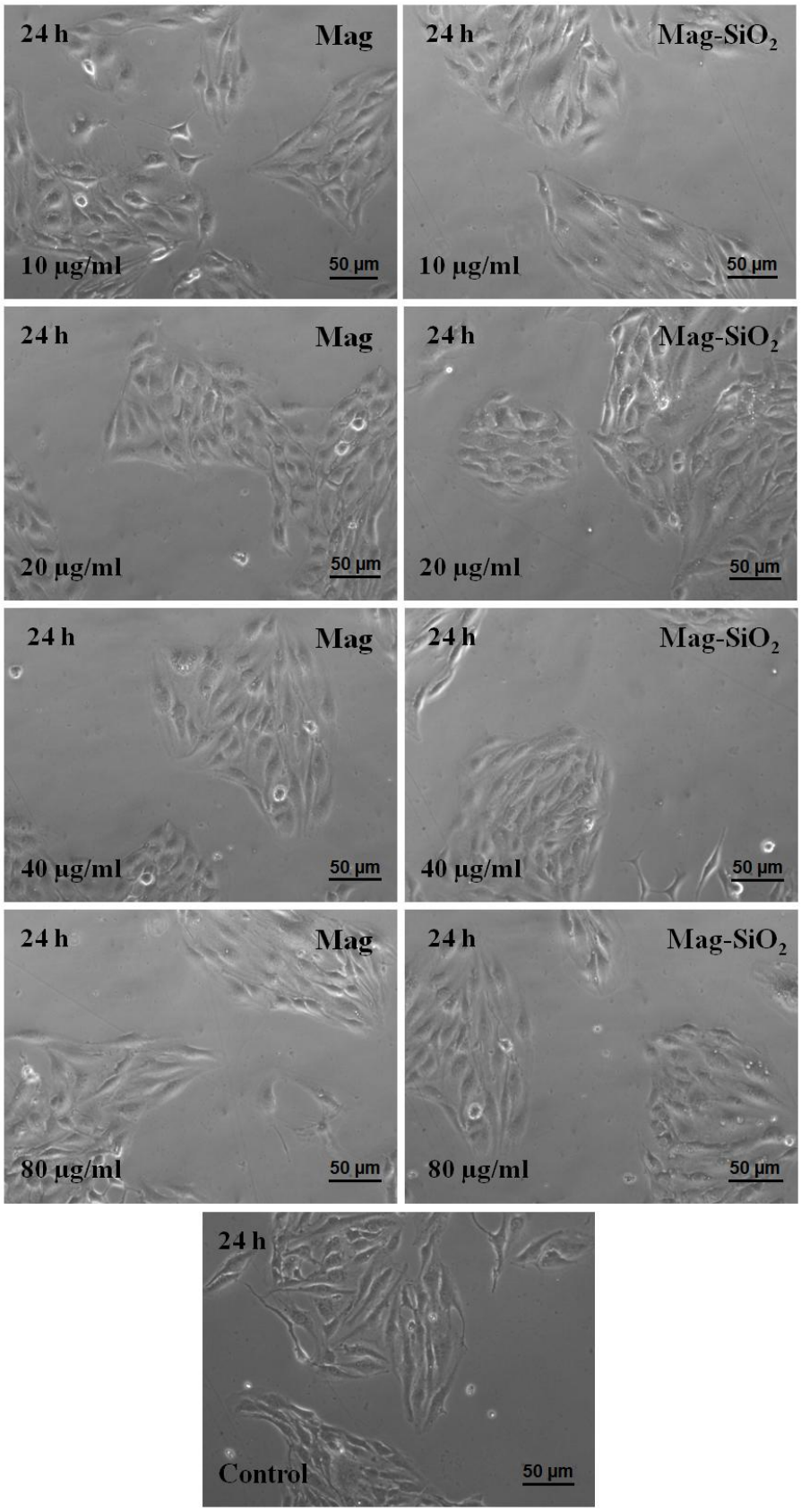

Figure 10. Optical microscopic images of endothelial cells (MS1 cells) after direct contact with MNPs (10-80 µg/ml) for 24 hours. Magnification: 20x, bar scale = 50 µm. No effects are observed on cell morphological features.

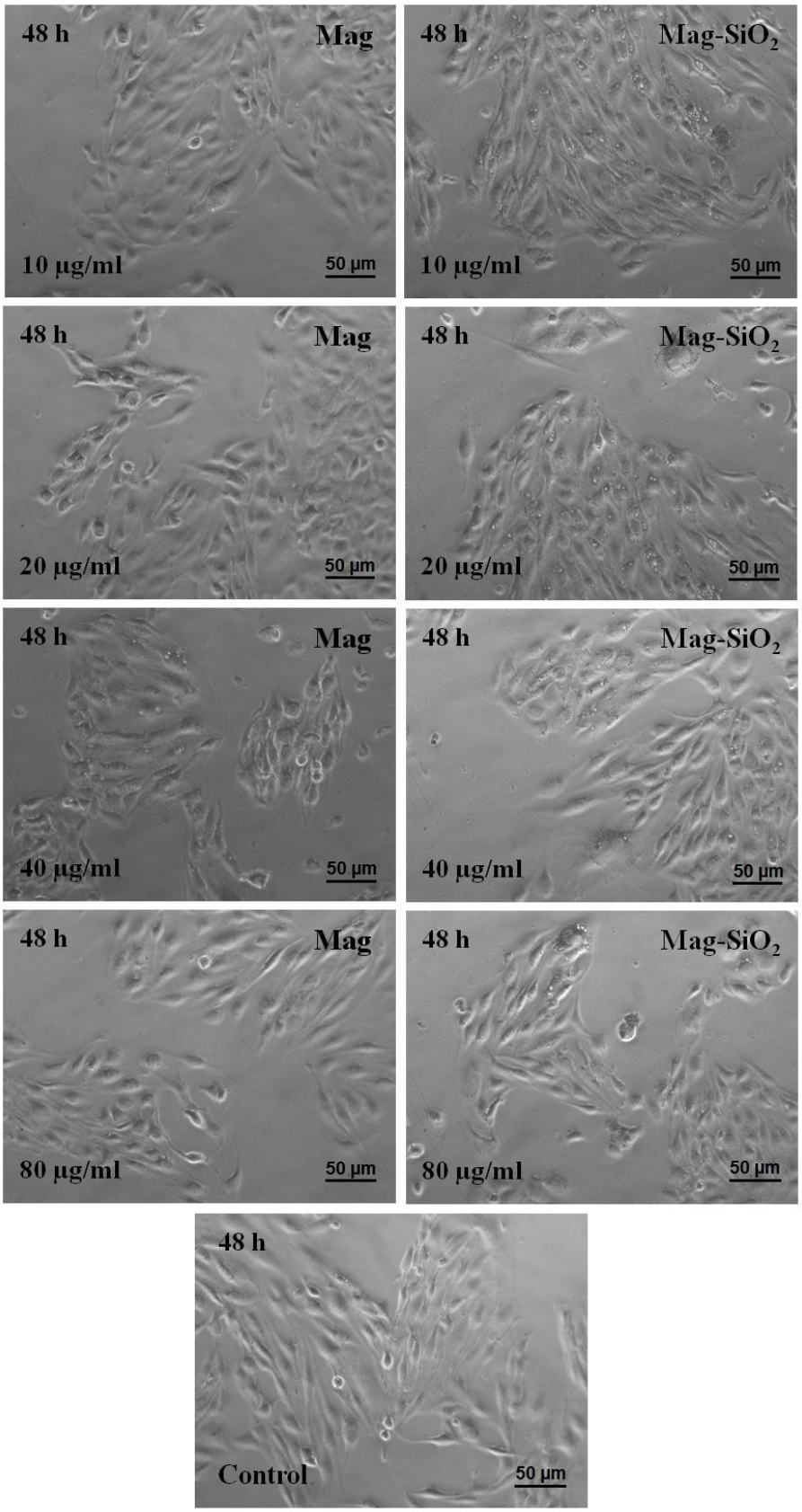

Figure 11. Optical microscopic images of endothelial cells (MS1 cells) after direct contact with MNPs (10-80 µg/ml) for 48 hours. Magnification: 20x, bar scale = 50 µm No effects are observed on cell morphological features.

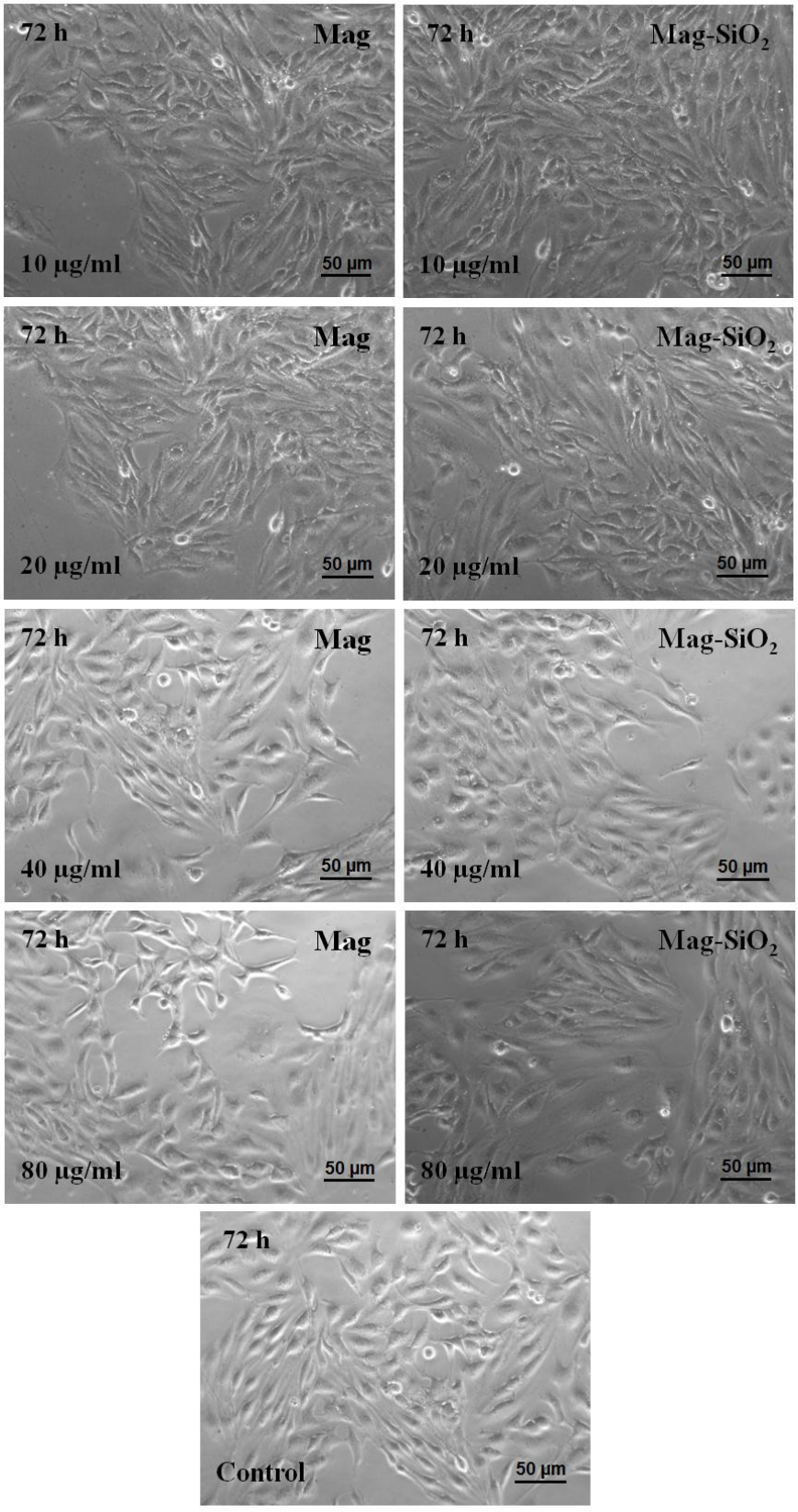

Figure 12. Optical microscopic images of endothelial cells (MS1 cells) after direct contact with MNPs (10-80 µg/ml) for 24 hours. Magnification: 20x, bar scale = 50 µm. No effects are observed on cell morphological features.

2.3.4 ROS generation induced by MNPs

Naked and silica core-shell type iron oxide nanoparticles could induce the generation of intracellular reactive oxygen species (ROS) depending on the concentration of nanoparticles, and oxidative stress followed by ROS generation may cause damage to mitochondria and DNA. We investigated whether Mag and Mag-SiO_2 NPs could induce the generation of intracellular ROS. CellROX Green Reagent was used to determine the generation of intracellular ROS induced by MNPs.

ROS generation was observed in MS1 cells exposed to Mag and Mag-SiO_2 NPs at 10, 20, 40 and 80 µg/ml concentrations for 24 h (**Figure 13**). An increase in ROS generation was observed in both Mag and Mag-SiO_2 NPs in a concentration-dependent manner following the exposure of 10, 20, 40 and 80 µg/ml MNPs for 24 hours (1.15%, 5.66%, 8.76% and 15.72% of ROS expression for Mag NPs and 2.11%, 20.78%, 22.64% and 24.13% of ROS expression for Mag-SiO_2 NPs, respectively). All data were considered statistically significant ($p < 0.05$).

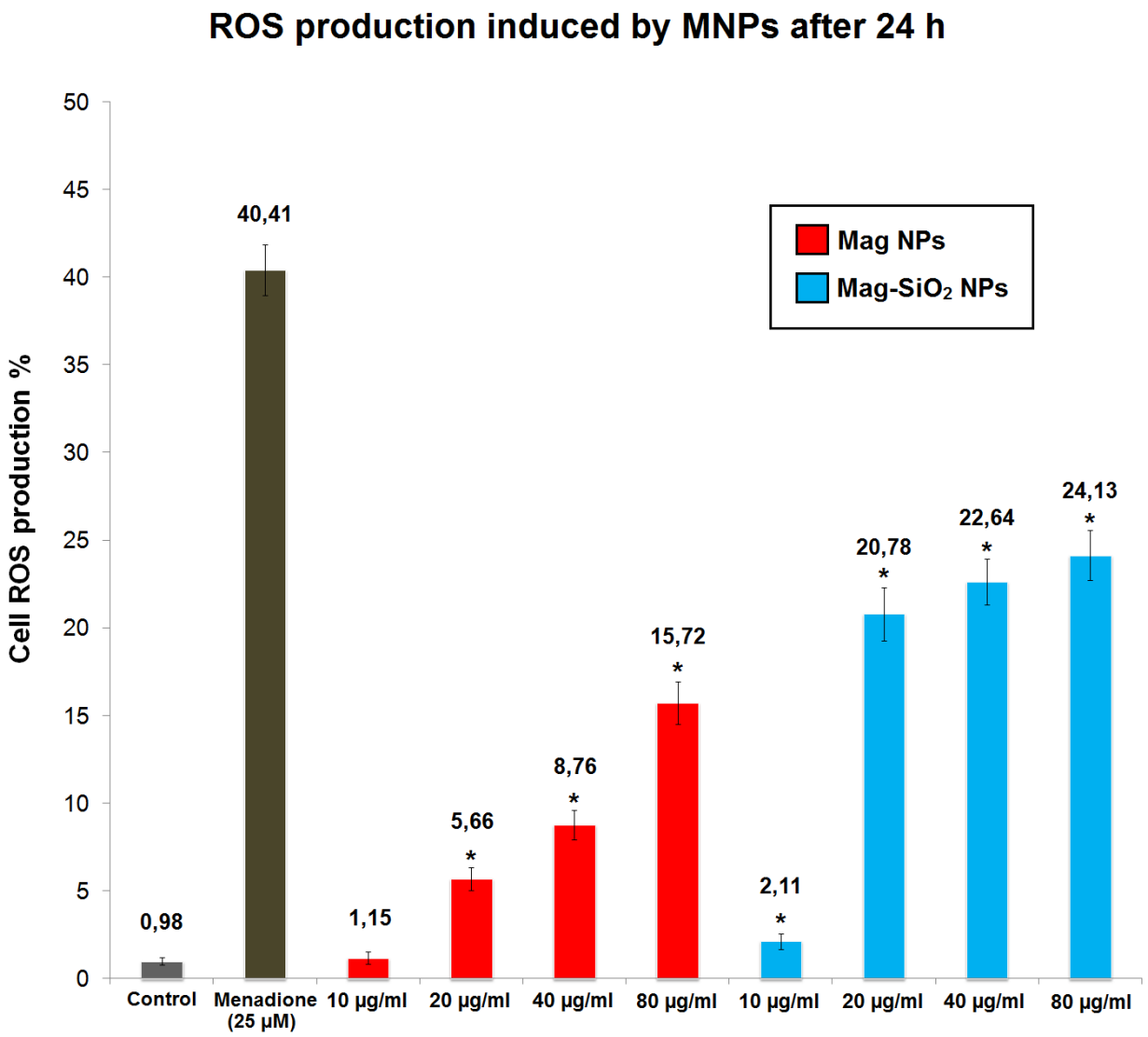

Figure 13. Effect of MNPs on the generation of ROS. Cells were treated with a designated concentration of MNPs for 24 hours. Results are expressed as mean ± SD. *P < 0.05 compared with control untreated and positive control (Menadione 25 µM).

2.4 Discussion

In this chapter we used a chemical co-precipitation method to synthesize magnetic nanoparticles. The advantages of this procedure include ease of synthesis, good control of chemical conditions, and repeatable experimental results [106]. Morphological observations and chemical compositional evaluation using EDS analyses and various electron microscopic methods confirmed that we successfully prepared naked and silica core-shell type iron oxide nanoparticles with uniform electron density, regular morphology, and homogeneous particle size, which are all fundamental

factors for biomedical applications. The bad points of this first synthesis of magnetic nanoparticles were the low dispersibility and colloidal stability of MNPs and a slight cell mortality observed for Mag NPs in not direct cytotoxicity. In vitro preliminary cytocompatibility is one of the most important prerequisite for the clinical application of any biomaterial [54]. The European Medicines Agency (EMA) and the U.S. Food and Drug Administration (FDA) are paying more attention to the safety of medical materials. Before any clinical study of a new biomaterial can take place, its compatibility must be evaluated by in vitro testing according to ISO standard 10993-12: 1996 that is a standard biological evaluation for medical instruments and is based on cell toxicity assays. The present study also carried out two cell toxicity tests based on mitochondrial dehydrogenase assessment (MTT assay) and plasma membrane damage evaluation (Trypan Blue (TB) staining). These cell toxicity assays are basic methods of evaluating the biocompatibility of biomaterials when studying cytotoxicity [54]. They are, fast, simple, flexible, and reproducible techniques. Therefore, we performed for MNPs a direct contact cytotoxicity evaluation and an *in vitro* not direct cytotoxicity test using a leaching solution. In not direct contact cytotoxicity evaluation Mag nanoparticles caused higher cell mortality after 24, 48 and 72 hours for both leaching conditions respect to Mag-SiO_2 nanoparticles. Our results showed that Fe_3O_4/SiO_2 magnetic nanoparticle leaching solutions have a very limited influence on cell viability.

In direct static contact cytotoxicity evaluation a trend of cell viability comparable to control was observed after 24, 48 and 72 hours for both Mag and Mag-SiO_2 nanoparticles. The cells maintained >80% cell viability even after 72 h of treatment with the samples at the concentration of 80 µg/ml. The trypan blue exclusion assays were also employed to determine the effect of iron-oxide nanoparticles on cell mortality of MS1 cells (Tables 3, 4 and 5). The obtained data were consistent with the results of the MTT assay. MTT assay and TB staining were used like two complementary tests for the evaluation of the cytocompatibility of magnetic nanoparticles constituting in this way a mutual confirmation of the experimental data. These results clearly confirmed the low cytotoxicity of the Mag and Mag-SiO_2 NPs compared to control in direct static contact conditions. All cell viability rates of direct contact cytotoxicity were greater than 75%. Thus, it can be considered a promising cytocompatible biomaterial. ROS production induced from the first synthesis of MNPs on MS1 cells was investigated. ROS are important intracellular mediators of the inflammatory response and cell death following uptake of nanoparticles. ROS generation induced by the first synthesis of MNPs was in a concentration-dependent manner after 24 hours.

Chapter 3

Biological characterization of magnetic nanoparticles synthesized via co-precipitation methods using citric acid as dispersant

3.1 Aim

The purpose of this part was to improve dispersibility and cytocompatibility of naked and silica core-shell type iron oxide nanoparticles respect to the first synthesis of MNPs. Dispersibility of the second synthesis of MNPs was improved respect to the first synthesis using citric acid as dispersant. In addition, calcium-silica core-shell type iron-oxide nanoparticles were introduced between the magnetic nanoparticles produced to exploit their positive surface charge for MNPs functionalization with targeting moieties. The first synthesis of MNPs showed problems of dispersibility and colloidal stability. In fact MNPs of first synthesis were observed to precipitate in solution. Physical-chemical, magnetic and *in vitro* biological characterization of the second synthesis of nanoparticles was carried out to investigate their colloidal stability, superparamagnetic properties and cytocompatibility.

3.2 Materials and methods

3.2.1 Nanoparticles preparation

Four different types of magnetic nanoparticles were preapared: Mag, Mag-SiO_2, Mag-SiO_2-Ca(3), Mag-SiO_2-Ca(17). The preliminary physico-chemical characterization of the nanoparticles was performed by Politecnico di Torino as following reported. Their main characteristics are described in table 7. One samples were naked magnetite while three consisted of a magnetite core covered by an amorphous silica shell (Mag-SiO_2) (**Figure 14**). The silica or silica-based glass layer (e.g. SiO_2-CaO) is useful to increase NP surface reactivity (e.g. by exposition of hydroxyl groups) and allow functionalization with targeting moieties (e.g. folic acid, monoclonal antibodies, fatty acids), drugs (e.g. cisplatinum, doxorubicin) and lentiviral vectors or other drug/tracers.

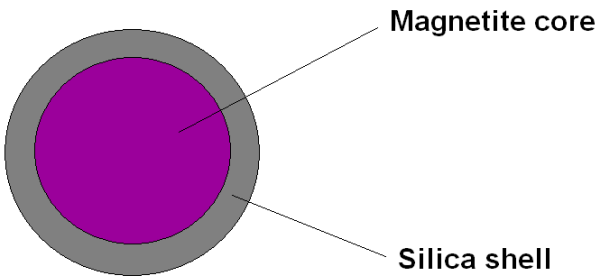

Figure 14. Schematic representation of silica core-shell type magnetic nanoparticles.

SAMPLE	MATERIAL	MEDIUM	Concentration of stock solution	pH approx	Notes
Mag	Citric acid treated magnetite nanoparticles	Water	5 mg/ml	4.12	Stable in solution for weeks
Mag-SiO_2	SiO_2 coated citric acid stabilized magnetite nanoparticles	Water	1,4 mg/ml	6.96	Stable in solution for weeks
Mag-SiO_2-Ca(3)	SiO_2 - Ca (low amount Ca) coated citric acid stabilized magnetite nanoparticles	Water	1,3 mg/ml	7.10	Stable in solution for weeks
Mag-SiO_2-Ca(17)	SiO_2 - Ca (high amount Ca) coated citric acid stabilized magnetite nanoparticles	Water	2,6 mg/ml	8.01	Tendency to partial precipitation

Table 7. Main characteristics of MNPs synthesized via co-precipitation methods using citric acid.

3.2.2 Nanoparticles: synthesis of MNPs

Magnetite nanoparticles (Mag) were produced by co-precipitation method [101] as explained in chapter 2.2.1. Aqueous solutions of $FeCl_2$ and $FeCl_3$ were mixed and pH was brought to basic values (about 10.0) by dropwise NH_4OH addition.

To improve water dispensability of the MNPs, a treatment of magnetite with citric acid was carried out by soaking nanoparticles in citric acid solution (0.05 M) for 24h and then exhaustively washed with water.

At the end of nanoparticles synthesis and fictionalization with citric acid, by adding tetraethyl orthosilicate (TEOS) (a silica precursor), with ethanol and water as solvent, an amorphous silica shell (Mag-SiO_2) was obtained.

To avoid the uncontrolled TEOS polymerization in the reaction media and to optimize the silica shell [107], the TEOS amount was reduced and concomitantly ethanol was added in the synthesis step, as described in the Stöber method [102].

To obtain calcium-silica magnetite NPs, calcium citrate was selected as precursor of Ca^{2+} ions and thus added in the synthesis process together with TEOS. Two different amounts of calcium citrate were tested to reach 99:1 (Mag-SiO_2-Ca(3)) and 95:5 ((Mag-SiO_2-Ca(17)) Si:Ca ratios, respectively.

3.2.3 Nanoparticle characterization

The size and shape of MNPs were characterized by means of transmission electron microscopy (TEM, Philips CM12, working at 120 kV operating voltage with a LaB6 filament), field emission scanning electron microscopy (FESEM - SUPRATM 40, Zeiss), scanning transmission electron microscopy (STEM-FESEM MERLIN Zeiss.) and energy dispersive x-ray spectroscopy (EDS) (Edax PV9800). Selected area electron diffraction (SAED) patterns were obtained for each sample to observe the morphology and structure.

FESEM micrographs of magnetic nanoparticles were captured using a SUPRATM 40, Zeiss field emission microscope operated at an excitation voltage of 10 kV. The elemental compositional study was investigated through energy dispersive spectroscopy (EDS) by using EDAX PV 9900 instrument coupled with STEM-FESEM.

A droplet of an aqueous dispersion of nanoparticles was placed on a copper grid for FESEM, TEM and STEM-FESEM sample preparation, allowed to dry, and examined under electron microscopy previously cited.

3.2.4 X-ray diffraction (XRD) analysis

XRD analysis of the synthesized magnetic nanoparticles was carried out in D8 Advance Powder X-ray diffractometer (Bruker, Germany) using CuKα radiation (λ = 1.54 nm). The XRD patterns were obtained between 2θ of 10° and 80° at a scanning rate of 4° min^{-1}. The obtained pattern from the XRD analysis was used to identify the crystalline structure of the samples.

3.2.5 Magnetic performance testing

A vibrating sample magnetometer (VSM-Lakeshore) was used to measure the magnetic hysteresis of naked iron-oxide nanoparticles and silica or silica-based glass layer core shell-type nanoparticles at 300 K under an applied field of ±15000 g.

3.2.6 Determination of sedimentation rates

Sedimentation tests were performed in order to evaluate the stability over time of iron oxide nanoparticles suspensions with and without different dispersants. The sedimentation rates of magnetic nanoparticles were measured by the change of optical absorbance with time, which can be related to the normalized nanoparticle concentration C/C_0, where C is the concentration in time t, and C_0 is the initial concentration (i.e. the initial absorbance at time 0). The sedimentation rate is then $d(C/C_0)/dt$ [108]. For relatively fast sedimentation conditions, the initial sedimentation rate was estimated from the decrease in the normalized particle concentration within the first 90 min, while for slower sedimentation conditions (C/C_0 decrease less than 80% in 600 min), all data within 50 hours were included. The following dispersants with the same concentration of MNPs (10 μg/ml) were used: citric acid, PEI (polyethylenimine), Dispex (polyacrylate dispersant) and Dolapix (deflocculant polycarboxylic acid). The tests were performed with and without the presence under the samples of a magnet for a period of time of 50 h.

3.2.7 AFM/MFM

AFM/MFM images of magnetic nanoparticles were acquired at room temperature with a Shimadzu Scanning Probe Microscope (SPM-9600). Tapping-mode was used to obtain the sample surfaces topography and lift-mode was used for the magnetic phase. In lift-mode, the tip-sample distance varied by tens to hundreds of nanometres. Magnetic force microscopy (MFM) images were obtained by allowing the cobalt coated magnetic tip (oscillating at its resonance frequency) to scan the air dried magnetic nanoparticles at the start height of 20 nm in 5 μm × 5 μm area using the MFM facility of Nanoscope IV.

3.2.8 Zeta potential

Zeta potential of nanoparticles was detected using a laser-scattering method (Zetasizer Nano ZS90; Malvern Instruments, Malvern, UK). The nanodispersions were diluted 100-fold with deionized water before testing. The measurement was repeated three times per sample at room temperature and the values reported as the average ± SD. Zeta potential was measured to different acid and basic pH values to evaluate the colloidal properties of MNPs by varying the isoelectric point of MNPs solutions.

Zeta potential can be related to the stability of colloidal dispersions. The relationship between the zeta potential value of the solution measured and the colloidal stability are indicated in Table 8 [109].

Zeta potential [mV]	**Stability behavior of the colloid**
from 0 to ±5,	Rapid coagulation or flocculation
from ±10 to ±30	Incipient instability
from ±30 to ±40	Moderate stability
from ±40 to ±60	Good stability
more than ±61	Excellent stability

Table 8. Relationship between the value of Zeta Potential measured and colloidal stability of the solution [109].

3.2.9 Cell culture

As previously described in the paragraph 2.2.2.

3.2.10 Not direct contact cytotoxicity evaluation of MNPs

As previously described in the paragraph 2.2.3.

3.2.11 Direct static contact cytotoxicity evaluation of MNPs

Direct static contact cytotoxicity evaluation of MNPs was done according to ISO standard 10993-5: 2009. Direct contact cytotoxicity was evaluated on MS1 cells for the following MNPs: Mag, Mag-SiO_2, Mag-SiO_2-Ca(3) and Mag-SiO_2-Ca(17). The cells were seeded in 24-well plates (1.6×10^4 cells per well) in DMEM medium and cultured for 24 h at 37°C in 5% CO_2 atmosphere-controlled incubator. After 24 hours the medium was substituted with a new one obtained by adding MNPs to DMEM to obtain the following concentrations: 10 μg/ml, 20 μg/ml, 40 μg/ml and 80 μg/ml (w/v). MS1 endothelial cells cultivated onto polystyrene wells in presence of DMEM additioned with 2 mM L-glutamine, 10% FBS and 1% antibiotics/antimycotics were used as control. Afterwards, cell viability was evaluated after 24, 48 and 72 hours using MTT assay, as above described for the indirect cytocompatibility assay. The viability of controls were considered as 100% viability. Even for direct contact cytotoxicity evaluation the percentages of cell viability observed in MTT assay were validated by Trypan Blue (TB) staining. Furthermore, cells morphology was visually investigated at each experimental time by light microscopy (Leica AF 6500, Leica Microsystems) at 20x magnification.

3.2.12 Lactate dehydrogenase assay

The effect of the NPs on the integrity of the cell membrane was assayed using a LDH Cytotoxicity Assay Kit (Gesan group). The assay was performed as per the manufacturer's instructions. LDH is released by cells in response to damage or loss of integrity of cell membrane and is a cellular toxicity indicator. Briefly, 1.6×10^4 cells/well were seeded in 24-well plates and treated with the following concentrations of MNPs: 10 μg/ml, 20 μg/ml, 40 μg/ml and 80 μg/ml (w/v) for 24, 48 and 72 hours. Untreated cells were taken as the negative control and cells treated with lysis buffer were taken as the high control (total LDH in the cell). As a positive control, 1 μL of LDH was used to validate the assay. Following the incubation with NPs, the well plates were centrifuged at 600 g for 10 minutes and 10 μL of the medium was transferred to a fresh 96-well plate. The medium was then incubated with 100 μL of LDH reaction mixture for 15 minutes at room temperature and the absorbance was measured at 450 nm using the microplate reader (Victor X4 - PerkinElmer) with the reference wavelength at 650 nm. LDH was quantified using the following formula:

$$LDH\% = \frac{\text{Test} - \text{low control}}{\text{High control} - \text{low control}} \times 100$$

in which “low control” was the cells without any treatment and “high control” was the cells treated with lysis buffer (total LDH).

3.2.13 Cells morphology evaluation by fluorescent microscopy

MNPs influence on cell morphology and cytoskeleton was evaluated by immunofluorescence (IF) staining. MS1 cells morphology in contact with magnetic nanoparticles (40 μg/ml for 72 h) was investigated by immunofluorescence (IF) staining. Briefly, after direct contact (72 h) with MNPs, cells were gently washed with PBS and fixed for 5 min with 4% formaldehyde-3% sucrose solution (in PBS) at RT. Afterwards, samples were washed three times with PBS and stained to visualize F-actins and nucleic acids by phalloidin (Molecular Probes Inc.) and 49,6-diamidino-2- phenylindole (DAPI, Molecular Probes Inc.). Fluorescence images were collected with a fluorescent microscope (Leica AF 1500, Leica Instruments).

3.2.14 Statistical analyses

All statistical analyses were performed using IBM Statistical Package for Social Sciences v. 20 software (SPSS - IBM). Data were expressed as means ± standard deviations. The results were analyzed using one way analysis of variance (ANOVA) followed by Scheffe’s test, and P values less than 0.05 were considered to be statistically significant.

3.3 Results

3.3.1 Physical-chemical characterization of MNPs

Small (10-15 nm) Mag NPs were obtained as observable with Field Emission Scanning Electron Microscopy (FESEM) (Figure 15a). X-ray diffraction (XRD) patterns confirmed that they consisted of magnetite/maghemite (Figure 15b). Spherical silica coated magnetite nanoparticles, with an evident core-shell structure were obtained, as observed by TEM and scanning transmission electron microscope (STEM) (Figure 16).

A good dispersion was reached for magnetite (Fig. 17a), and less for SiO_2-coated magnetite NPs (Figure 17b). Selected area electron diffraction (SAED) patterns detected signals of Mag NPs and Mag-SiO_2 NPs (Figure 18).

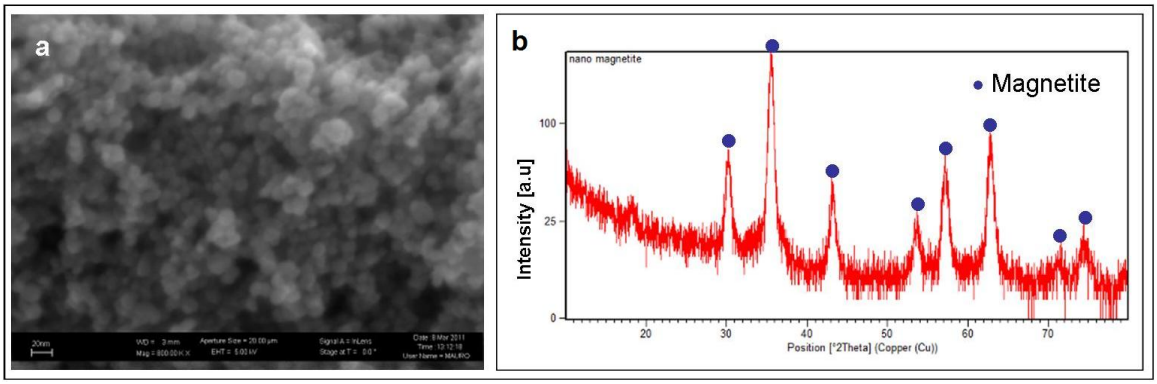

Figure 15. Magnetite obtained by co-precipitation a) FESEM observation, b) XRD analysis.

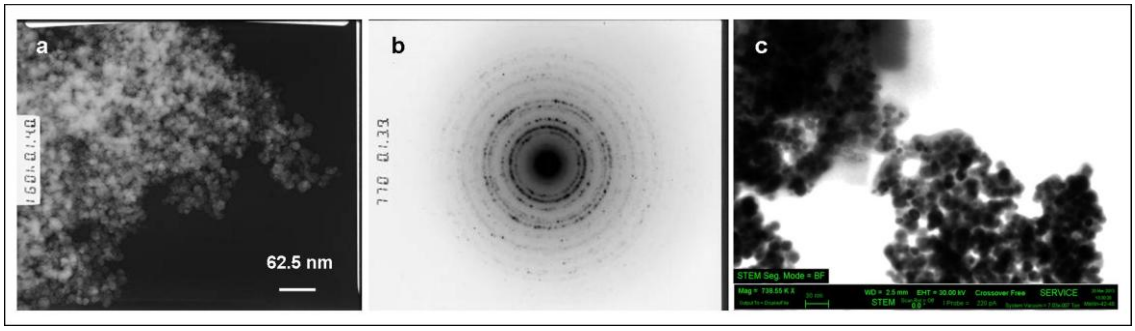

Figure 16. TEM image (a), SAED (b) and STEM (c) of optimized SiO_2 coated magnetite nanoparticles.

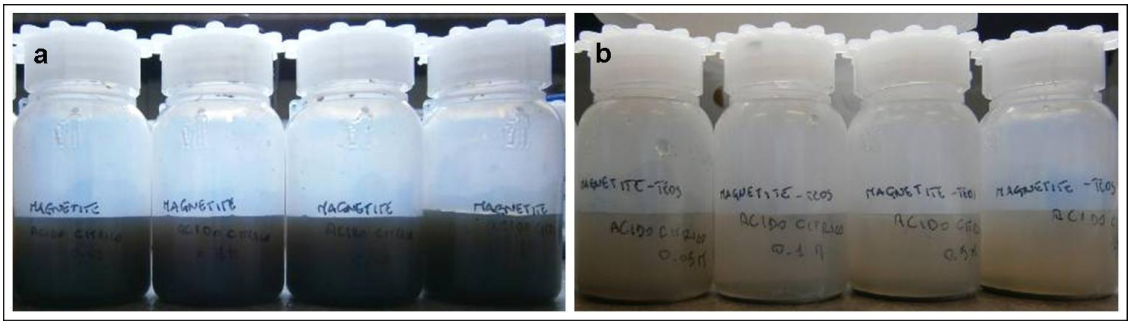

Figure 17. a) citric acid treated magnetite nanoparticles, b) citric acid treated SiO_2-coated magnetite nanoparticles.

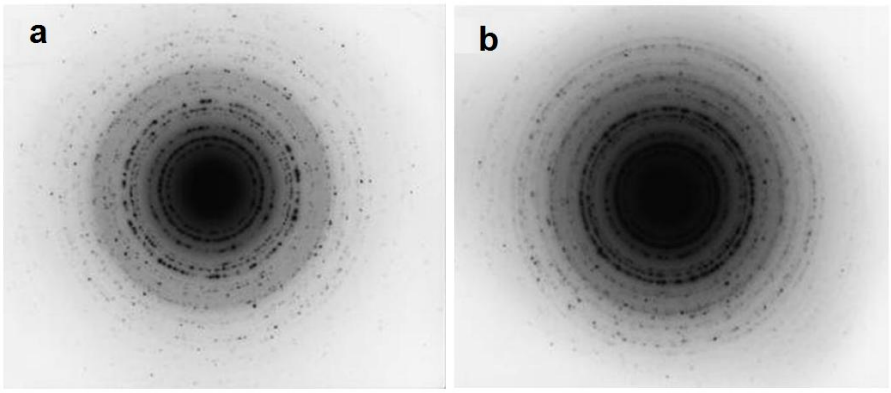

Figure 18. SAED patterns of Mag NPs (a) and Mag-SiO_2 NPs (b).

3.3.2 Mag-SiO_2-Ca NPs characterization

In view of the fact that MNPs should be functionalized, their surface reactivity was enhanced. This aim was approached by adding calcium ions to their surface. Mag-SiO_2-Ca nanoparticles (10-15 nm) with calcium and with a good dispersion in water were obtained. An effective enrichment in Ca^{2+} was verified for both formulations with an increased calcium content, according to expectancies by means of compositional analysis (**Figure 19**).

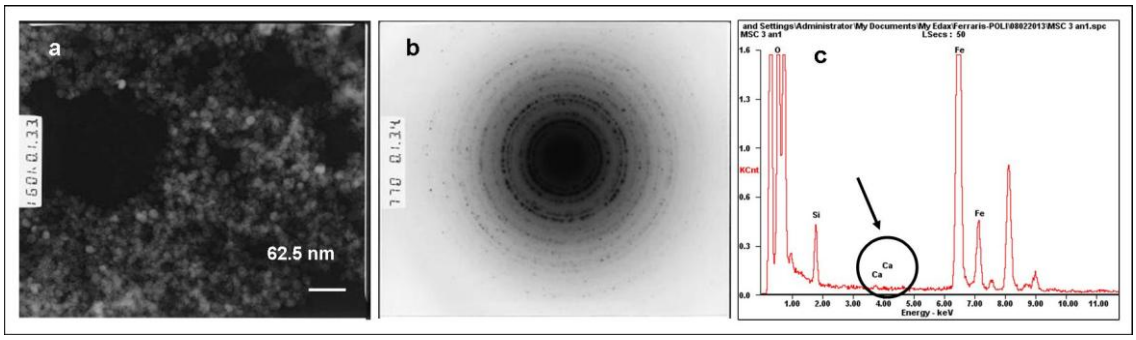

Figure 19. TEM image (a), SAED patterns (b) and EDS spectrum (c) of Mag-SiO_2-Ca nanoparticles.

3.3.3 Morphological observations

TEM showed that the electron density of the magnetic particles was relatively high, and that the particles, which were spherical and partially agglomerated (**Figure 20**). Mag, Mag-SiO_2, Mag-SiO_2-Ca(3) and Mag-SiO_2-Ca(17) NPs obtained after citric acid (CA) treatment were analyzed for their size at transmission electron microscope (TEM) and shown to be small (10-15 nm) and spherical with a shell (silica) with a thickness of 1-2 nm (**Figure 20**). EDS analysis confirmed the composition of the nanoparticles through a rough estimate (data not shown).

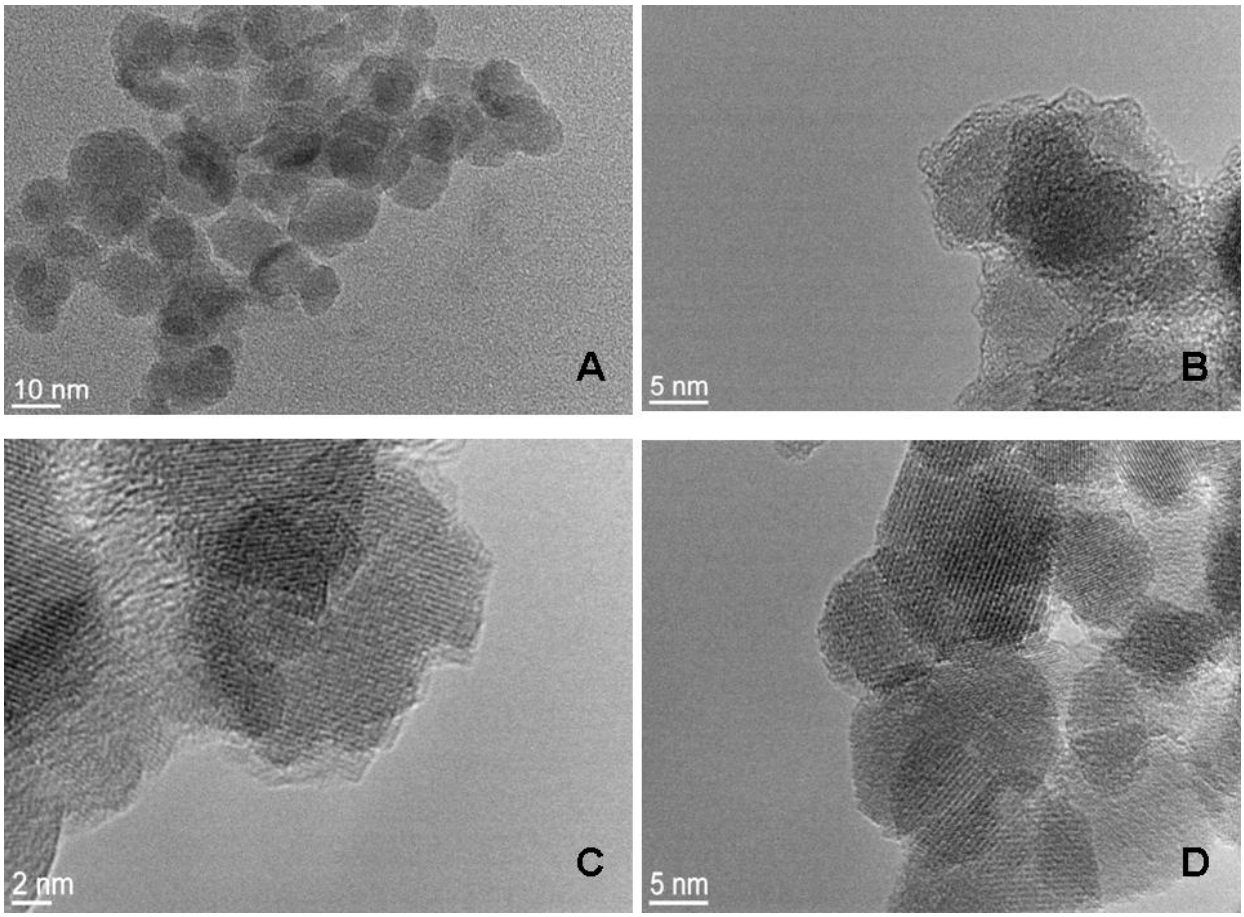

Figure 20. TEM images of magnetic nanoparticles: Mag (A), Mag-SiO_2 (B), Mag-SiO_2-Ca3 (C) and Mag-SiO_2-Ca17 (D).

3.3.4 Magnetic performance

A vibrating sample magnetometer was used to measure the magnetic hysteresis of the magnetic nanoparticles at 300 K in an applied field of ± 15000 g. The results showed that the saturated magnetic intensity of Mag NPs and Mag-SiO_2 NPs were ± 20.2 emu/g and ± 5.3 emu/g respectively. Instead, the saturated magnetic intensities were ± 7.3 emu/g and ± 7.4 emu/g for Mag-SiO_2-Ca(3) NPs and Mag-SiO_2-Ca(17) NPs respectively (**Figure 21**). The four lines of the hysteresis loop overlapped, ie, no coercivity was noted, indicating that the magnetic nanoparticles prepared were superparamagnetic.

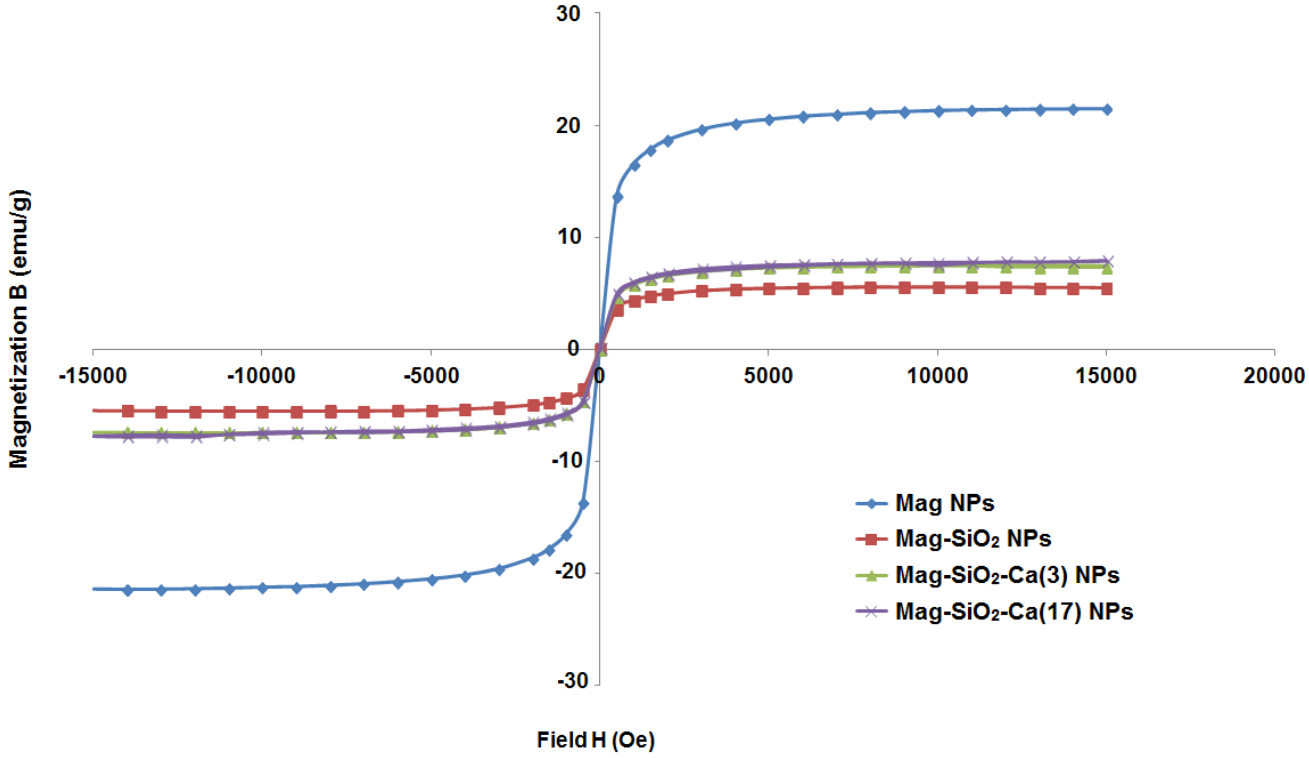

Figure 21. Measurement of the magnetic hysteresis of Mag, Mag-SiO_2, Mag-SiO_2-Ca(3), Mag-SiO_2-Ca(17) NPs - Magnetic performance.

3.3.5 AFM/MFM

MFM images of magnetic nanoparticles along with its AFM image counterpart in 5 μm × 5 μm scan area were shown in the **Figure 22**. The image clearly indicated the core structure of magnetic nanoparticles. The dark contrasts appearing in the MFM image are the signals due to presence of iron oxide MNPs. Consequently, it is observed a high frequency change (up to 125 Hz) in the vertically oscillating magnetic tip nearby the surfaces of magnetic nanoparticles. The sample presents a relative constant magnetism all over the scanned MNPs surface regardless of the sample's corresponding height. The relative intensity of the magnetic phase has a scale of 1°, indicating a weak detected field. The phase images shown in the right side of Figures present a magnetic response from the sample induced by the magnetization of the tip. The results here cannot be considered to be quantitative measurements because the principle of magnetic force microscopy (MFM) involves measuring a phase change in the resonance frequency spectrum of the (magnetized) cantilever, compared to the original resonance frequency while scanning different regions of the sample.

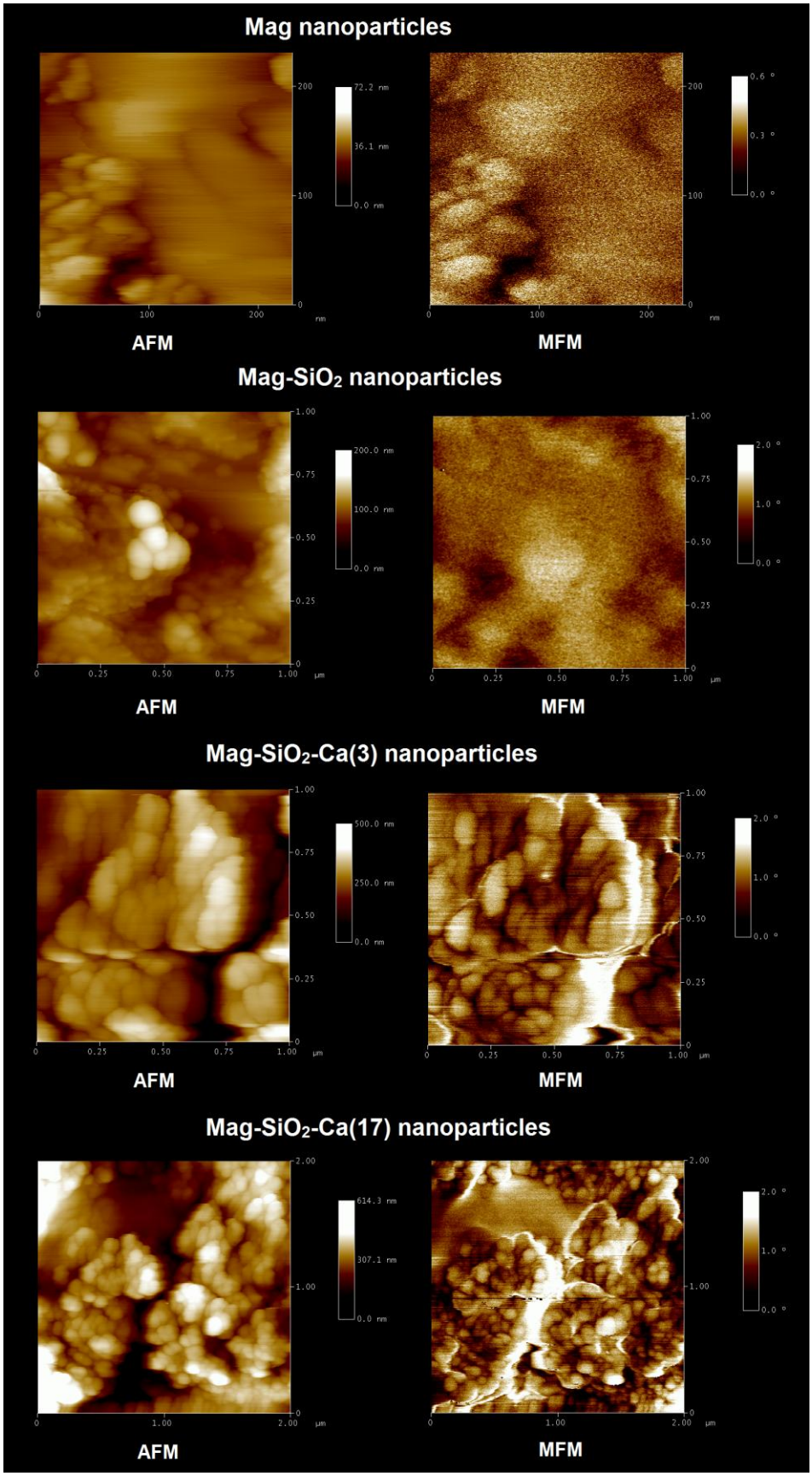

Figure 22. Representative AFM/MFM images of Mag, Mag-SiO_2, Mag-SiO_2-Ca(3) and Mag-SiO_2-Ca(17) NPs with their respective size distributions.

3.3.6 Zeta potential evaluation

Zeta-potential measurement is considered as a key parameter for providing an insight into the colloidal stability of the resulting magnetic nanoparticles. The zeta-potential results are shown in Fig. 23. The zeta potential of suspension for Mag NPs, Mag-SiO_2 NPs, Mag-SiO_2-Ca(3) NPs and Mag-SiO_2-Ca(17) NPs is - 32.46 mV, - 29.88 mV, - 42.21 mV and - 21.74 mV, respectively (Table 9). Zeta potential measurements revealed an incipient colloidal instability for Mag-SiO_2 NPs and Mag-SiO_2-Ca(17) NPs, a moderate colloidal stability for Mag NPs and a good colloidal stability for Mag-SiO_2-Ca(3) NPs.

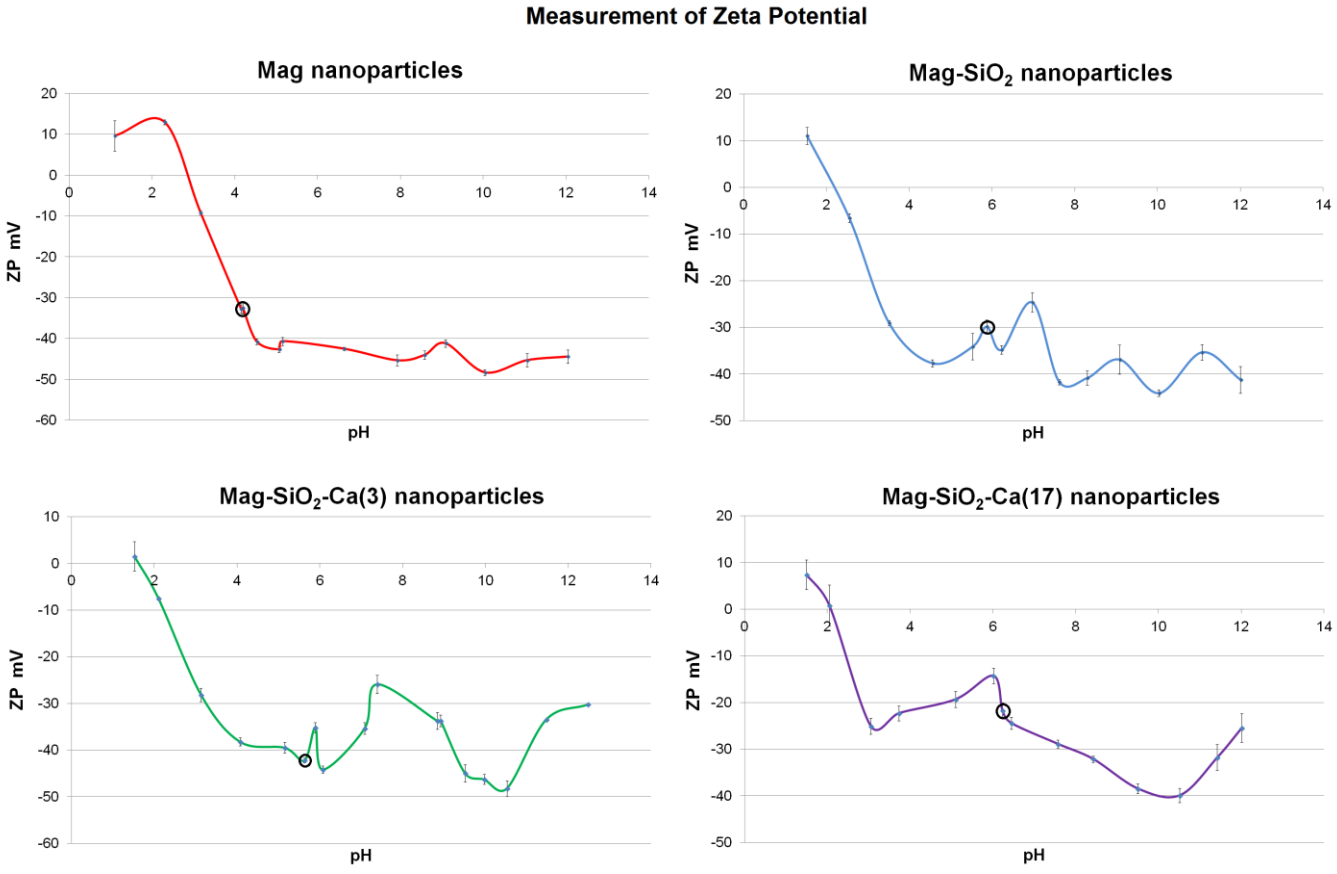

Figure 23. Zeta Potential measurements of MNPs. Data are shown as the mean ± standard deviation (n = 3). The black circles indicate starting pH of the solutions with MNPs.

Sample	Starting pH	ZP (mV)	Stability behaviour of the colloid
Mag NPs	4.19	- 32.46 ± 1.61 mV	Moderate stability
Mag-SiO_2 NPs	5.87	- 29.88 ± 1.42 mV	Incipient instability
Mag-SiO_2-Ca(3) NPs	5.63	- 42.21 ± 0.56 mV	Good stability
Mag-SiO_2-Ca(17) NPs	6.23	- 21.74 ± 1.61 mV	Incipient instability

Table 9. Zeta Potential measurements of MNPs. Data are shown as the mean ± standard deviation (n = 3).

3.3.7 Sedimentation tests

The sedimentation test showed the evolution of nanoparticles over a period of time of 48 h with and without the presence under the nanoparticles of a magnet. In the sedimentation test of MNPs without the presence of a magnet surnatant thickness decreased over time, while the thickness of the sediment increased (**Figure 24**). The suspension of MNPs with PEI was very unstable because the precipitation of the colloid was quicker even compared to the pure magnetite suspension. This was due because at pH around 8 this suspension of MNPs with PEI was close to isoelectric point and nanoparticles had not almost any surface charge. Samples with Dispex and Dolapix were very stable and only after one day they showed a sediment of 1 mm of thickness. Sample with citric acid did not show any sediment during the test time. This indicated high colloidal stability of the suspension of MNPs with citric acid (**Figure 24**). Test performed with the presence of a magnet under the samples showed a similar behavior, only faster. In fact with the presence of a magnet the suspension of MNPs with PEI was again the most unstable, because nanoparticles rapidly (few minutes) sedimented on the bottom of the tube and the surnatant was very clear. A similar behavior was also visible in the suspension of pure magnetite, dolapix and dispex, but they reached the 2 mm of sediment thickness in a slower way. In this case even the suspension with citric acid showed a little amount of sediment due to the presence of the magnet, but it was still the most stable suspension (**Figure 25**). The thickness of the sediment was different between the first and second test because the presence of the magnet made the sediment more compact, thus the thickness was lower in the second test.

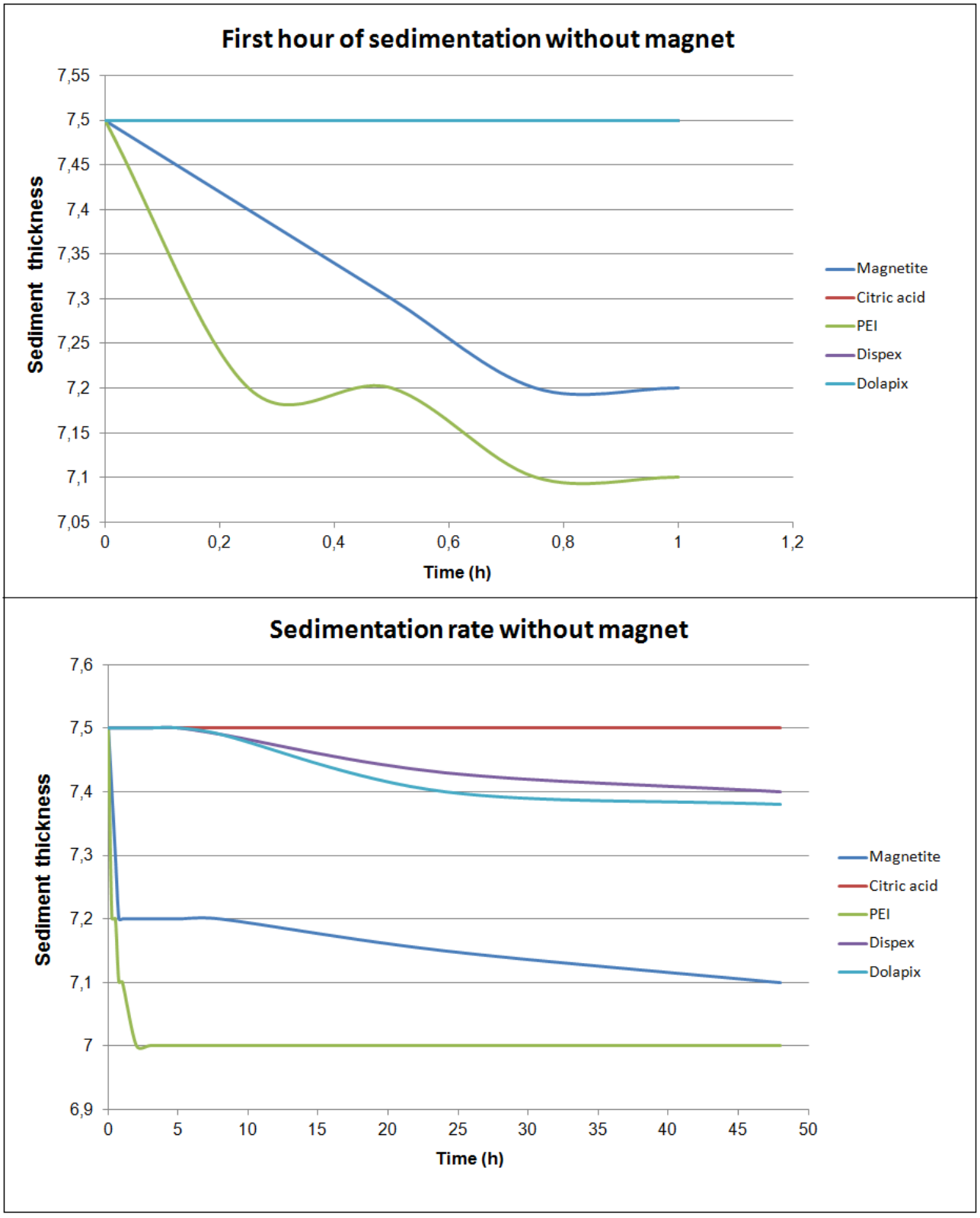

Figure 24. Sedimentation test of magnetic nanoparticles without magnet.

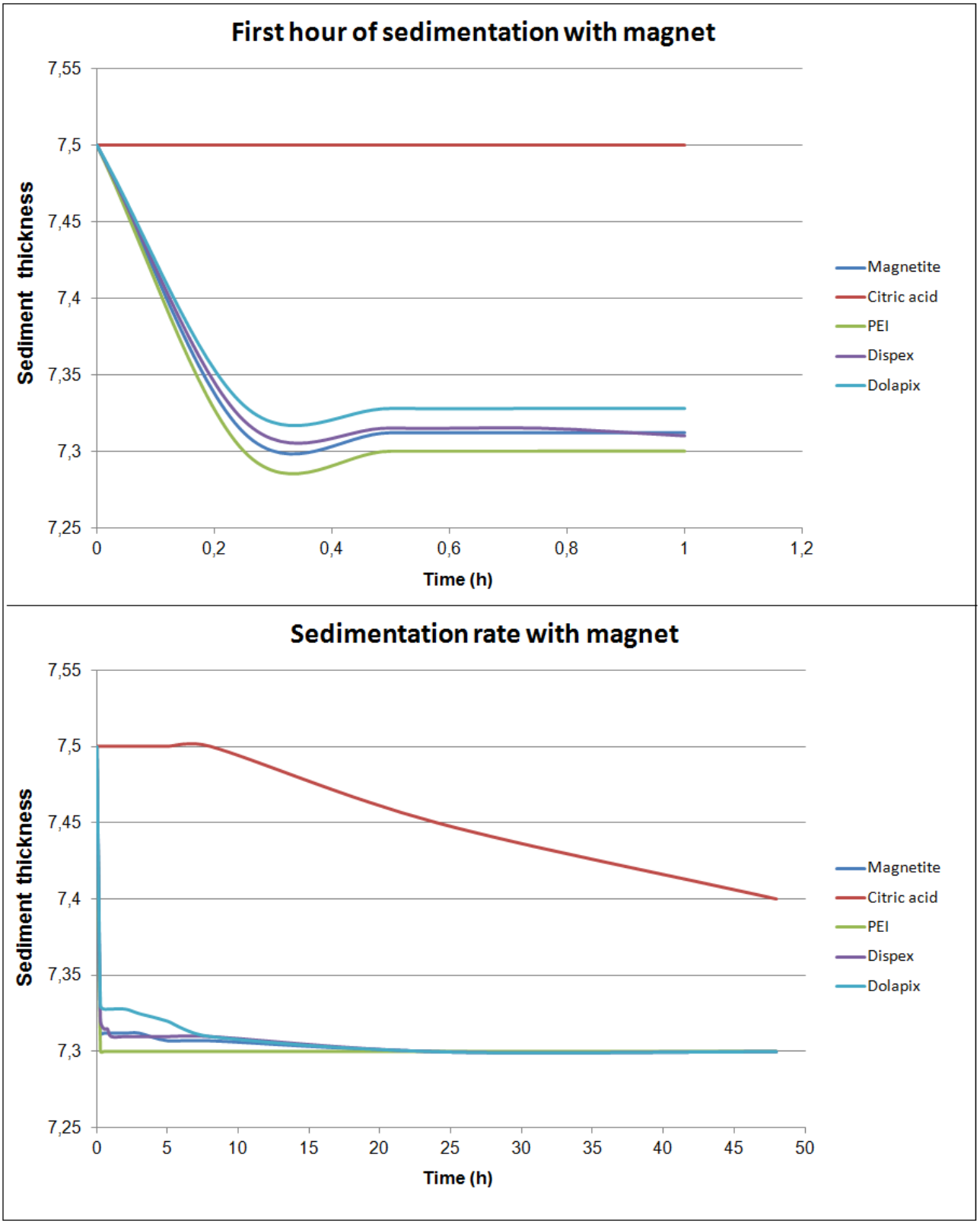

Figure 25. Sedimentation test of magnetic nanoparticles with magnet.

3.3.8 Not direct contact cytotoxicity evaluation of second synthesis of MNPs

Cell viability results were evaluated with MTT assay (**Figures 26-27**). The percentages of cell viability for not direct contact cytotoxicity evaluation of 24 h were in a range between 90% and 95% for Mag NPs leaching solution (**Fig. 26**). Cell viability after contact with Mag-SiO_2 NPs leaching solution (**Fig. 26**) was in a range between 92% and 97%. Moreover, the percentages of cell viability were in a range between 91% and 97% for Mag-SiO_2-Ca(3) NPs leaching solution and between 87% and 93% for Mag-SiO_2-Ca(17) NPs leaching solution respectively (**Fig. 26**).
Not direct contact cytotoxicity evaluation of 72 h showed a cell viability in range between 88% and 94% for Mag NPs leaching solution (**Fig. 27**). Cell viability after contact with Mag-SiO_2 NPs leaching solution was in a range between 89% and 95% (**Fig. 27**). Moreover, cell viability after contact with Mag-SiO_2-Ca(3) NPs leaching solution was in a range between 88% and 94% (**Fig. 27**). Finally, cell viability after contact with Mag-SiO_2-Ca(17) NPs leaching solution was in a range between 85% and 91% (**Fig. 27**). The results of cytotoxicity evaluation for not direct contact of culture medium DMEM with MNPs using ISO 10993 standards showed a cell viability comparable to control. Trypan blue assay validated the results obtained with MTT assay (**Tables 10 and 11**). Differences were statistically significant at 24, 48 and 72 h time-points ($p < 0.05$).

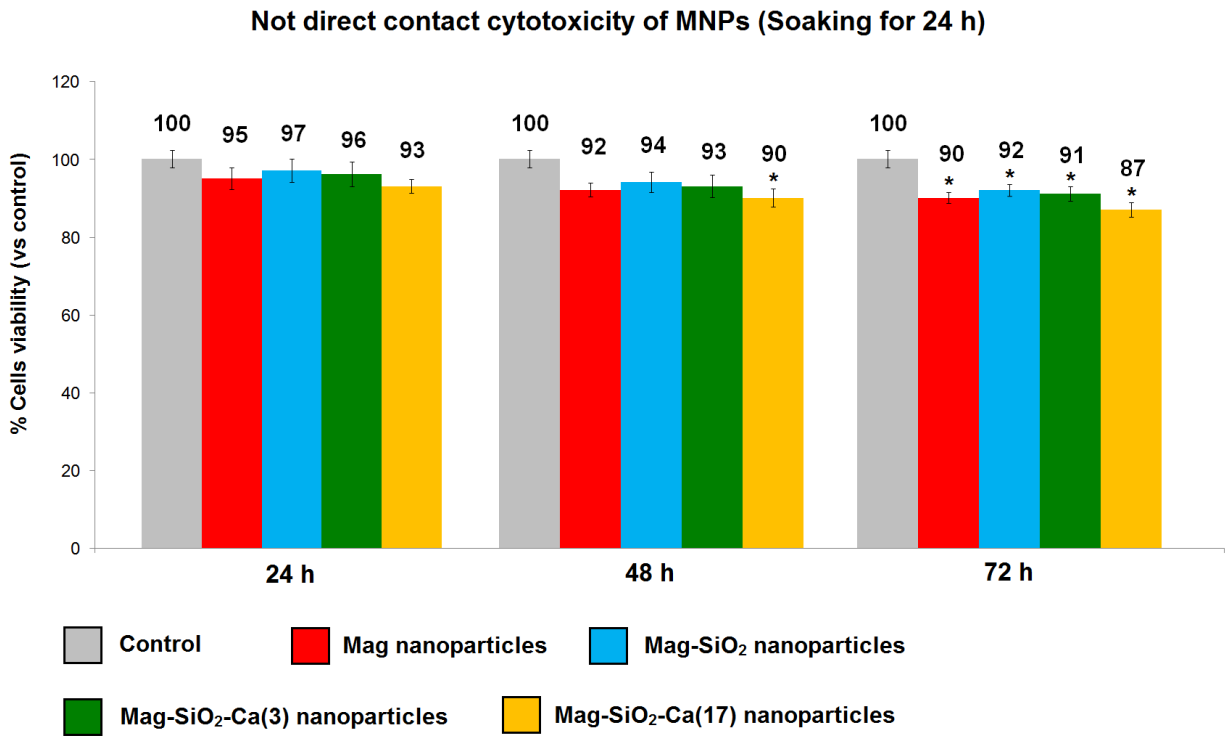

Figure 26. Not direct contact cytotoxicity evaluation of MNPs using murine endothelial cells (MS1 cells) and eluates (24 h of soaking); MTT assay. Data are shown as the mean ± standard deviation (n = 4). *P < 0.05 compared with control.

Not direct contact cytotoxicity (37°C for 24 h) - Percentage of TB positive MS1 cells

Samples	24 h	48 h	72 h
Mag	4.8 ± 0.7	8.0 ± 0.9	9.6 ± 0.8*
Mag-SiO_2	3.2 ± 0.4	5.5 ± 0.5	8.9 ± 1.0*
Mag-SiO_2-Ca(3)	3.9 ± 0.5	6.8 ± 0.7	7.8 ± 0.7*
Mag-SiO_2-Ca(17)	6.5 ± 0.6	9.7 ± 0.8*	13.2 ± 0.9*

Table 10. Trypan blue exclusion test. MS1 cell mortality after not direct contact with MNPs (37°C for 24 h). Data are shown as the mean ± standard deviation (n = 4). *P < 0.05 compared with control.

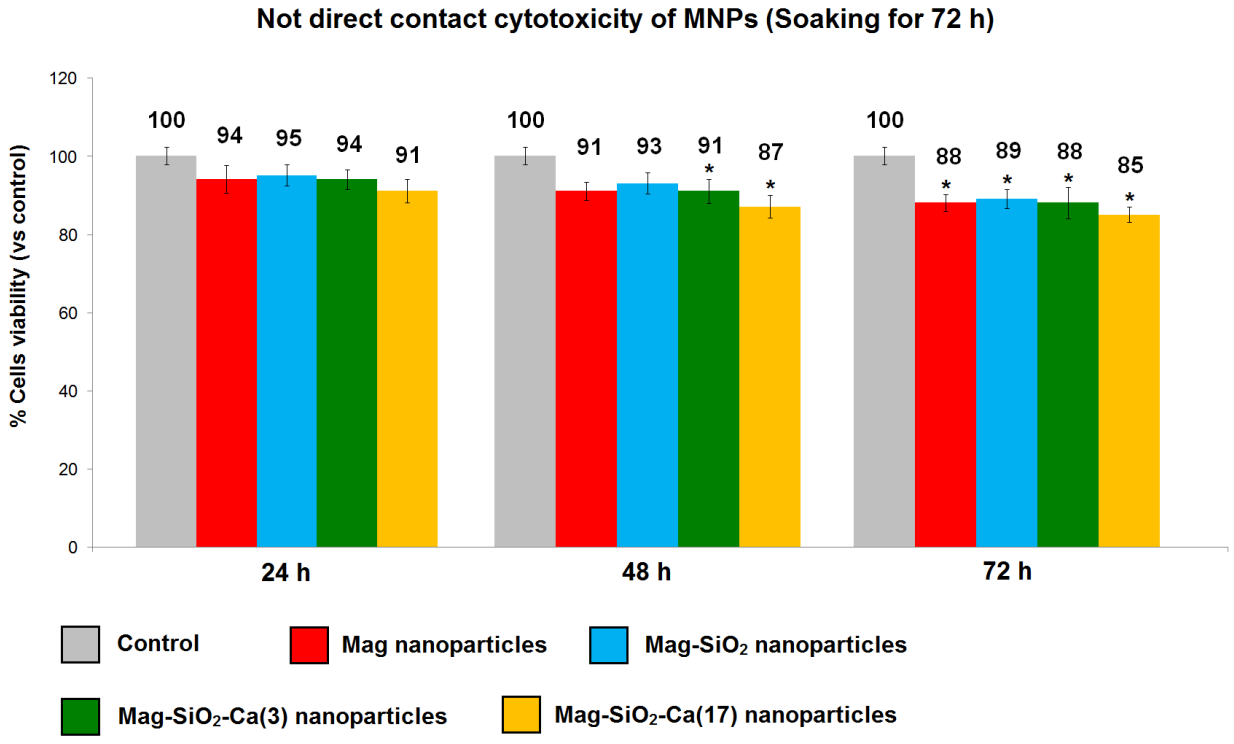

Figure 27. Not direct contact cytotoxicity evaluation of MNPs using murine endothelial cells (MS1 cells) and eluates (72 h of soaking). Data are shown as the mean ± standard deviation (n = 4). *P < 0.05 compared with control.

Not direct contact cytotoxicity (37°C for 72 h) - Percentage of TB positive MS1 cells			
Samples	24 h	48 h	72 h
Mag	6.1 ± 0.7	8.7 ± 0.8	11.8 ± 0.8*
Mag-SiO_2	4.9 ± 0.5	6.8 ± 1.0	10.9 ± 1.1*
Mag-SiO_2-Ca(3)	5.8 ± 0.9	9.4 ± 0.7	12.7 ± 0.9*
Mag-SiO_2-Ca(17)	9.3 ± 1.2	12.1 ± 1.1*	15.2 ± 1.0*

Table 11. Trypan blue exclusion test. MS1 cell mortality after not direct contact with MNPs (37°C for 72 h). Data are shown as the mean ± standard deviation (n = 4). *P < 0.05 compared with control.

3.3.9 Direct static contact cytotoxicity evaluation of second synthesis of MNPs

In direct static contact cytotoxicity tests, MS1 endothelial cells showed a cell viability ranging between 80% and 97% for Mag NPs, 86% and 95% for Mag-SiO_2 NPs, 59% and 85% for Mag-SiO_2-Ca(3) NPs, 45% and 82% for Mag-SiO_2-Ca(17) NPs (**Figures 28-30**). Calcium-silica MNPs displayed a higher toxicity respect to calcium-free MNPs on MS1 cells. MS1 cells viability after contact with calcium-silica MNPs was dose-dependent and time-dependent. Moreover, the amount of Ca^{2+} ions incorporated in the nanoparticles could have played a role on the cytocompatibility of the MNPs, since at higher ratios a lower cell survival was observed ($p < 0.05$). Trypan blue assay validated the results obtained using MTT assay (**Tables 12-14**). Data were considered statistically significant ($p < 0.05$). No cellular morphological alterations were observed after direct contact with MNPs (**Fig. 31-33**).

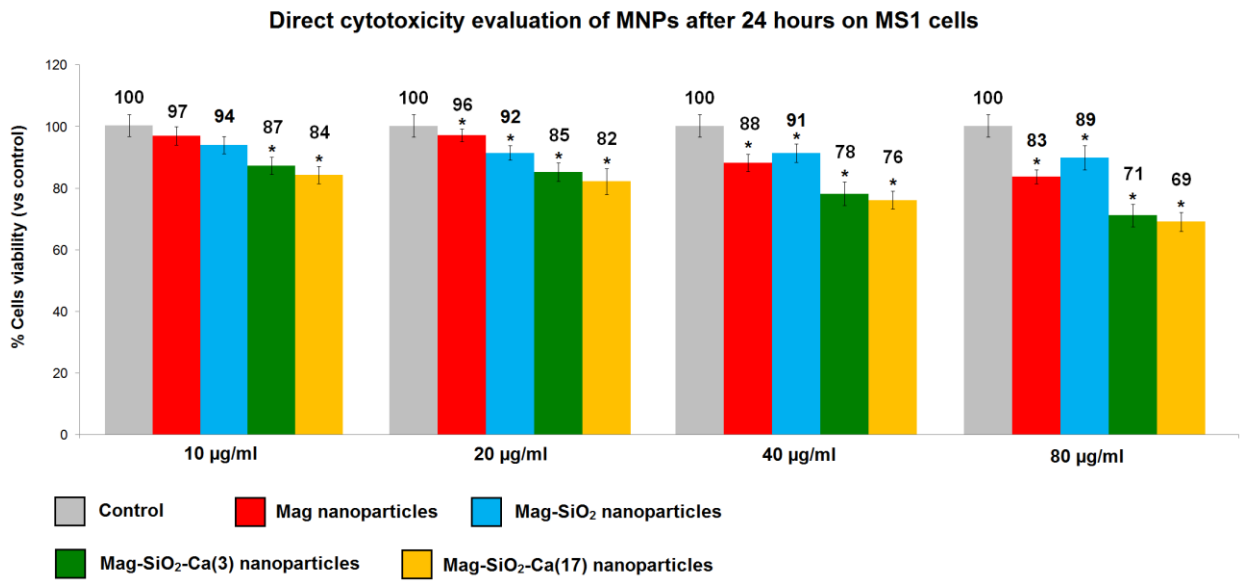

Figure 28. Cytocompatibility assessment of MS1 cells after 24 hours in contact with different concentration of MNPs. Data are shown as the mean ± standard deviation (n = 4). *P < 0.05 compared with control samples.

Percentage of TB positive MS1 cells after 24 hours of contact with MNPs

Sample	10 µg/ml	20 µg/ml	40 µg/ml	80 µg/ml
Mag NPs	3.2 ± 0.5	4.6 ± 0.7	11.7 ± 0.8*	16.9 ± 0.9*
Mag-SiO_2 NPs	6.3 ± 0.8	8.4 ± 0.6	9.2 ± 0.6*	11.2 ± 1.0*
Mag-SiO_2-Ca(3) NPs	13.5 ± 1.0*	15.0 ± 0.9*	22.1 ± 1.2*	28.8 ± 0.7*
Mag-SiO_2-Ca(17) NPs	15.8 ± 1.2*	17.8 ± 1.1*	24.4 ± 1.3*	31.3 ± 1.1*

Table 12. Trypan blue exclusion test. MS1 cell mortality after contact of 24 hours with nanoparticles. Data are shown as the mean ± standard deviation (n = 4). *P < 0.05 compared with control samples.

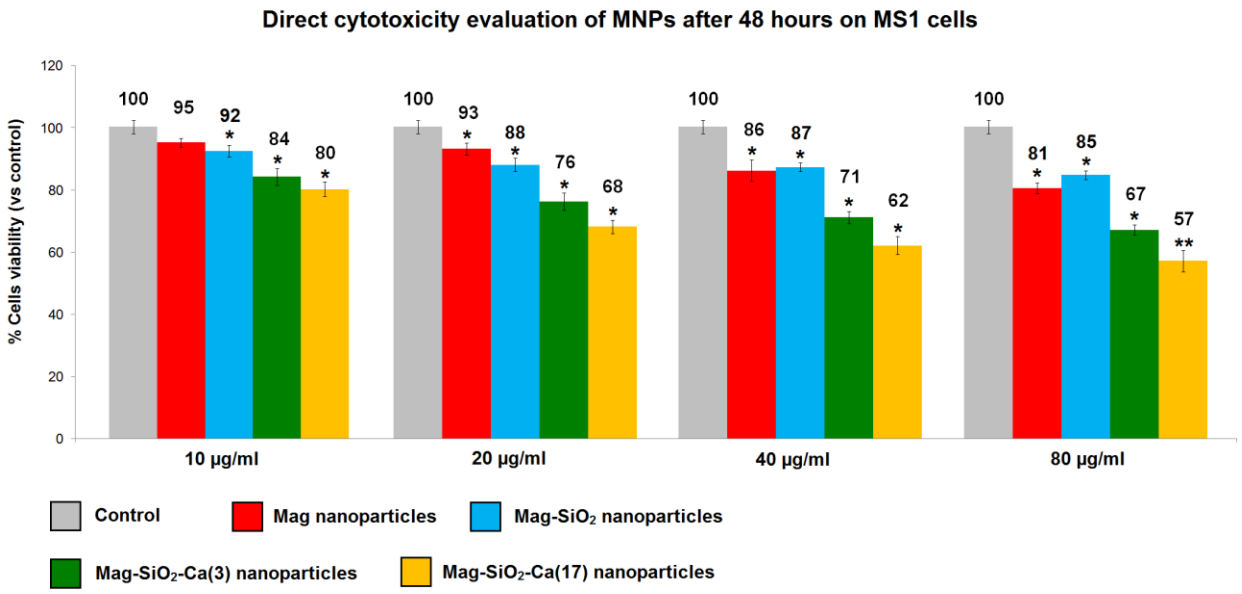

Figure 29. Cytocompatibility assessment of MS1 cells after 48 hours in contact with different concentration of MNPs. Data are shown as the mean ± standard deviation (n = 4). *P < 0.05 compared with control. **P < 0.05 compared with Mag-SiO_2-Ca(3) and control samples.

Percentage of TB positive MS1 cells after 48 hours of contact with MNPs

Sample	10 µg/ml	20 µg/ml	40 µg/ml	80 µg/ml
Mag NPs	5.2 ± 0.6	7.4 ± 0.9	14.3 ± 1.2*	19.2 ± 0.7*
Mag- SiO_2 NPs	8.2 ± 0.9	12.2 ± 0.5*	12.8 ± 0.7*	15.3 ± 1.2*
Mag-SiO_2-Ca(3) NPs	16.5 ± 1.3*	24.3 ± 1.1*	29.3 ± 0.8*	33.1 ± 0.9*
Mag-SiO_2-Ca(17) NPs	19.7 ± 0.9*	31.8 ± 1.4*	38.4 ± 1.2*	42.8 ± 1.3*

Table 13. Trypan blue exclusion test. MS1 cell mortality after contact of 48 hours with nanoparticles. Data are shown as the mean ± standard deviation (n = 4). *P < 0.05 compared with control samples.

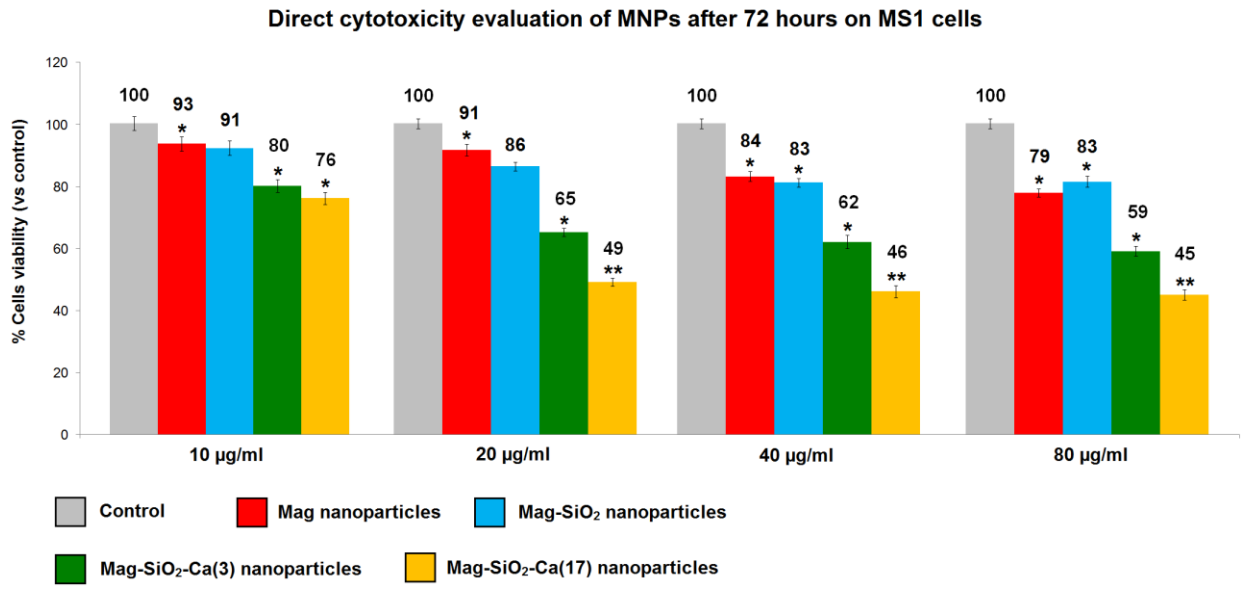

Figure 30. Cytocompatibility assessment of MS1 cells after 72 hours in contact with different concentration of MNPs. Data are shown as the mean ± standard deviation (n = 4). *P < 0.05 compared with control samples. **P < 0.05 compared with Mag-SiO_2-Ca(3) and control samples.

Percentage of TB positive MS1 cells after 72 hours of contact with MNPs

Sample	10 µg/ml	20 µg/ml	40 µg/ml	80 µg/ml
Mag NPs	7.2 ± 0.9	9.2 ± 1.1	16.5 ± 0.6*	21.4 ± 0.8*
Mag- SiO_2 NPs	9.1 ± 0.7	14.2 ± 0.8*	17.2 ± 0.8*	17.4 ± 1.0*
Mag-SiO_2-Ca(3) NPs	20.4 ± 1.1*	35.4 ± 1.2*	38.1 ± 1.2*	41.6 ± 1.2*
Mag-SiO_2-Ca(17) NPs	24.2 ± 0.6*	50.7 ± 1.0*	54.2 ± 0.9*	55.8 ± 0.9*

Table 14. Trypan blue exclusion test. MS1 cell mortality after contact of 72 hours with nanoparticles. Data are shown as the mean ± standard deviation (n = 4). *P < 0.05 compared with control samples.

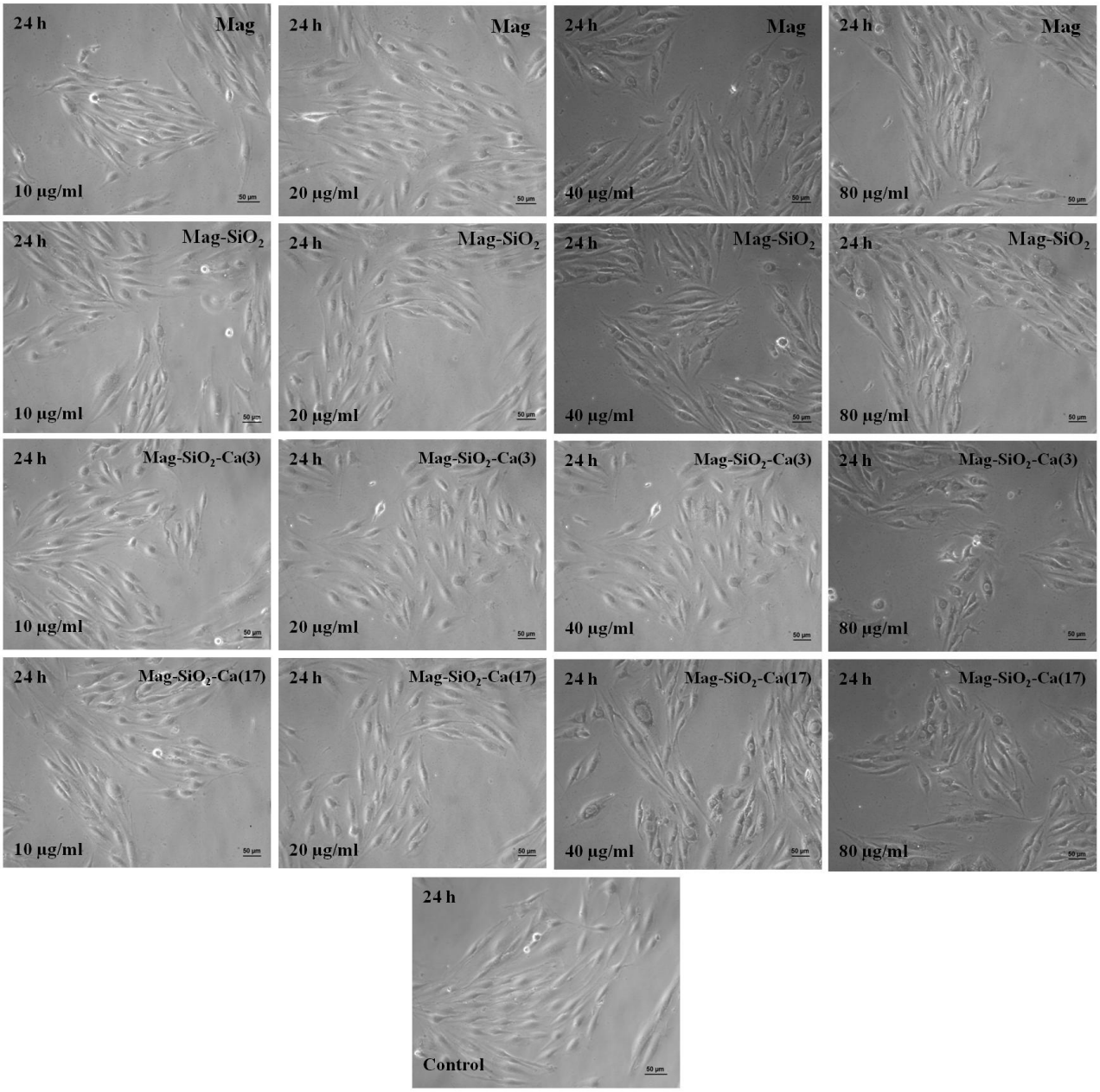

Figure 31. Optical microscopic images of endothelial cells (MS1 cells) after direct contact with MNPs (10-80 µg/ml) for 24 hours. Magnification: 20x, bar scale = 50 µm. No effects are observed on cell morphological features.

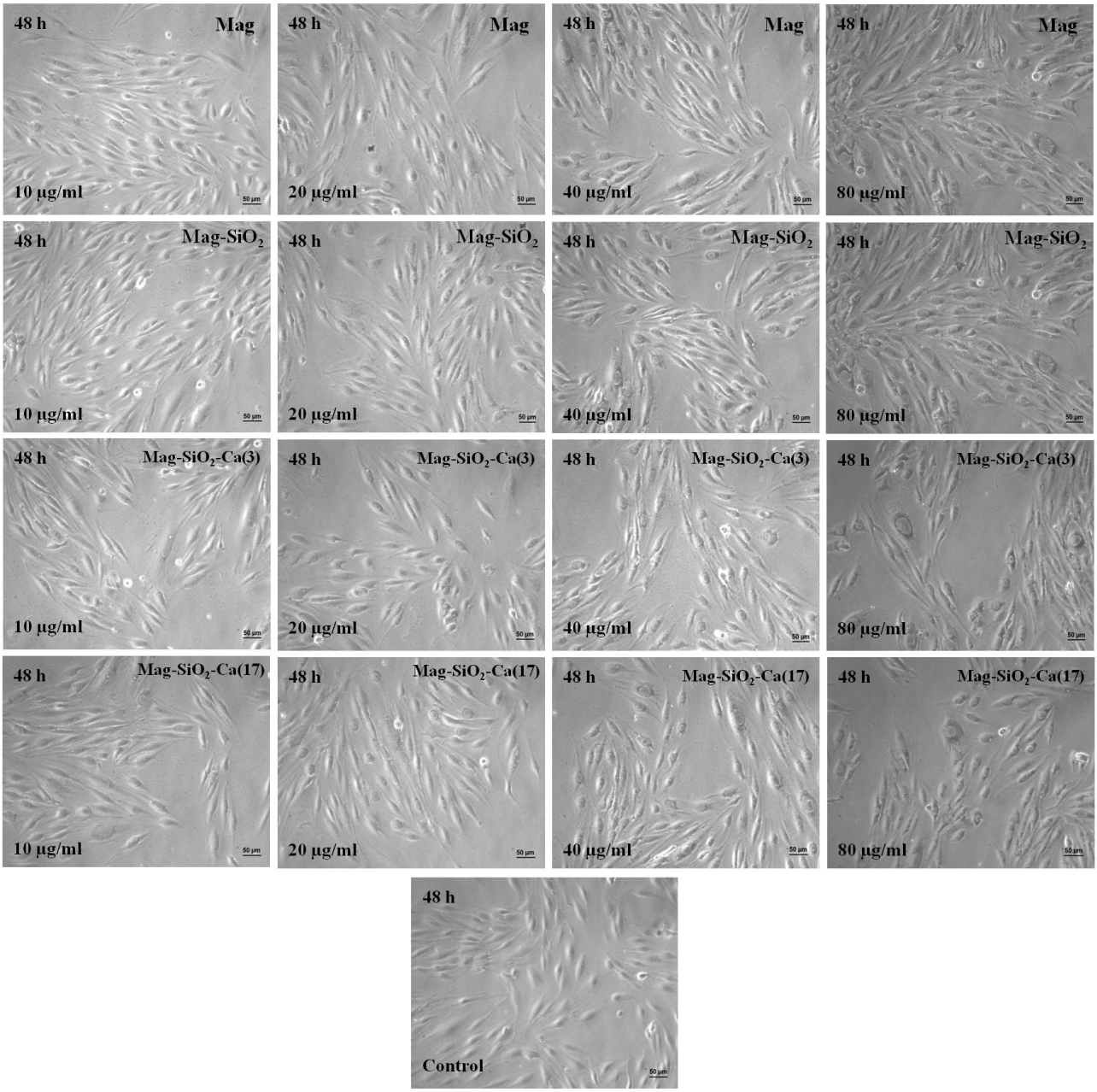

Figure 32. Optical microscopic images of endothelial cells (MS1 cells) after direct contact with MNPs (10-80 µg/ml) for 48 hours. Magnification: 20x, bar scale = 50 µm. No effects are observed on cell morphological features.

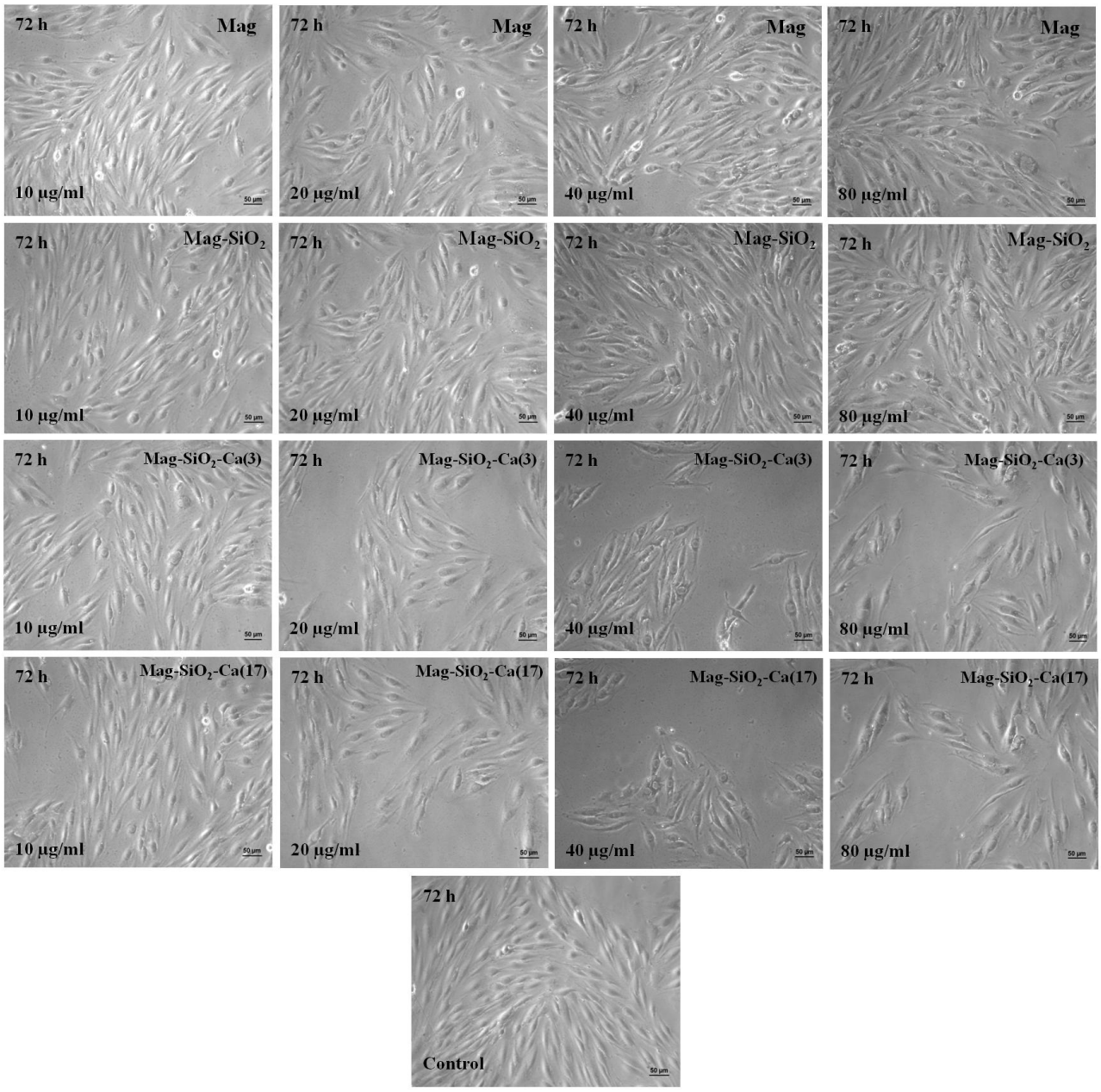

Figure 33. Optical microscopic images of endothelial cells (MS1 cells) after direct contact with MNPs (10-80 µg/ml) for 72 hours. Magnification: 20x, bar scale = 50 µm. No effects are observed on cell morphological features.

3.3.10 Lactate dehydrogenase assay

The lactate dehydrogenase assay is a convenient method for evaluation of cell damage, as indicated by lactate dehydrogenase release from the cytosol of lysed cells. LDH leakage from MNPs reflects cell membrane disruption. The lactate dehydrogenase results on MS1 cells were consistent with those of the MTT assay (**Figures 34-36**). All types of MNPs stimulated LDH release in a

concentration-dependent manner. LDH release of Mag NPs and Mag-SiO_2 NPs (in a range between 3.09 and 5.13%) was lower than calcium-silica core-shell type iron oxide nanoparticles (in a range between 4.69 and 8.87%) after 24, 48 and 72 hours, suggesting less cell membrane damage. Data were considered statistically significant ($p < 0.05$).

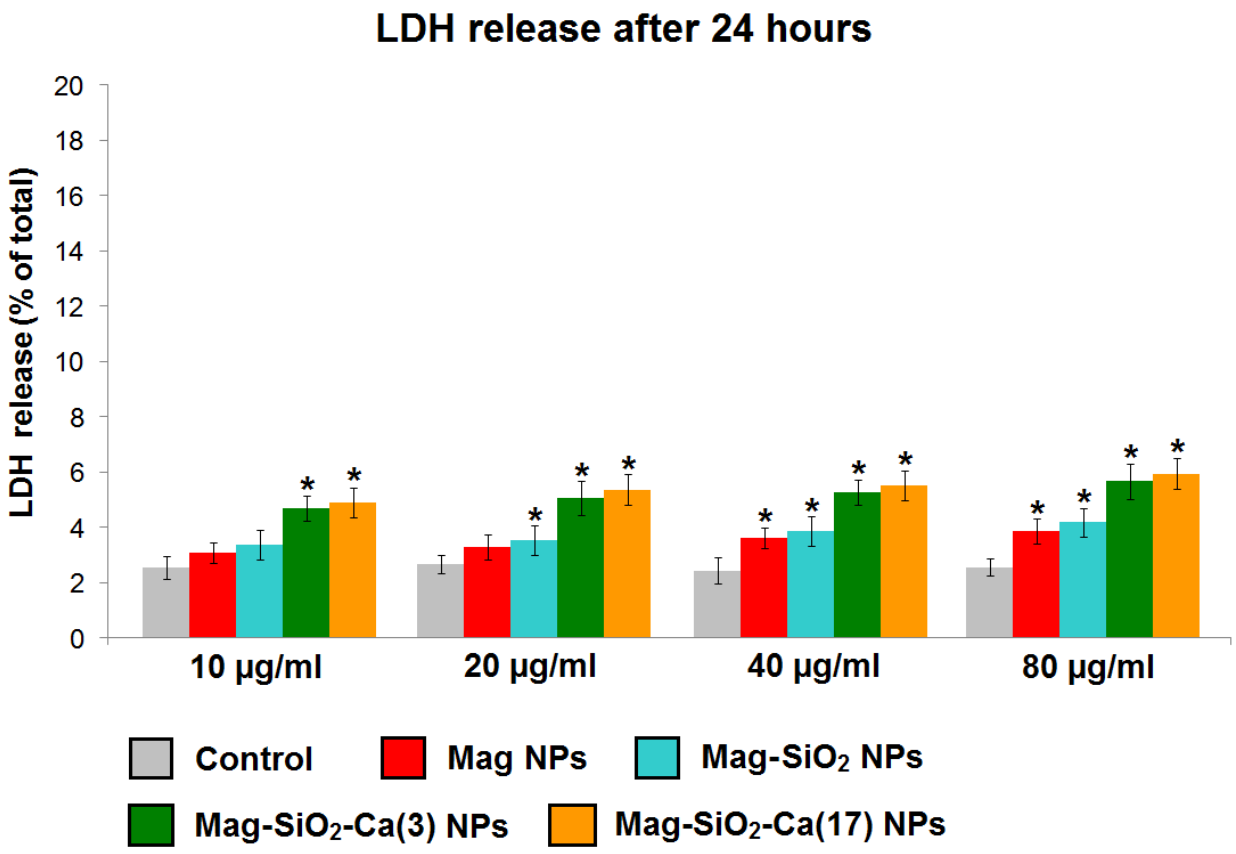

Figure 34. Effect of MNPs on cell-membrane integrity following exposure to increasing concentrations of MNPs for 24 hours. The relative lactate dehydrogenase (LDH) release was co-related to percentage cytotoxicity. Data are shown as the mean ± standard deviation (n = 4). *P < 0.05 compared with control.

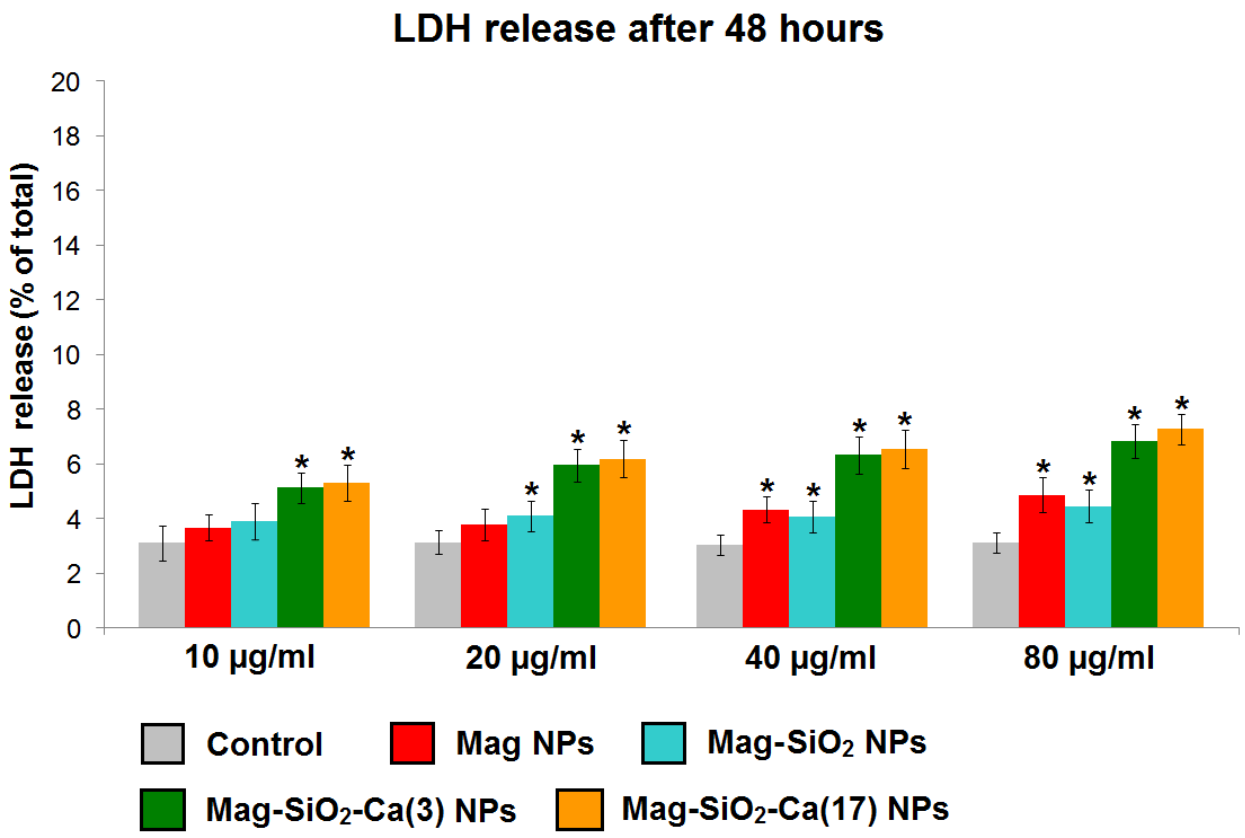

Figure 35. Effect of MNPs on cell-membrane integrity following exposure to increasing concentrations of MNPs for 48 hours. The relative lactate dehydrogenase (LDH) release was co-related to percentage cytotoxicity. Data are shown as the mean ± standard deviation (n = 4). *P < 0.05 compared with control.

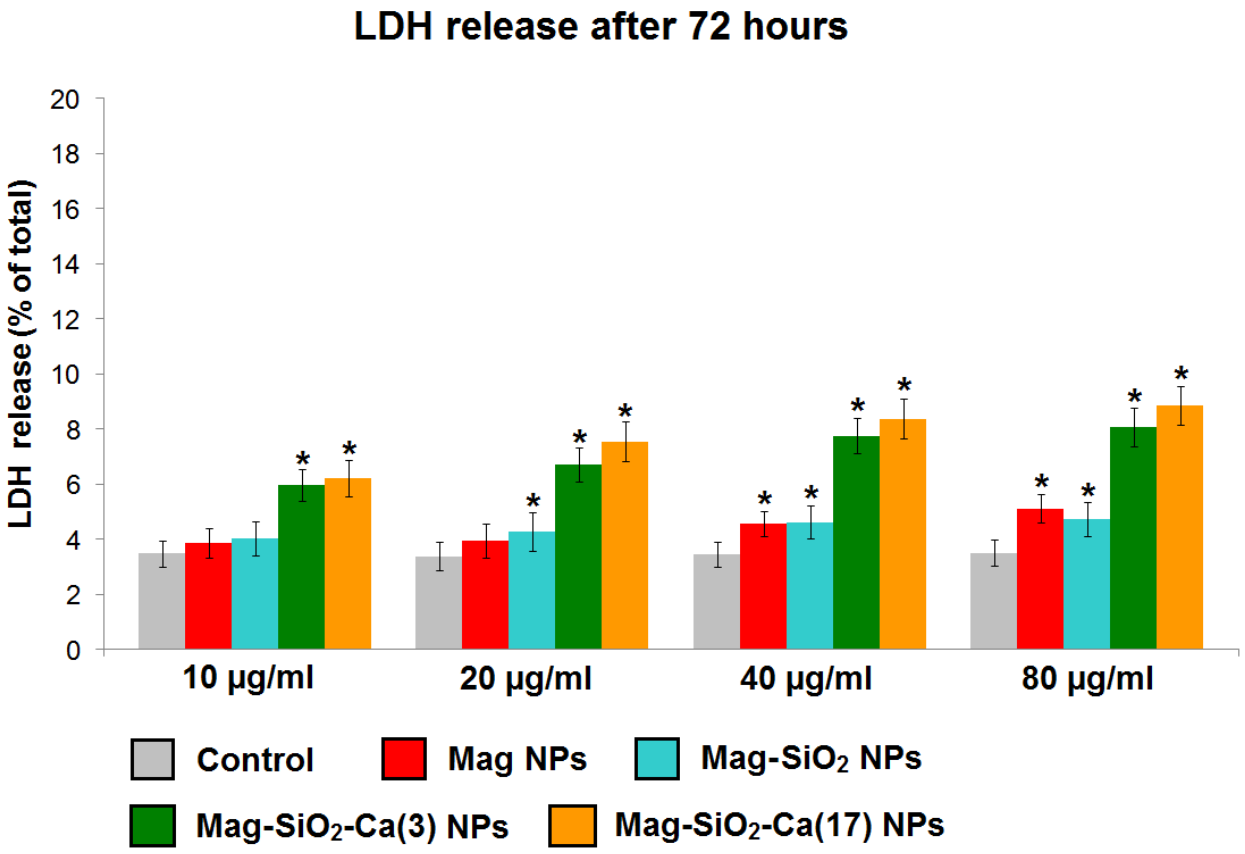

Figure 36. Effect of MNPs on cell-membrane integrity following exposure to increasing concentrations of MNPs for 72 hours. The relative lactate dehydrogenase (LDH) release was co-related to percentage cytotoxicity. Data are shown as the mean ± standard deviation (n = 4). *P < 0.05 compared with control.

3.3.11 Cells morphology evaluation by fluorescent microscopy

No cellular morphological alterations were observed between cells in direct contact with MNPs and control using IF staining (**Figures 37-39**). These results confirmed that MNPs had not adverse effects on the cytoskeleton and cell morphology. Some problem of MNPs cytotoxicity could be related to their accumulation in tissues and organs. Afterwards this aspect will be investigated in next chapter by using a bioreactor with microfluidic technology and by in vivo biodistribution of MNPs.

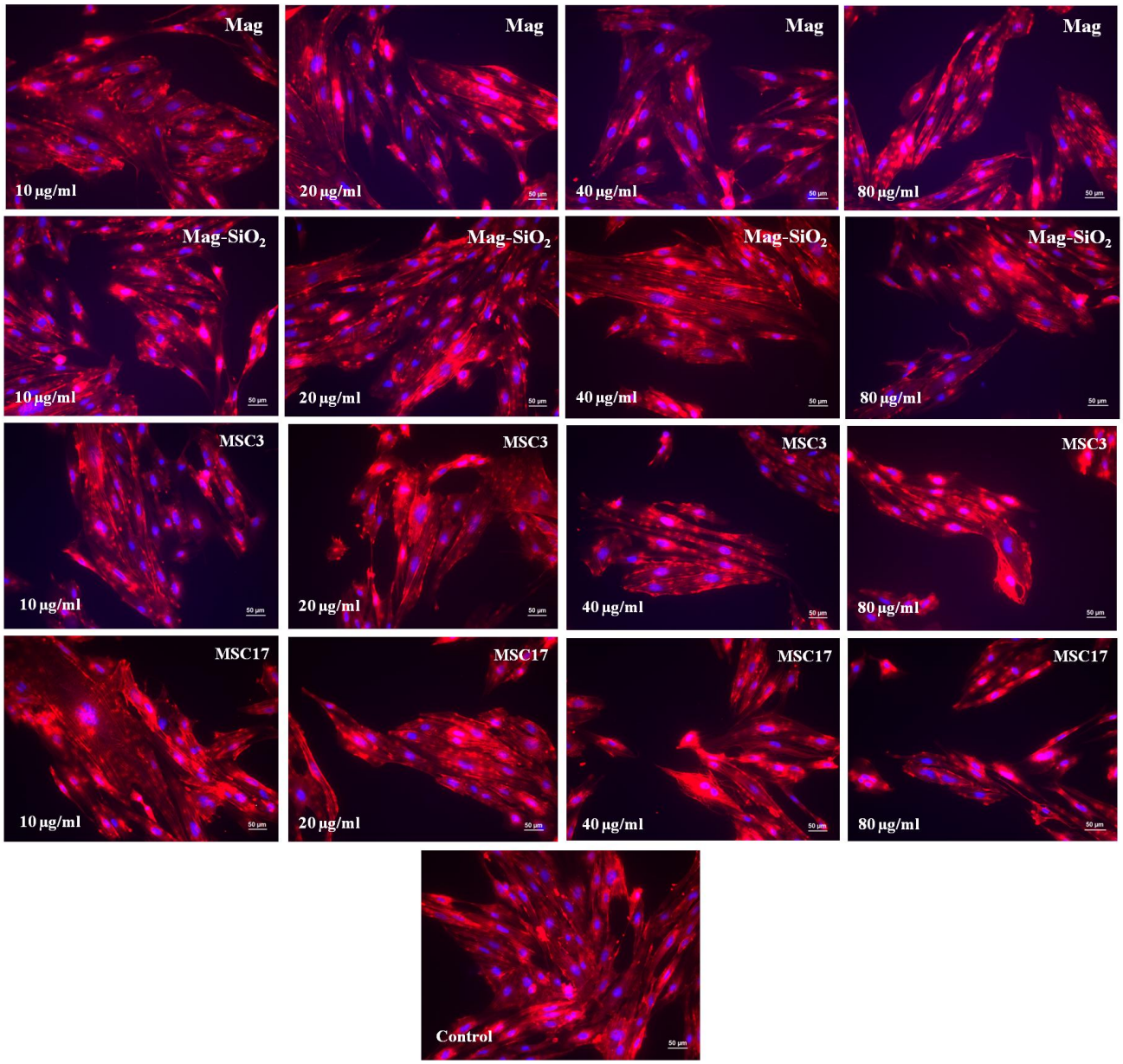

Figure 37. IF staining with DAPI (blue) and phalloidin (red) of cells seeded for 24 h in contact with nanoparticles: Mag, Mag-SiO_2, Mag-SiO_2-Ca(3), Mag-SiO_2-Ca(17) and control. Magnification: 20x, bar scale = 50 µm.

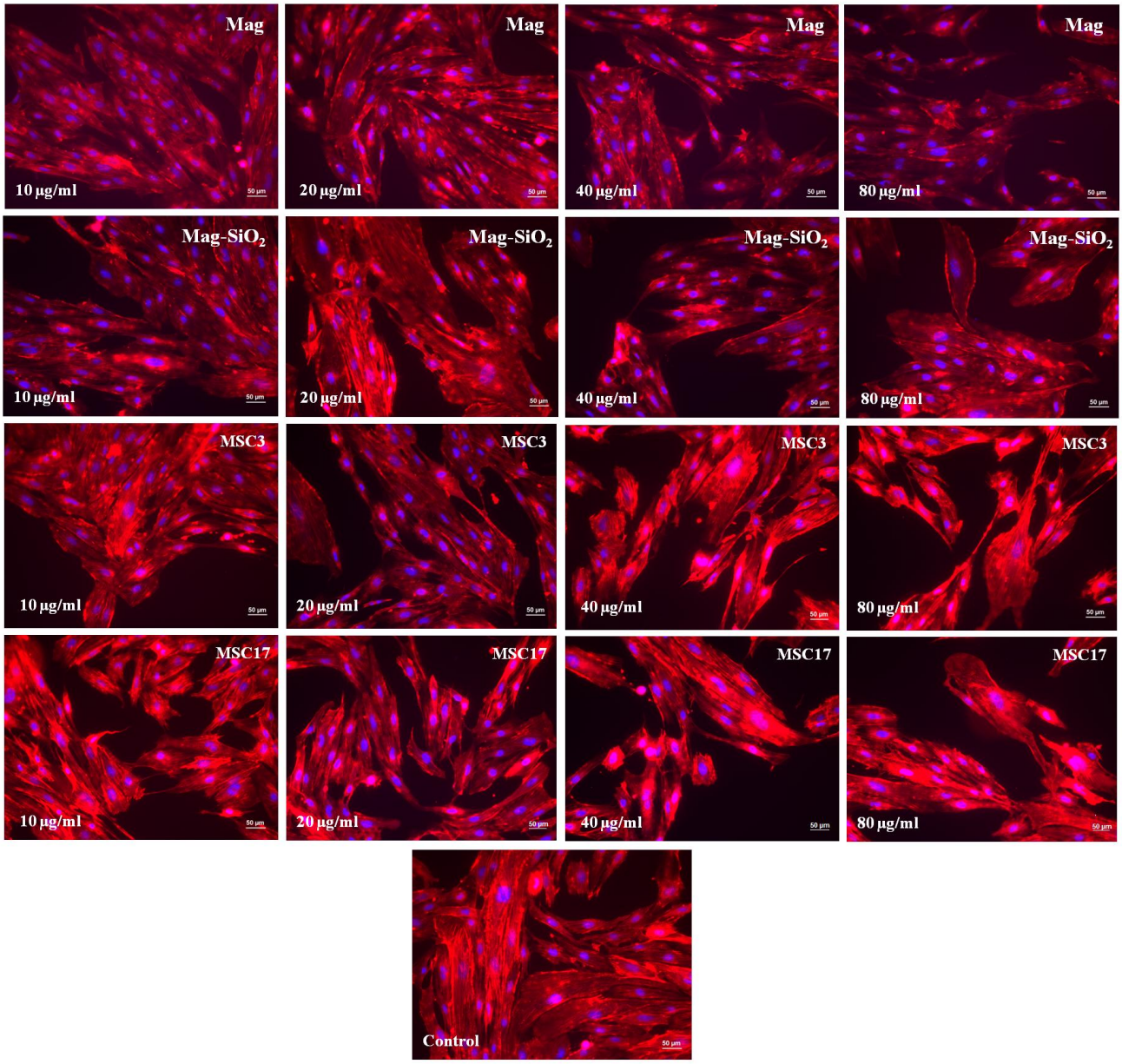

Figure 38. IF staining with DAPI (blue) and phalloidin (red) of cells seeded for 48 h in contact with nanoparticles: Mag, Mag-SiO_2, Mag-SiO_2-Ca(3), Mag-SiO_2-Ca(17) and control. Magnification: 20x, bar scale = 50 µm.

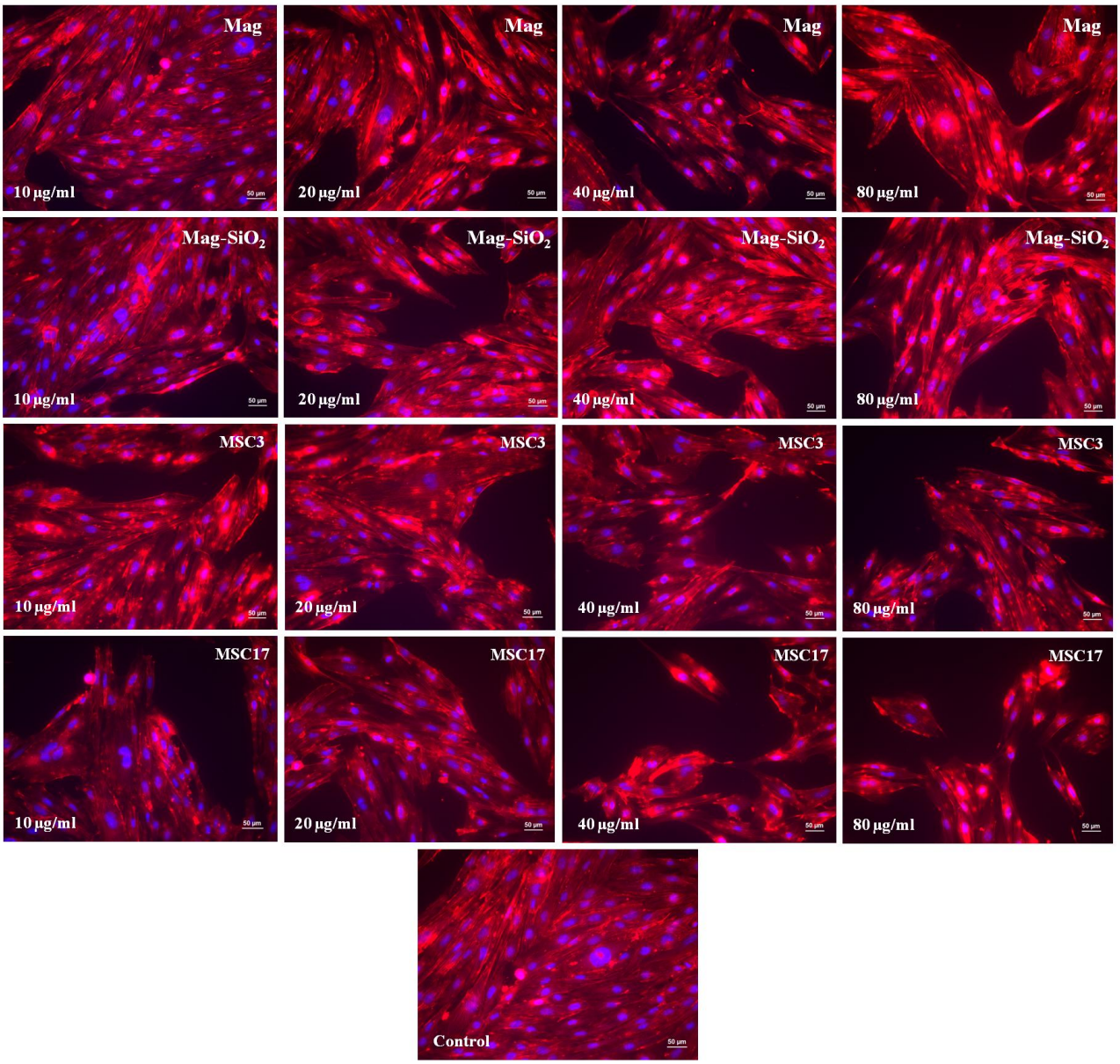

Figure 39. IF staining with DAPI (blue) and phalloidin (red) of cells seeded for 72 h in contact with nanoparticles: Mag, Mag-SiO_2, Mag-SiO_2-Ca(3), Mag-SiO_2-Ca(17) and control. Magnification: 20x, bar scale = 50 µm.

3.4 Discussion

Spherical MNPs were synthesized, with a diameter around 10-15 nm. MNPs consisting of magnetite or a core of magnetite coated with silica or calcium-silica were obtained. The addition of citric acid during the synthesis process increased their dispersibility and colloidal stability compared to the first synthesis of MNPs. Moreover, a second synthesis of MNPs was produced to improve their cytocompatibility compared to first synthesis. Ca^{2+} ions were introduced in order to enhance

MNPs surface reactivity for future functionalization with different moieties. Zeta potential was measured to determine the degree of the electrostatic or charge repulsion or attraction between nanoparticles, and is one of the fundamental parameters known to affect stability. In addition, it is useful to determine the best coating to be used to enhance the properties of the surface charge of the nanoparticles. Zeta potential of magnetic nanoparticles was measured to different acid and basic pH values in order to evaluate the overall trend of colloidal properties by varying the isoelectric point of the solution that contains the nanoparticles. Zeta potential measurements revealed a greater colloidal stability behavior of second synthesis of MNPs compared to the first synthesis.

The magnetic characterization of second synthesis of MNPs by using vibrating sample magnetometer (VSM-Lakeshore) to measure magnetic hysteresis showed that all types of MNPs have superparamagnetic properties. AFM/MFM observation of MNPs was useful to investigate magnetic forces, but also atomic and electrostatic forces.

Cell viability evaluation demonstrated that Mag NPs and Mag-SiO_2 NPs are cytocompatible and comparable to the control till the concentration of 80 µg/ml. The NP surface is crucial to improve dispersibility and biocompatibility of MNPs.

On the contrary Mag-SiO_2-Ca(3) NPs and Mag-SiO_2-Ca(17) were not cytocompatible. A possible explanation of the cytotoxicity effect observed could be the transient absorption of Ca^{2+} ions on the amorphous shell and their subsequent release of Ca^{2+} ions in cell culture medium, which are toxic to the cells. In fact, NPs with a higher ratio of Ca^{2+} ions displayed a higher level of toxicity compared to low Si:Ca ratio ($p < 0.05$). Finally to further improve the dispersibility and separation of MNPs, the implementation of ultrafiltration techniques will be achieved in the next chapter. The future goal is to realize functionalized magnetic nanoparticles which minimize not direct and direct toxic effects and improve assembling of MNPs with drugs, chemicals and antibodies.

3.5 Conclusion

This new synthesis of MNPs showed a considerable improvement of colloidal properties of nanoparticles using citric acid like dispersant respect to first synthesis. Mag and Mag-SiO_2 NPs prepared with the addition of citric acid showed cytocompatibility comparable to control in both direct and not direct conditions. In addition the new formulation for the preparation of Mag and Mag-SiO_2 NPs in the second synthesis improved their cytocompatibility in not direct conditions respect to the first synthesis. However the new nanoparticles with calcium synthesized in the second synthesis did not show cytocompatibility comparable to control, probably due to the release of Ca^{2+}

ions from MNPs in cell culture media which affected cell viability of MS1 cells. In fact in the next chapter this aspect will be addressed by preparing calcium-silica iron-oxide nanoparticles with a more efficient synthesis procedure.

Chapter 4

In vitro and in vivo biological characterization of magnetic nanoparticles obtained via co-precipitation methods using citric acid as dispersant

4.1 Aim

The third synthesis of magnetic nanoparticles was optimized to reach the best physical-chemical properties and evaluate the biocompatibility of the nanoparticles in different conditions. MNPs of third synthesis were assessed for their cytocompatibility using various approaches including leaching tests, static and dynamic direct contact tests. In fact naked Fe_3O_4 nanoparticles (Mag) were compared with those covered by silica shell (Mag-SiO_2) in static and dynamic conditions of cytocompatibility. Two concentrations of MNPs: 2 and 20 µg/ml were standardized for cytocompatibility tests to avoid problems of cytotoxicity related to high concentrations of MNPs, as observed in the previous chapters. In addition, the characterization of magnetic nanoparticles was extended analyzing the aspects of *in vivo* biocompatibility of MNPs. Dynamic cell *in vitro* evaluation was implemented to minimize the MNPs cluster effect on cytocompatibility of MS1 cells. Noteworthy is the fact that the static cytotoxicity may, however, be more pronounced *in vitro* than *in vivo* because in cell culture conditions the NPs and/or their degradation products (which can affect cell viability) remain in close contact with the cells and may act as a depot showing continuous effect. For this reason, we implemented a cytotoxicity test of MNPs in dynamic conditions. On the contrary, NPs are in vivo continuously eliminated from the body when they are biodegradable, as reported in literature [54]. Thus, it is obvious that the assessment of *in vivo* safety of MNPs is essential for any type of application.

The investigation of third synthesis of MNPs was aimed to evaluate systemic biodistribution, after intravenous injection, of magnetic nanoparticles with and without silica coating. Only Mag and Mag-SiO_2 NPs were tested for *in vivo* biodistribution because *in vitro* cell viability tests showed that they were more cytocompatible in comparison with calcium-silica core-shell type MNPs, as described in the previous chapter. A further synthesis of MNPs was prepared for two reasons: 1) the

previous synthesis of MNPs had a low yield production and 2) calcium-silica core-shell type MNPs showed problems of cytotoxicity on murine endothelial cells. Thus, yield production of third synthesis of MNPs was improved by separating and washing MNPs extensively with water using an ultrafiltration device. Moreover, it was investigated the reason of cytotoxicity observed for calcium-silica MNPs in the previous synthesis if it's due to the Ca^{2+} precursor used for their production. To solve this problem two different Ca^{2+} precursors (calcium citrate and calcium hydroxide) were compared. In this way it was possible to compare the precursor (calcium citrate) used in the second synthesis of MNPs respect to the final preparation of MNPs.

4.2 Materials and methods

4.2.1 Nanoparticles preparation

Four different types of magnetic nanoparticles (MNPs) were studied: Mag, Mag-SiO_2, Mag-SiO_2-Ca(3) IDR, Mag-SiO_2-Ca(3) CITR. In the third synthesis a different method of preparation of calcium-silica MNPs with Si:Ca ratio 99:1 (MSC(3)) was implemented by using two different Ca^{2+} precursors: calcium citrate and calcium hydroxide. These nanoparticles were produced by Politecnico di Torino in the laboratory of the Applied Science and Technology Department directed by Prof. Enrica Vernè. The preliminary physico-chemical characterization of the nanoparticles was performed by Politecnico di Torino as following reported. Their main characteristics are described in Table 15. Three of them consisted of a magnetite core covered by an amorphous silica shell (Mag-SiO_2) (**Figure 40**).

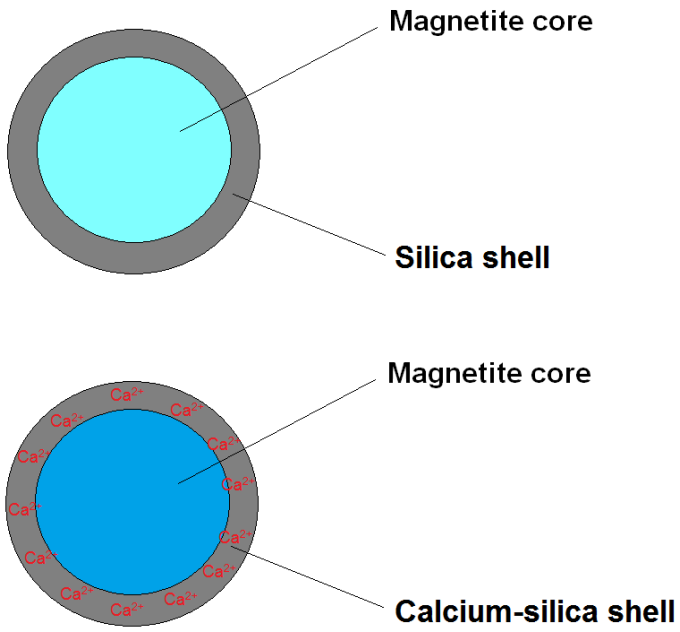

Figure 40. Schematic representation of silica core-shell type magnetic nanoparticles.

SAMPLE	MATERIAL	MEDIUM	Concentration of MNPs stock solution	pH approx	Notes
Mag	Citric acid treated magnetite nanoparticles	Water	1.8 mg/ml	9.6	Stable in solution for weeks
Mag-SiO_2	SiO_2 coated citric acid stabilized magnetite nanoparticles	Water	3.4 mg/ml	7.9	Stable in solution for weeks
Mag-SiO_2-Ca(3) IDR	SiO_2 – Ca (low amount Ca) coated citric acid stabilized magnetite nanoparticles produced from the precursor: calcium hydroxide	Water	4.4 mg/ml	9.2	Stable in solution for weeks
Mag-SiO_2-Ca(3)	SiO_2 - Ca (low amount Ca) coated citric acid stabilized	Water	4.5 mg/ml	8.3	Stable in solution

CITR	magnetite nanoparticles produced from the precursor: calcium citrate				for weeks

Table 15. Main characteristics of MNPs synthesized via co-precipitation methods using citric acid.

4.2.2 Nanoparticles: synthesis of MNPs

Magnetite nanoparticles (Mag) were produced by co-precipitation method [101] as explained in chapter 2.2.1. Aqueous solutions of $FeCl_2$ and $FeCl_3$ were mixed and pH was brought to basic values (about 10.0) by dropwise NH_4OH addition.

To improve water dispensability of the MNPs, a treatment of magnetite with citric acid was carried out by soaking nanoparticles in citric acid solution (0.05 M) for 3 h and then exhaustively washed with water.

At the end of nanoparticles synthesis and fictionalization with citric acid, by adding tetraethyl orthosilicate (TEOS) (a silica precursor), with ethanol and water as solvent, an amorphous silica shell (Mag-SiO_2) was obtained.

To avoid the uncontrolled TEOS polymerization in the reaction media and to optimize the silica shell [107], the TEOS amount was reduced and concomitantly ethanol was added in the synthesis step, as described in the Stöber method [102]. The nanoparticles were then separated and washed extensively with water using an ultrafiltration device.

To obtain calcium-silica magnetite NPs, calcium citrate and calcium hydroxide were selected as precursors of Ca^{2+} ions and thus added in the synthesis process together with TEOS to reach 99:1 (Mag-SiO_2-Ca(3) CITR and IDR) Si:Ca ratio.

4.2.3 Nanoparticles characterization

As previously described in the paragraph 3.2.3.

4.2.4 Magnetic performance testing

As previously described in the paragraph 3.2.5.

4.2.5 Zeta potential

As previously described in the paragraph 3.2.8.

4.2.6 Cell culture

As previously described in the paragraph 2.2.2.

4.2.7 Cell viability evaluation using MTT assay

As previously described in the paragraph 2.2.3.

4.2.8 Not direct contact cytotoxicity evaluation of MNPs

As previously described in the paragraph 2.2.3.

4.2.9 Direct contact cytotoxicity evaluation of MNPs in static conditions

Mag, Mag-SiO_2, Mag-SiO_2-Ca(3) CITR and Mag-SiO_2-Ca(3) IDR nanoparticles were tested for cytocompatibility in static conditions. Direct contact static cytotoxicity evaluation was done according to ISO standard 10993-5: 2009. The cells were seeded in 24-well plates (1,6 x 10^4 cells per well) in DMEM medium and cultured for 24 h at 37°C in 5% CO_2 atmosphere-controlled incubator. After 24 hours the medium was substituted with a new one obtained by adding MNPs to DMEM to obtain the following concentrations: 2 μg/ml, 20 μg/ml (w/v). Media without MNPs were used as comparison. Cells viability of MS1 cells was evaluated using MTT assay after 24, 48 and 72 h. Furthermore, cells morphology for direct contact cytotoxicity evaluation in static conditions was visually investigated at each experimental time by light microscopy (Leica AF 6500, Leica Microsystems) at 20x magnification.

4.2.10 Cells morphology evaluation by fluorescent microscopy

As previously described in the paragraph 3.2.13.

4.2.11 Reactive oxygen species (ROS) in cells

The production of ROS in cells was measured using CellROX Oxidative Stress Reagents (Life Technologies) as an oxidation-sensitive probe. CellROX Oxidative Stress Reagents are fluorogenic probes designed to reliably measure reactive oxygen species (ROS) in live cells. CellROX Green Reagent is a DNA dye, and upon oxidation, it binds to DNA; thus, its signal is localized primarily in the nucleus and mitochondria. Briefly, 2.5 mM CellROX Green Reagent stock solution was diluted 500-fold with cell culture medium without serum or other additives to prepare a 5 µM working solution. MS1 cells were seeded in 12-well plates (7.5×10^4 cells per well). After exposure to Mag, Mag-SiO_2, Mag-SiO_2-Ca(3) CITR and Mag-SiO_2-Ca(3) IDR NPs at the concentrations of 2 and 20 µg/ml for 24 h, the cells were washed with PBS and incubated in 1 mL of CellROX Green Reagent at a final concentration of 5 µM at 37°C in the dark for 30 min. Experimental time-point (24 h) of ROS production induced by MNPs was chosen according to literature [103, 104]. Menadione (25 µM) was used as a positive control. Then, MS1 cells were analyzed with Flow cytometry at an excitation wavelength of 485 nm for CellROX Green Reagent. Statistical data were obtained from the dot plots using CellQuest software (BD Biosciences).

4.2.12 Apoptosis evaluation

MS1 cells were seeded at a density of $2{,}5 \times 10^5$ cells for 24 hours and $1{,}75 \times 10^5$ cells for 48 and 72 hours on Petri dishes, then treated with Mag and Mag-SiO_2 NPs at different concentrations (2 and 20 µg/ml in DMEM respectively) at 37 °C. Following incubation for 24, 48 and 72 h, Annexin V-FITC and PI double staining was performed according to the manufacturer's instructions. Cells were collected by centrifugation, washed twice with cold PBS, and a cell suspension was prepared by adding 400 µl x 1 binding buffer and 10 µl Annexin V-FITC, which was incubated for 15 min at 4 °C in the dark. Finally, 10 µl PI was added and incubated for 15 min under the same conditions. Flow cytometry experiments were carried out at an excitation wavelength of 488 nm for Annexin V-FITC and PI. The obtained data from the dot plots using CellQuest software (BD Biosciences) were analyzed by means of frequency distribution table and descriptive statistics using IBM SPSS (version 20) and Chi-square test.

4.2.13 Direct contact cytotoxicity evaluation of MNPs in dynamic conditions

Experiments were repeated in dynamic conditions using a continuous flow bioreactor (**Figure 41**) with a peristaltic pump simulating the blood stream in a capillary. MS1 cells were seeded at confluence on a strip (2.4 cm x 0.6 cm) of polycaprolactone (PCL) supports (30.000 cells/cm^2). When MS1 cells were confluent, the strips were inserted in the bioreactor and the cells were subjected to a continuous flow of cell culture medium (DMEM) with MNPs at the concentration of 20 µg/ml. Experiments were carried out in humidified incubator at 37°C, 5% CO_2 atmosphere and stopped at the following experimental times: 2 h, 12 h and 24 h. Cell viability was then evaluated using LDH assay and XTT assay. Moreover, cell morphology was analyzed with FESEM equipped to EDS probe, in order to evaluate the presence, if any, of Mag and Mag-SiO_2 nanoparticles deposits.

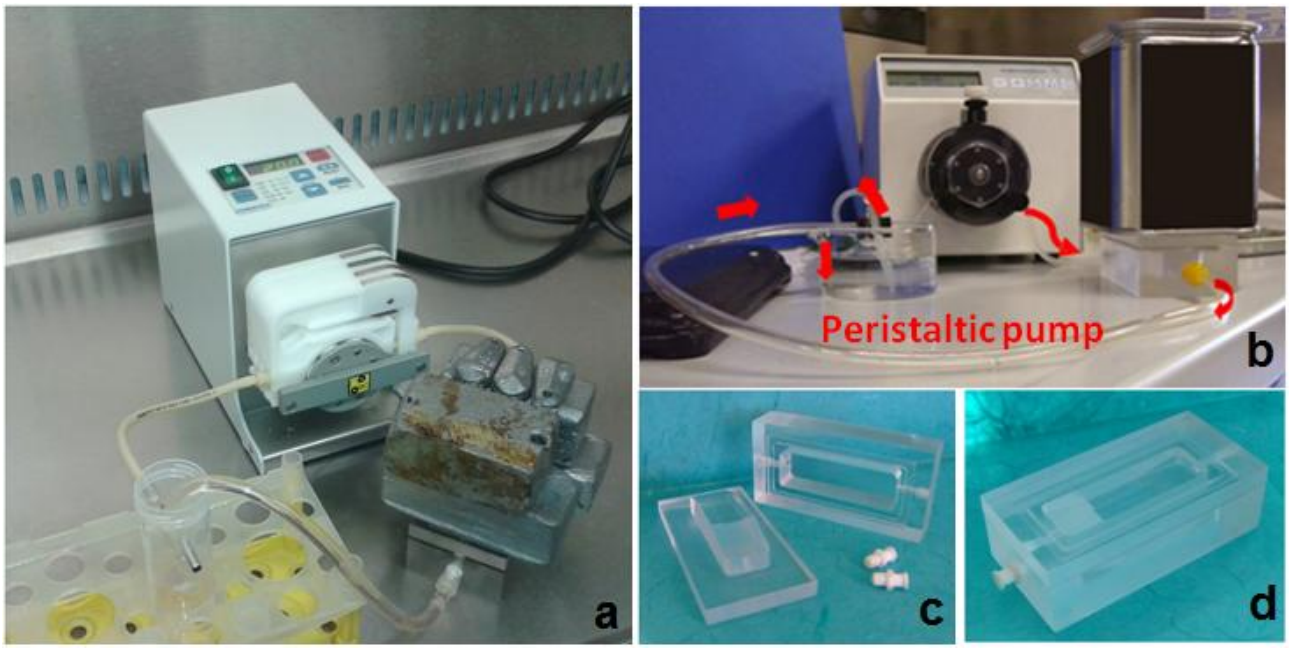

Figure 41. a) Microfluidics bioreactor used for cytocompatibility evaluation of MNPs in dynamic conditions, b) Peristaltic pump of bioreactor, c) Perfusion chamber of bioreactor disassembled, d) Perfusion chamber of bioreactor assembled. Bioreactor was kindly set up and provided by Prof. Silvia Farè - Politecnico di Milano.

4.2.14 Lactate dehydrogenase assay

The possible adverse effects of MNPs on MS1 cells subjected to a continuous flow in a bioreactor were assayed using a LDH Cytotoxicity Assay Kit (Gesan group). The assay was performed as per the manufacturer's instructions. LDH is released by cells in response to damage or loss of integrity of cell membrane and is a cellular toxicity indicator. Briefly, MS1 cells were seeded at confluence on a strip of polycaprolactone (PCL) and subjected to a continuous flow of cell culture medium (DMEM) with MNPs at concentration of 20 µg/ml for three experimental times: 2, 12 and 24 h. Untreated cells were taken as the negative control and cells treated with lysis buffer were taken as the high control (total LDH in the cell). As a positive control, 1 µL of LDH was used to validate the assay. Following the incubation with NPs, the well plates were centrifuged at 600 g for 10 minutes and 10 µL of the medium was transferred to a fresh 96-well plate. The medium was then incubated with 100 µL of LDH reaction mixture for 15 minutes at room temperature and the absorbance was measured at 450 nm using the microplate reader (Victor X4 - PerkinElmer) with the reference wavelength at 650 nm. LDH was quantified using the following formula:

$$\text{LDH\%} = \frac{\text{Test} - \text{low control}}{\text{High control} - \text{low control}} \times 100$$

in which "low control" was the cells without any treatment and "high control" was the cells treated with lysis buffer (total LDH).

4.2.15 XTT assay

The 2,3-bis (2-methoxy-4-nitro-5-sulphophenyl)-5-[(phenyl amino) carbonyl]-2H-tetrazolium hydroxide (XTT; Sigma) colorimetric assay was used to determine mitochondrial dehydrogenase activity as an indicator of the metabolic state of MS1 cells seeded at confluence on a strip of polycaprolactone (PCL) and subjected to a continuous flow of cell culture medium (DMEM) with MNPs at concentration of 20 µg/ml for three experimental times: 2, 12 and 24 h. 50 µL XTT solution (1 mg/mL in PBS) and 4 µL menadione solution (1 mM in acetone) were used for each strip. Plates were incubated for 5 hours in the dark at 37°C. After the supernatant was centrifuged into new 1-mL Eppendorf tubes and centrifuged (5 min, 13,000 rpm) to remove residual cells. From each tube, 200 µL was transferred to a new 96-well plate and XTT formazan [OD] (optical density) in the supernatant was determined spectrophotometrically at 690 nm.

4.2.16 Biodistribution of MNPs

Biocompatibility and biodistribution of the MNPs were studied after 7 days of administration in mice. The same concentrations of MNPs of in vitro experiments were tested for biodistribution in vivo. Mag and Mag-SiO_2 nanoparticles were tested in vivo in mice using the following concentrations: 2 and 20 mg/kg body weight. In this way it was possible to investigate the dose-dependent toxic effects induced in vivo by the magnetic nanoparticles.

4.2.17 Animal experiments

C57BL6 wild-type mice (8-10 weeks old with body weight of 20-25 g - purchased form Harlan) were treated according to protocols evaluated and approved by the Ethical Committee of University of Piemonte Orientale, Novara and to the National and European laws.
Two doses of 2 and 20 mg/kg of Mag and Mag-SiO_2 NPs were separately given to the mice via tail vein injections. 7 days post-injection, the mice were anesthetized with i.p. injection of an aqueous solution of 6 % chloral hydrate (6 ml/kg). Control experiments were carried out by injecting physiological saline solution (NaCl 0.9%). Four mice (2 males and 2 females) were used for each sample: Mag NPs, Mag-SiO_2 NPs and control. Twelve mice were used for each dose of MNPs.

4.2.18 Serum biochemical analysis

The mice were intravenously administrated MNPs with a dose of 2 and 20 mg/kg. At 7 days post-injection, 1 ml of blood was collected by removal through the eyeball before perfusion. Blood samples were allowed to clot at room temperature and centrifuged at 3,000 g for 10 min to separate the serum. The serum biochemical analysis were carried using a commercial kit according to the manufacturer's instruction (LDH kit assay, Gesan Production). Aspartate transaminase (AST), alanine transaminase (ALT), creatinine (CRE), lactic acid dehydrogenase (LDH) were measured. Saline was used as a control.

4.2.19 Hematological analysis

Hematological parameters: red blood cell (RBC) and white blood cell (WBC) were measured using trypan blue staining for counting of blood cells. The blood was collected from mice by removal through the eyeball after 3 and 7 days. The cell counting was performed using a hemocytometer.

Because the high density of blood cells to allow cell counting, a diluition 1:200 blood:isotonic solution was performed. Once the blood sample was diluted, trypan blue was added on a 1:1 proportion. Afterwards the blood cell counting was performed by hemocytometer according to literature [110]. The final number of RBC and WBC was calculated multiplying by 200 due to the initial dilution made, and additionally by 2 because of the viability dye. Cell counting was repeated three times.

4.2.20 Organs explant

The major organs (liver, spleen, brain, kidney, lung, and heart) were collected and analyzed from three points of view: 1) Macroscopic evaluation (organ weights); 2) Spectrometry evaluation for iron accumulation (Inductively coupled plasma-atomic emission spectrometry (ICP-AES)); 3) Histological evaluation of iron accumulation (Perls' Prussian blue staining).
After dissection organs were collected (from 4 mice for each MNP sample and control). The organs from three mice (per sample) were used for ICP-AES compositional evaluation, while organs from one mouse (per sample) were used for histological evaluation. For analysis in liver, only right lobes were used.

4.2.21 Inductively coupled plasma-atomic emission spectrometry (ICP-AES)

Inductively coupled plasma atomic emission spectroscopy (ICP-AES) is a very diffused analytical technique used for the detection of trace metals. It is a type of emission spectroscopy that uses the inductively coupled plasma to produce excited atoms and ions that emit electromagnetic radiation at wavelengths characteristic of a particular element [111, 112]. The intensity of this emission is indicative of the concentration of the element within the sample. The organs were digested overnight in an Erlenmeyer flask containing 8.0 ml of HNO_3 (68 %) and 2.0 ml of $HClO_4$ (70 %) at room temperature. Next, the digested sample was placed at 70 °C for 2 h, and then heated at 150 °C to remove the remaining acid. Finally, the remaining residue was dissolved in 1.0 ml of HNO_3 and made up to the final volume of 500 ml for the iron quantification using ICP-AES. The amount of iron and silicon present in the organs was measured using ICP-AES.

4.2.22 Histological evaluation of iron accumulation

The Perls' Prussian blue staining was performed to control the presence and the intracellular accumulation of iron ions in tissues and organs of mice injected with magnetic nanoparticles. The underlying principle of the staining is the formation of a bright blue pigment called Prussian blue due to chemical interaction of ferrous or ferric ions present in the tissue sections with ferrocyanide. In brief paraffin-embedded tissue sections were fixed for 30 minutes in 4% paraformaldehyde. To reveal the presence of ferrous ions (Fe^{2+}) paraffin-embedded tissue were pre-incubated for 20 minutes with ammonium sulphide solution. The tissue sections were then washed with phosphate-buffered solution and incubated with potassium hexacyanoferrate solution (2% potassium ferrocyanide/2% HCl, 1:1 v/v, Sigma, St Louis, MO) for 30 minutes to reveal ferric ions (Fe^{3+}). Instead the sections incubated with potassium hexacyanoferrate solution (5% potassium ferrocyanide/1% HCl, 1:1 v/v, Sigma, St Louis, MO) for 30 minutes to verify the presence of ferrous ions. Finally, the tissue sections were counterstained with Nuclear Fast Red solution (Sigma-Aldrich), and observed under an inverted optical microscope.

4.2.23 Statistical analyses

All statistical analyses were performed using IBM Statistical Package for Social Sciences v. 20 software (SPSS - IBM). Data were expressed as means ± standard deviations. The results were analyzed using one way analysis of variance (ANOVA) followed by Scheffe's test, and P values less than 0.05 were considered to be statistically significant.

4.3 Results

4.3.1 MNPs diffraction signals

Diffraction patterns of Mag, Mag-SiO_2, Mag-SiO_2-Ca(3) CITR and IDR NPs match the ones reported for magnetite [101] (**Figure 42**). The numbers in SAED patterns of MNPs refer to the distances of crystal planes of Mag, Mag-SiO_2, Mag-SiO_2-Ca(3) CITR and IDR NPs according to a defined crystallographic direction. In the case of Mag-SiO_2 and Mag-SiO_2-Ca(3) CITR and IDR samples broad halos can be observed together with the diffraction signals characteristics of

magnetite (that resulted a little attenuated), and can be attributed to the amorphous coating (**Figure 42**).

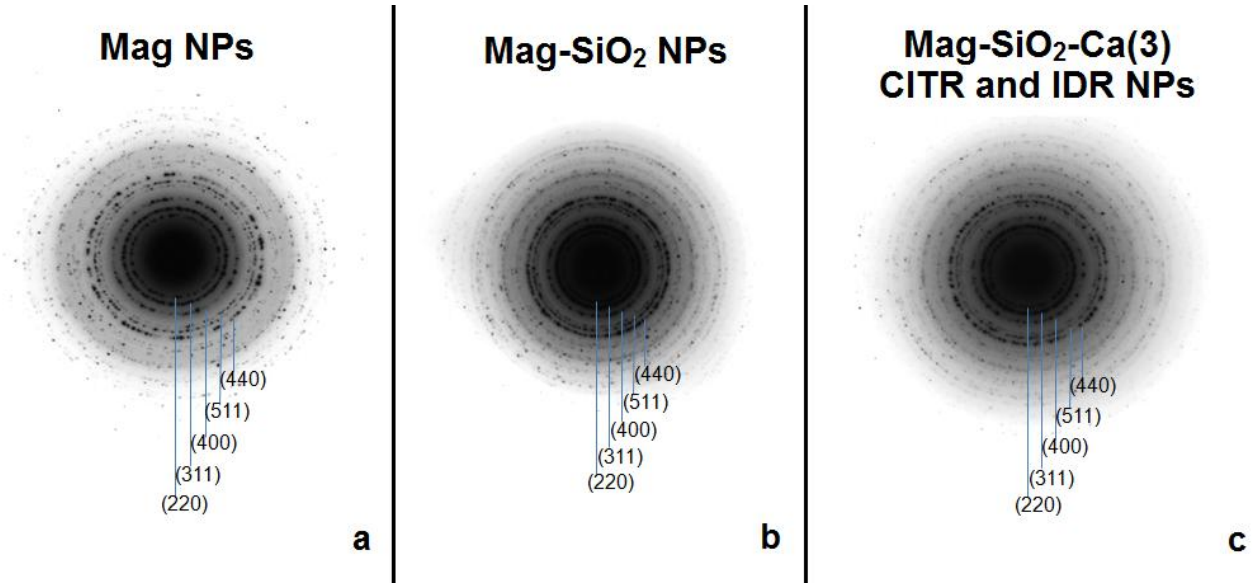

Figure 42. Diffraction signals of Mag NPs (a); Mag-SiO_2 NPs (b); and Mag-SiO_2-Ca(3) CITR and IDR NPs (c). The numbers in SAED patterns refer to the distances of crystal planes of Mag and Mag-SiO_2 NPs according to a defined crystallographic direction.

4.3.2 Morphological observations

TEM showed that the electron density of the magnetic nanoparticles was relatively high, and that the nanoparticles, which were spherical and partially agglomerated, had a primary diameter of 15 nm and a shell (silica) with a thickness of 1-2 nm. Nanometric spherical particles (10-15 nm) with calcium and with a good dispersion in water were obtained. An effective enrichment in Ca^{2+} was verified for both formulations with an increased calcium content, according to expectancies (**Figure 45-46**). EDS analysis confirmed the composition of the nanoparticles through a rough estimate (**Figures 43-46**).

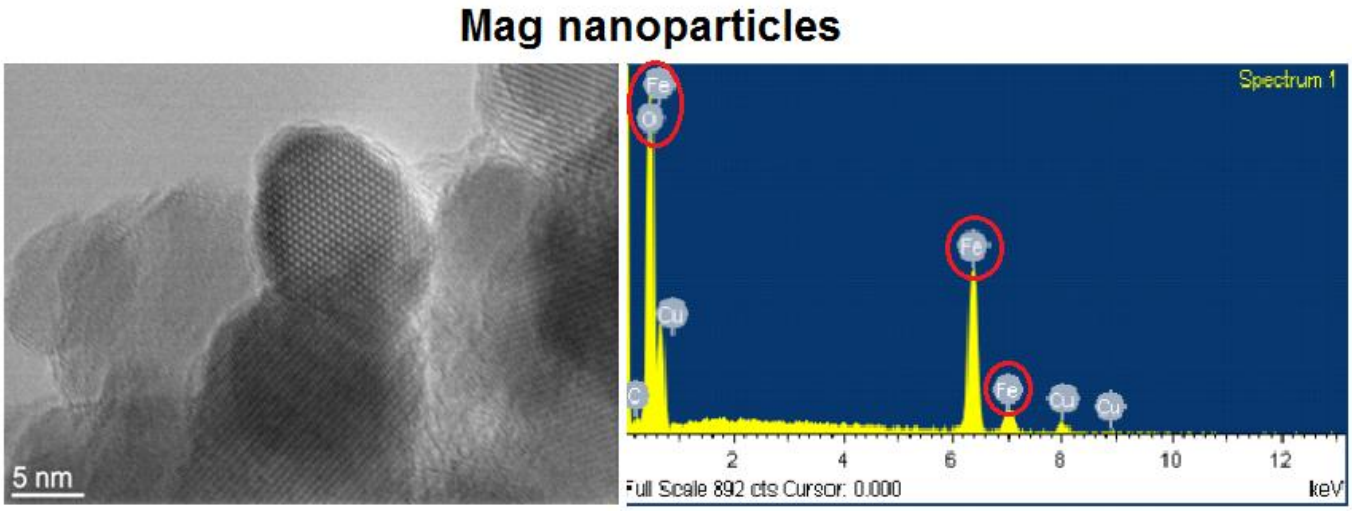

Figure 43. TEM image and EDS spectrum of Mag nanoparticles.

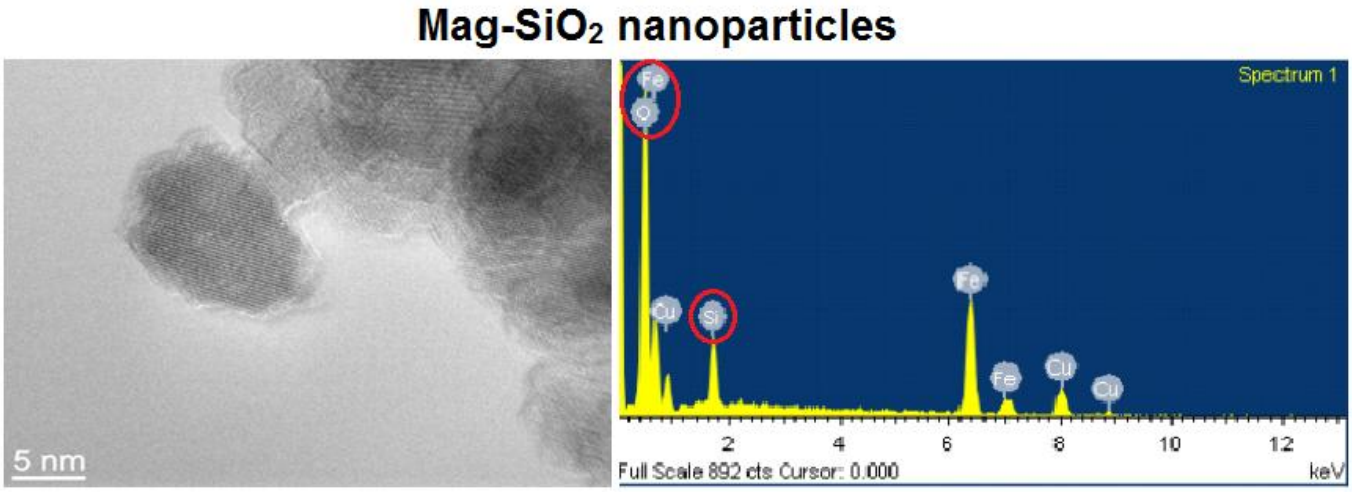

Figure 44. TEM image and EDS spectrum of Mag-SiO_2 NPs.

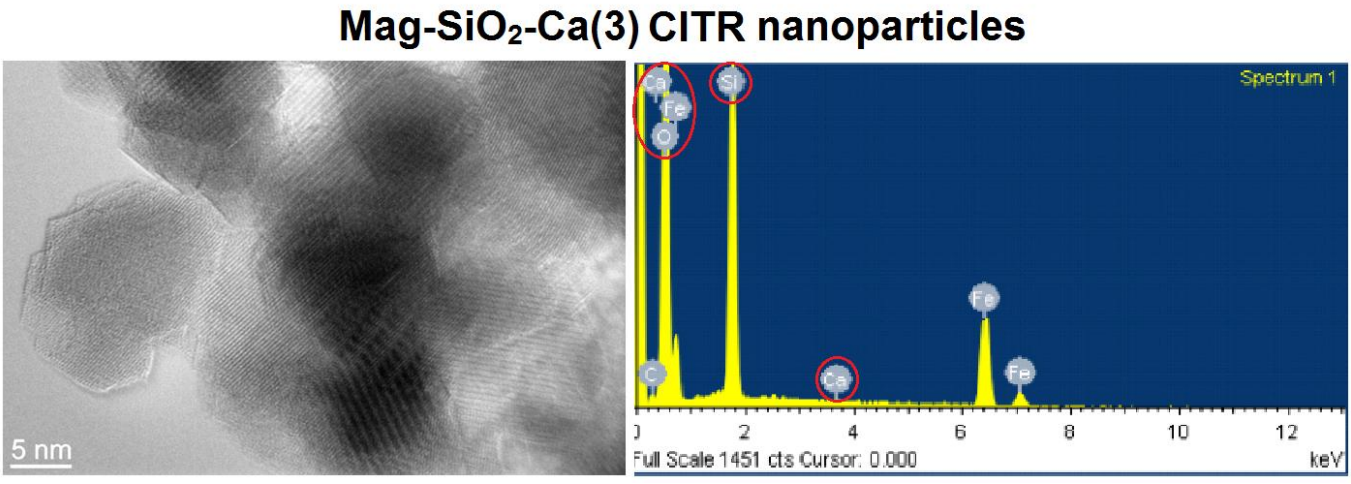

Figure 45. TEM image and EDS spectrum of Mag-SiO_2-Ca(3) CITR NPs.

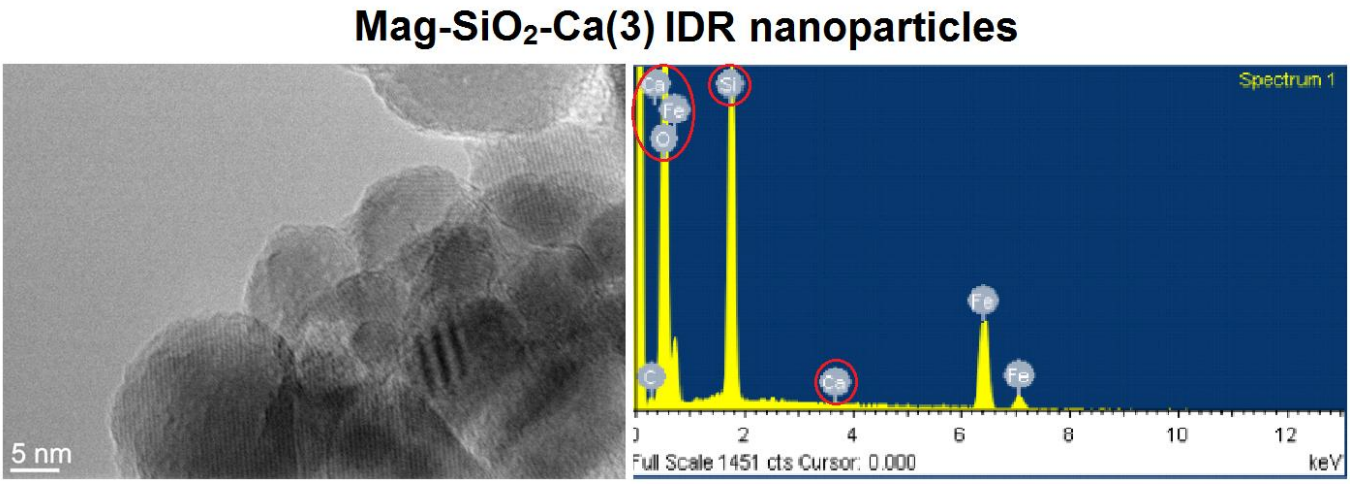

Figure 46. TEM image and EDS spectrum of Mag-SiO_2-Ca(3) IDR NPs.

4.3.3 Magnetic performance

A vibrating sample magnetometer was used to measure the magnetic hysteresis of the magnetic nanoparticles at 300 K in an applied field of ± 15000 g. The results showed that the saturated magnetic intensity of Mag NPs was ± 40.5 emu/g. Instead, the saturated magnetic intensities were ± 3.5 emu/g and ± 4.3 emu/g for Mag-SiO_2 NPs and Mag-SiO_2-Ca(3) CITR and IDR NPs respectively (**Figure 47**). The three lines of the hysteresis loop overlapped, ie, no coercivity was noted, indicating that the magnetic nanoparticles prepared were superparamagnetic.

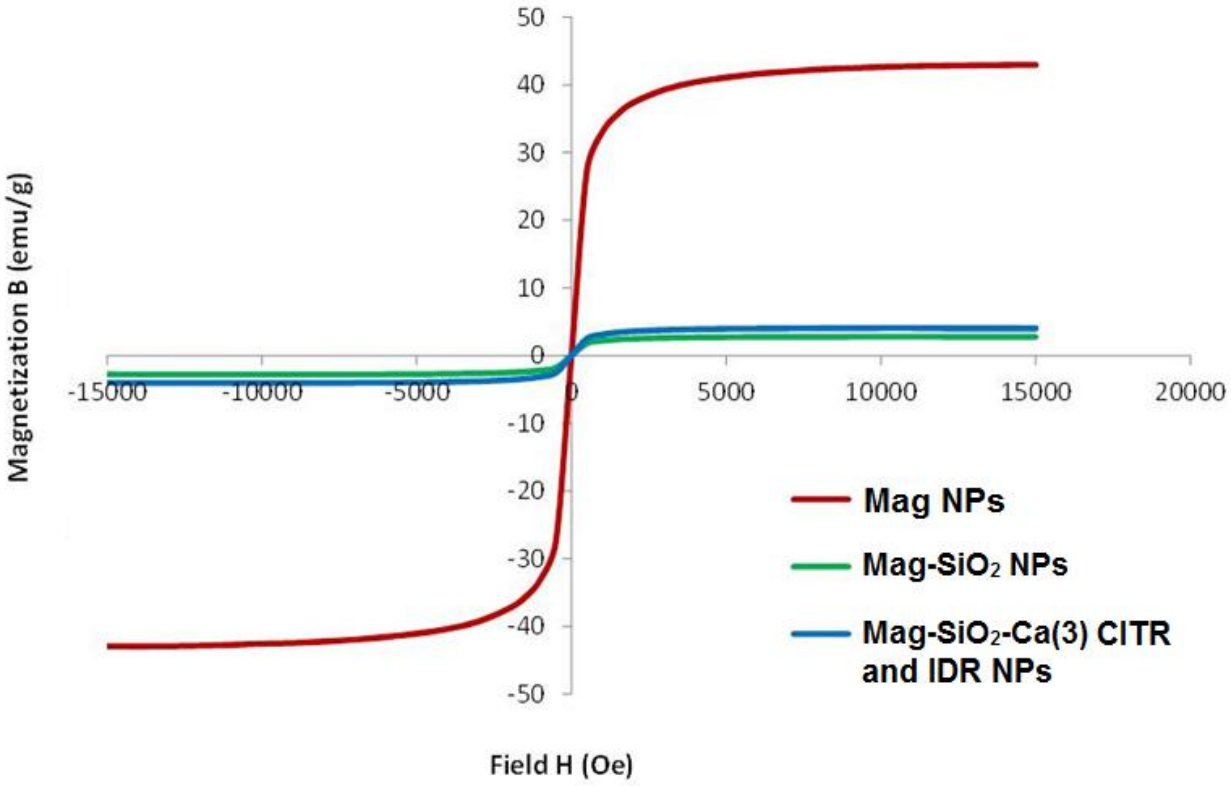

Figure 47. Measurement of the magnetic hysteresis of Mag, Mag-SiO_2, Mag-SiO_2-Ca(3) CITR and IDR NPs - Magnetic performance.

4.3.4 Zeta potential evaluation of third synthesis of MNPs

Zeta-potential measurement is considered as a key parameter for providing an insight into the colloidal stability of the resulting magnetic nanoparticles. The zeta-potential results are shown in **Fig. 48**. The zeta potential of suspension for Mag NPs, Mag-SiO_2 NPs, Mag-SiO_2-Ca(3) CITR and IDR NPs is - 30.23 mV, - 29.41 mV, - 43.14 mV respectively (Table 16). Zeta potential measurements revealed an incipient colloidal instability for Mag-SiO_2 NPs, a moderate colloidal stability for Mag NPs and a good colloidal stability for Mag-SiO_2-Ca(3) CITR and IDR NPs.

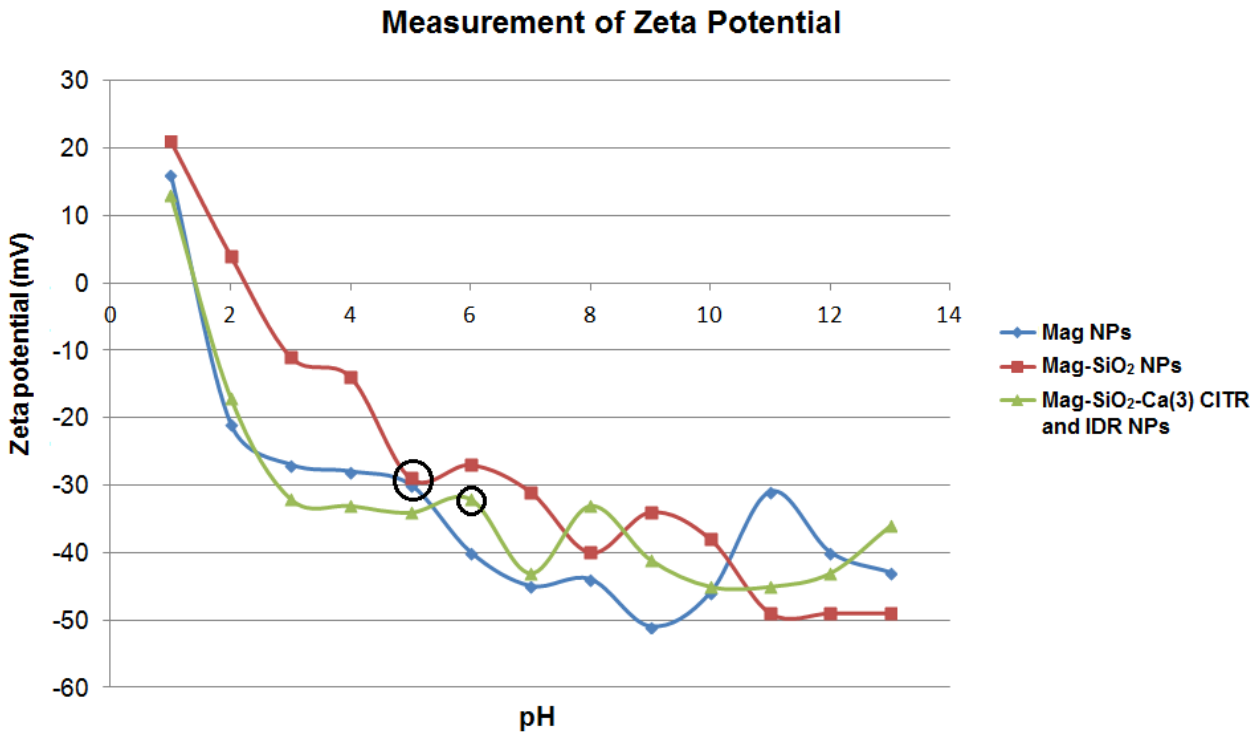

Figure 48. Zeta Potential measurements of third synthesis of MNPs. Data are shown as the mean ± standard deviation (n = 3). The black circles indicate starting pH of the solutions with MNPs.

Sample	Starting pH	ZP (mV)	Stability behaviour of the colloid
Mag NPs	4.26	- 30.23 ± 1.49 mV	Moderate stability
Mag-SiO_2 NPs	4.70	- 29.41 ± 0.81 mV	Incipient instability
Mag-SiO_2-Ca(3) CITR and IDR NPs	5.63	- 43.14 ± 1.95 mV	Good stability

Table 16. Zeta Potential measurements of third synthesis of MNPs. Data are shown as the mean ± standard deviation (n = 3).

4.3.5 Not direct contact cytotoxicity evaluation of third synthesis of MNPs

Cell viability was evaluated with MTT assay (**Figures 49-50**). The percentages of cell viability for not direct contact cytotoxicity evaluation after 24 h were in a range between 91% and 94% for Mag NPs leaching solution (**Fig. 49**). Cell viability after contact with Mag-SiO_2 NPs leaching solution was in a range between 92% and 96% (**Fig. 49**). Moreover, the percentages of cell viability were in

a range between 89% and 93% for Mag-SiO_2-Ca(3) IDR NPs leaching solution and between 88% and 94% for Mag-SiO_2-Ca(3) CITR NPs leaching solution respectively (**Fig. 49**).

Not direct contact cytotoxicity evaluation after 72 h showed a cell viability in range between 89% and 93% for Mag NPs leaching solution (**Fig. 50**). Cell viability after contact with Mag-SiO_2 NPs leaching solution (**Fig. 50**) was in a range between 90% and 95%. Moreover, cell viability after contact with Mag-SiO_2-Ca(3) IDR NPs leaching solution (**Fig. 50**) was in a range between 87% and 93%. Finally, cell viability after contact with Mag-SiO_2-Ca(3) CITR NPs leaching solution (**Fig. 50**) was in a range between 86% and 92%. The results of cytotoxicity evaluation for not direct contact of culture medium DMEM with MNPs using ISO 10993 standards showed a cell viability comparable to control. Trypan blue assay validated the results obtained with MTT assay (**Tables 17 and 18**). Differences were statistically significant at 24, 48 and 72 h time-points ($p < 0.05$).

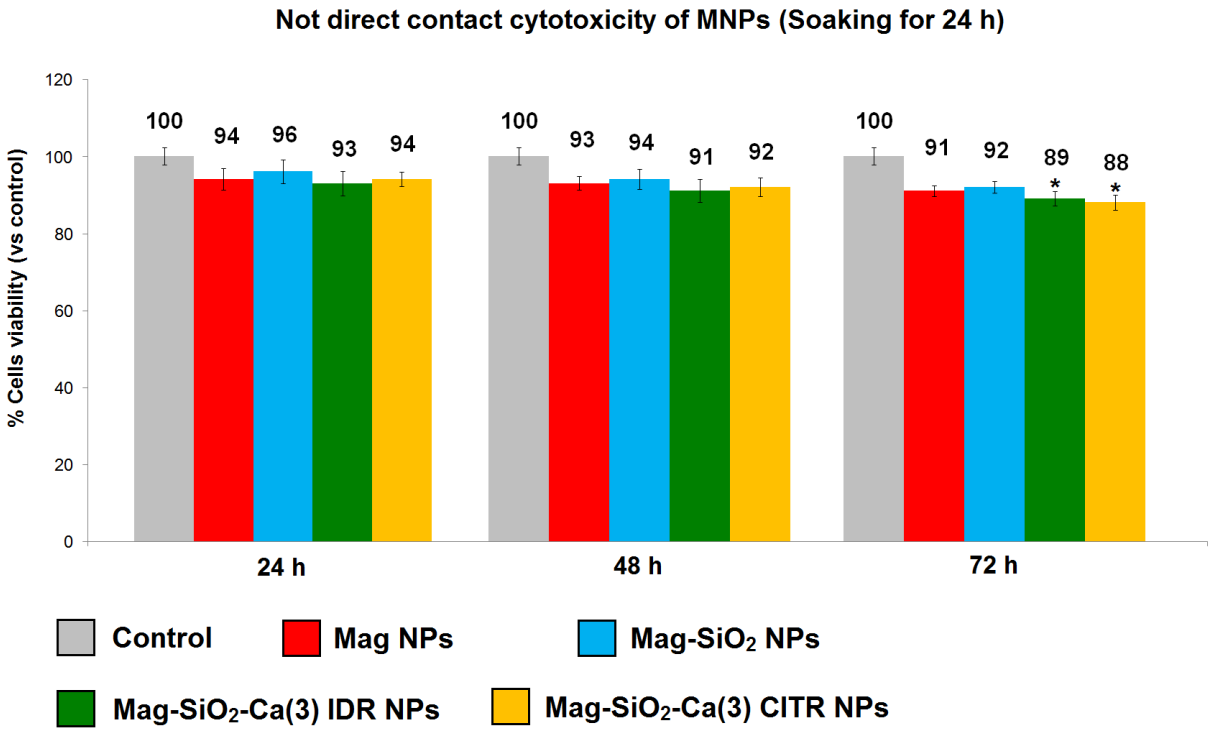

Figure 49. Not direct contact cytotoxicity evaluation of MNPs using murine endothelial cells (MS1 cells) and eluates (24 h of soaking); MTT assay. Data are shown as the mean ± standard deviation (n = 4).

Not direct contact cytotoxicity (37°C for 24 h) - Percentage of TB positive MS1 cells			
Samples	24 h	48 h	72 h
Mag NPs	6.4 ± 0.5	7.3 ± 0.8	9.0 ± 0.8
Mag-SiO_2 NPs	3.8 ± 0.7	5.7 ± 0.5	7.8 ± 0.6
Mag-SiO_2-Ca(3) IDR NPs	6.9 ± 0.8	8.6 ± 0.9	10.5 ± 0.9*
Mag-SiO_2-Ca(3) CITR NPs	5.5 ± 0.6	7.7 ± 0.7	11.7 ± 1.0*

Table 17. Trypan blue exclusion test. MS1 cell mortality after not direct contact with MNPs (37°C for 24 h). Data are shown as the mean ± standard deviation (n = 4).*P < 0.05 compared with control.

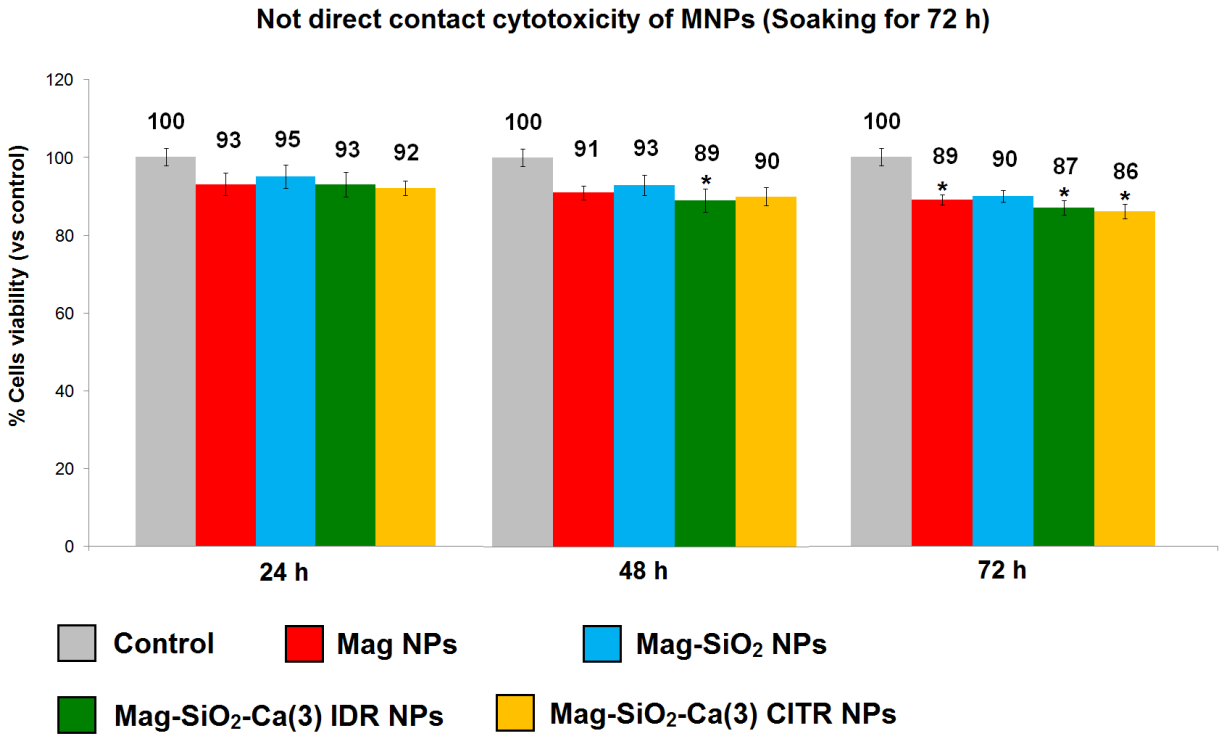

Figure 50. Not direct contact cytotoxicity evaluation of MNPs using murine endothelial cells (MS1 cells) and eluates (72 h of soaking); MTT assay. Data are shown as the mean ± standard deviation (n = 4).

Not direct contact cytotoxicity (37°C for 72 h) - Percentage of TB positive MS1 cells			
Samples	24 h	48 h	72 h
Mag NPs	6.8 ± 0.5	8.7 ± 1.0	10.5 ± 0.8*
Mag-SiO_2 NPs	4.3 ± 0.4	6.5 ± 0.7	9.3 ± 0.6
Mag-SiO_2-Ca(3) IDR NPs	6.7 ± 0.7	10.4 ± 0.8*	12.7 ± 1.1*
Mag-SiO_2-Ca(3) CITR NPs	7.5 ± 0.6	9.8 ± 0.9	13.6 ± 0.7*

Table 18. Trypan blue exclusion test. MS1 cell mortality after not direct contact with MNPs (37°C for 72 h). Data are shown as the mean ± standard deviation (n = 4).*P < 0.05 compared with control.

4.3.6 Direct static contact cytotoxicity

Two different concentrations of MNPs (2 and 20 µg/ml) were used in direct static cytotoxicity tests. After 24 hours, using a concentration of 2 µg/ml of MNPs it was not observed a reduction of cell viability for all MNPs (**Fig. 51**). Afterwards also raising 10-fold the concentration of nanoparticles tested (20 µg/ml) their cytotoxicity did not increase so much but only in a percentage ranging between 4% and 9%. The same trend of cell viability (MS1 cells) was observed after 48 and 72 hours of static direct contact for all nanoparticles (**Fig. 52 and 53**). Mag-SiO_2 nanoparticles (84-95%) showed the endothelial cell viability not significantly different compared to Mag nanoparticles (89-98%). Cell viabilities slightly decreased for Mag-SiO_2-Ca(3) IDR and Mag -SiO_2-Ca(3) CITR nanoparticles but these reductions of cell viability were generally modest (**Fig. 52 and 53**). Trypan blue assay validated the results obtained with MTT assay (**Tables 19-21**). In general these data of cell viability reassure on the cytocompatibility of these nanoparticles in static conditions comparable to the control. No morphological alterations were observed between cells in direct contact with MNPs and control using microscopic observation (**Fig. 54-56**).

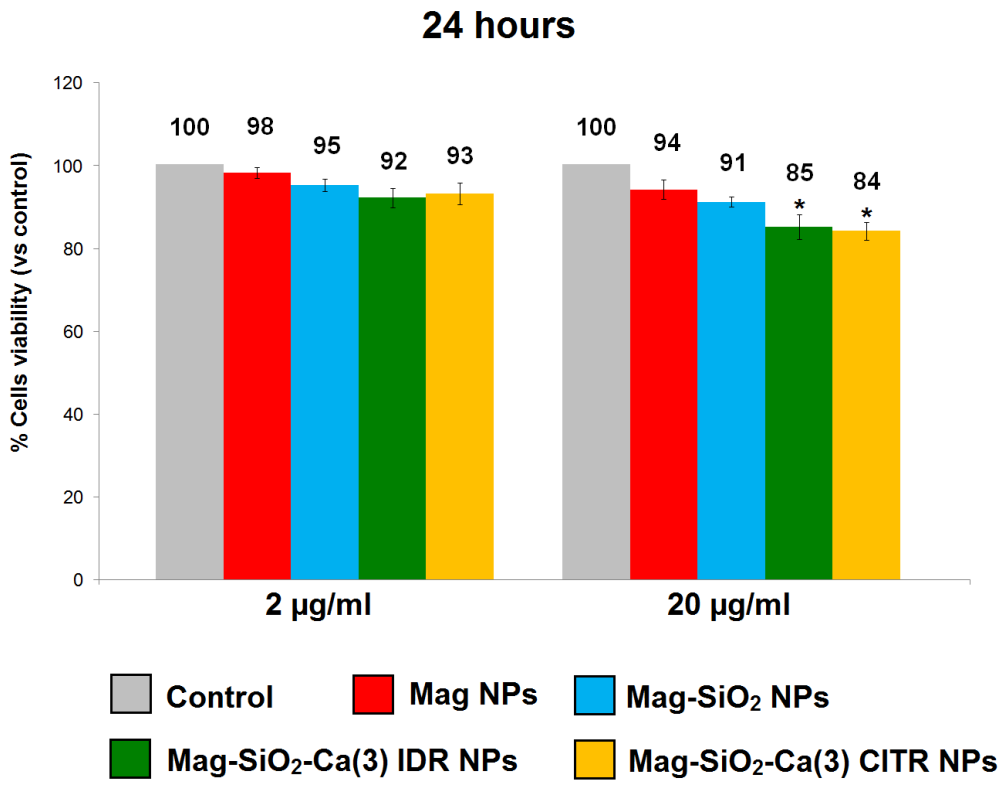

Figure 51. Cytocompatibility assessment of MS1 cells after 24 hours in contact with two concentrations of MNPs (2 and 20 µg/ml). Data are shown as the mean ± standard deviation (n = 4). *P < 0.05 compared with control.

Percentage of TB positive MS1 cells after 24 hours of contact with MNPs

Sample	2 µg/ml	20 µg/ml
Mag NPs	2.1 ± 0.5	6.2 ± 0.7
Mag-SiO_2 NPs	5.2 ± 0.8	8.9 ± 0.6
Mag-SiO_2-Ca(3) IDR NPs	7.8 ± 1.0	15.3 ± 0.9*
Mag-SiO_2-Ca(3) CITR NPs	7.1 ± 0.7	16.0 ± 1.0*

Table 19. Trypan blue exclusion test. MS1 cell mortality after direct contact of 24 hours with nanoparticles. Data are shown as the mean ± standard deviation (n = 4). *P < 0.05 compared with control.

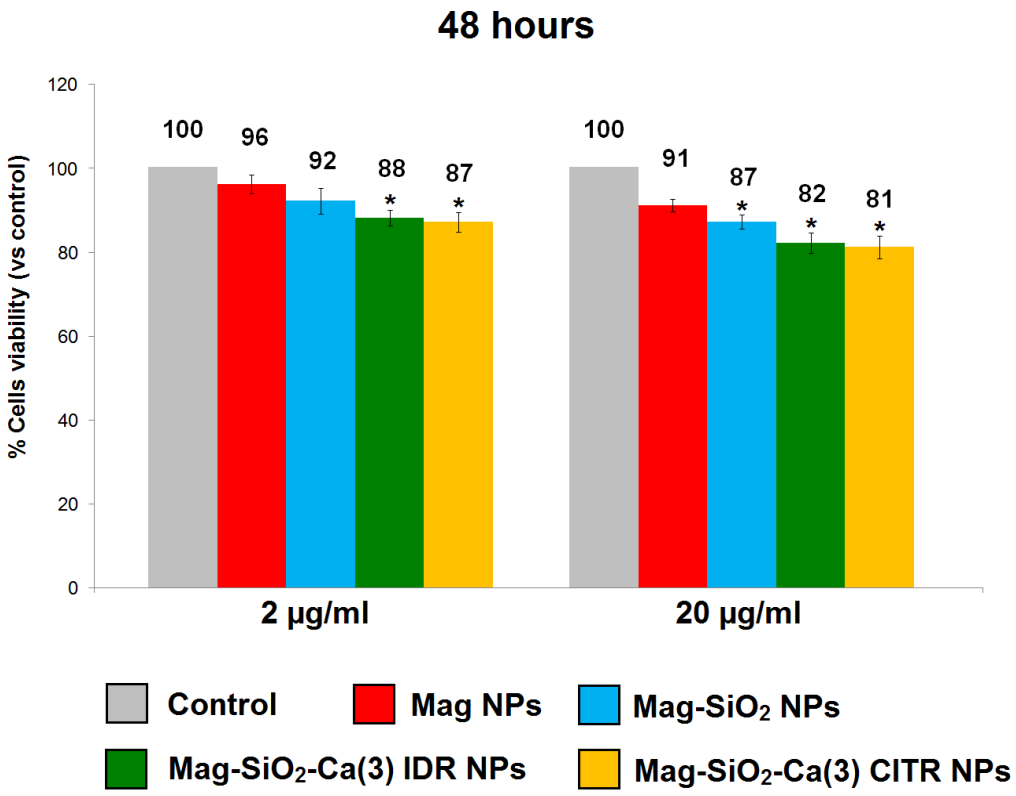

Figure 52. Cytocompatibility assessment of MS1 cells after 48 hours in contact with two concentrations of MNPs (2 and 20 µg/ml). Data are shown as the mean ± standard deviation (n = 4). *P < 0.05 compared with control.

Percentage of TB positive MS1 cells after 48 hours of contact with MNPs

Sample	2 µg/ml	20 µg/ml
Mag NPs	4.2 ± 0.6	9.1 ± 0.5
Mag-SiO_2 NPs	8.1 ± 0.7	13.3 ± 0.7*
Mag-SiO_2-Ca(3) IDR NPs	12.2 ± 0.9*	17.9 ± 0.6*
Mag-SiO_2-Ca(3) CITR NPs	13.1 ± 0.8*	19.2 ± 1.0*

Table 20. Trypan blue exclusion test. MS1 cell mortality after direct contact of 48 hours with nanoparticles. Data are shown as the mean ± standard deviation (n = 4). *P < 0.05 compared with control.

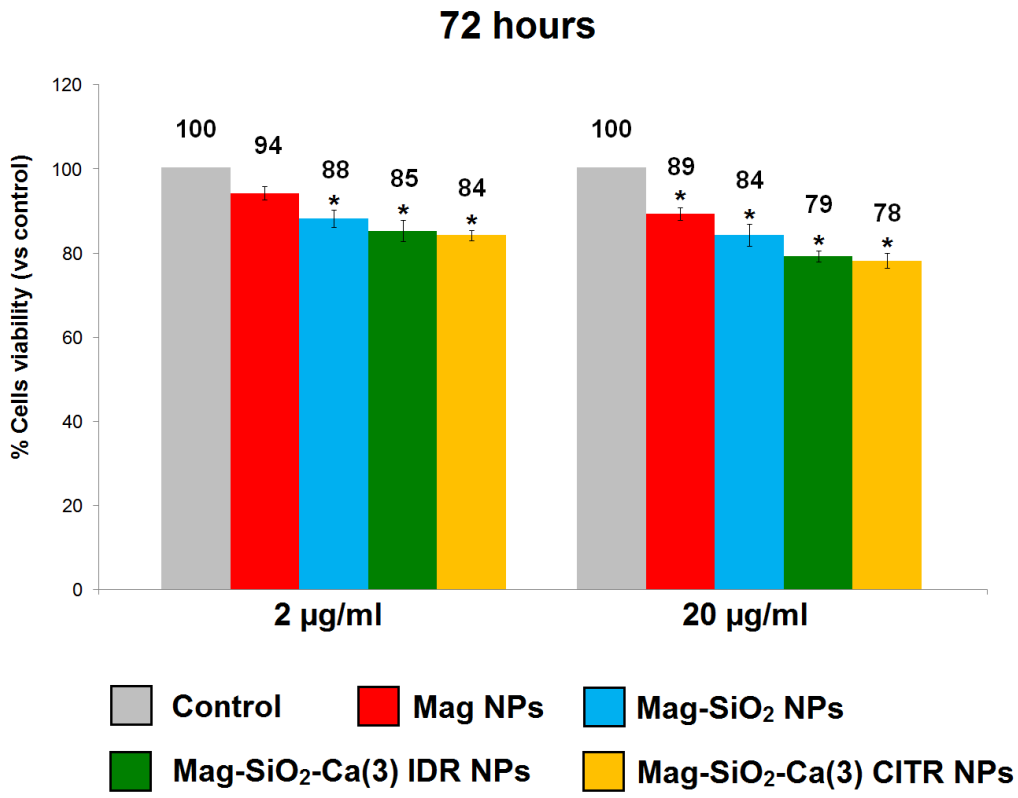

Figure 53. Cytocompatibility assessment of MS1 cells after 72 hours in contact with two concentrations of MNPs (2 and 20 µg/ml). Data are shown as the mean ± standard deviation (n = 4). *P < 0.05 compared with control.

Percentage of TB positive MS1 cells after 72 hours of contact with MNPs

Sample	2 µg/ml	20 µg/ml
Mag NPs	6.3 ± 0.8	10.9 ± 0.9*
Mag-SiO_2 NPs	12.1 ± 0.6*	15.6 ± 0.8*
Mag-SiO_2-Ca(3) IDR NPs	14.7 ± 0.8*	20.7 ± 1.1*
Mag-SiO_2-Ca(3) CITR NPs	15.5 ± 1.0*	21.8 ± 0.7*

Table 21. Trypan blue exclusion test. MS1 cell mortality after direct contact of 72 hours with nanoparticles. Data are shown as the mean ± standard deviation (n = 4). *P < 0.05 compared with control.

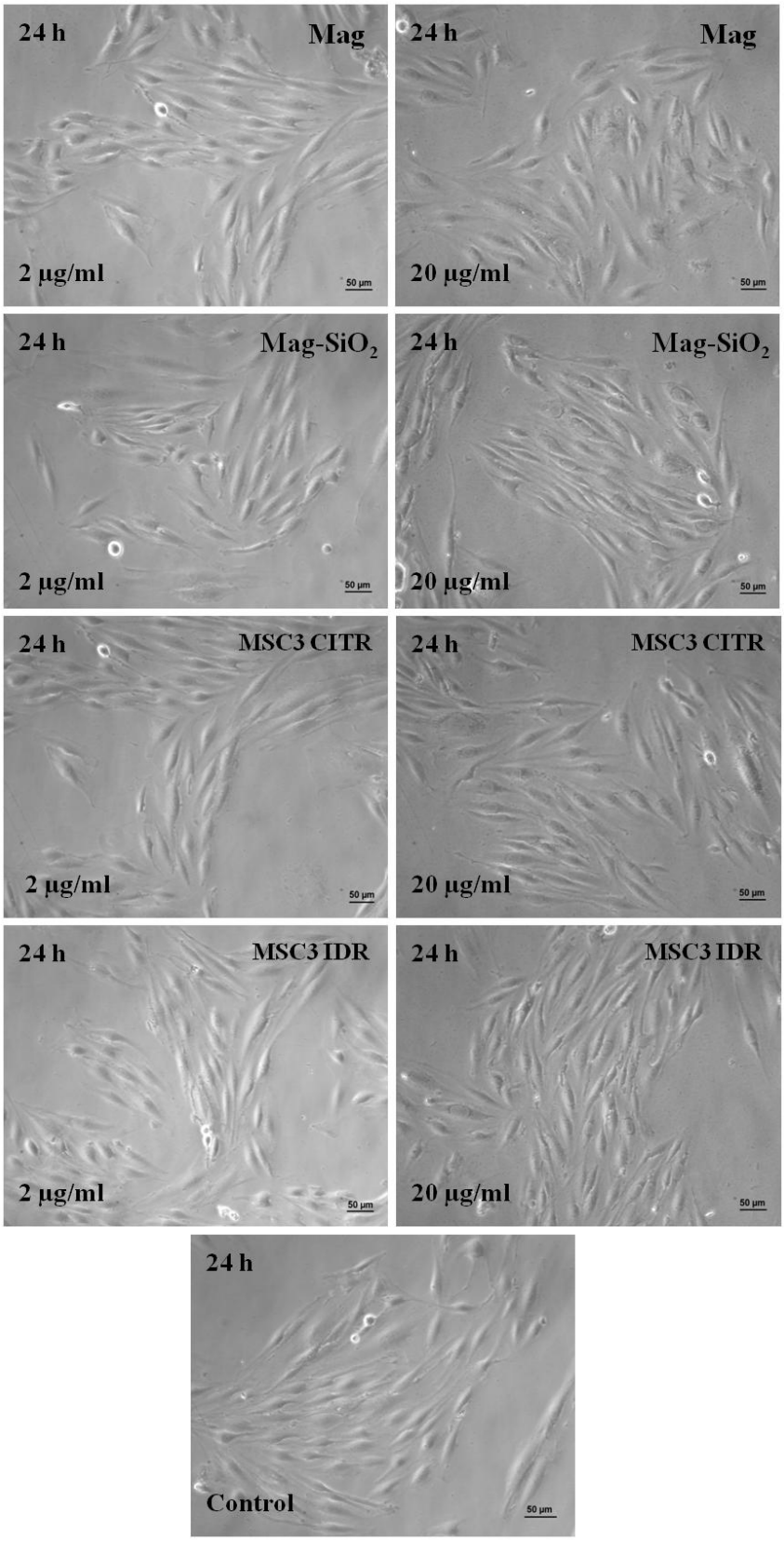

Figure 54. Optical microscopic images of endothelial cells (MS1 cells) after direct contact with MNPs (2 and 20 µg/ml) for 24 hours. Magnification: 20x, bar scale = 50 µm. No effects are observed on cell morphological features.

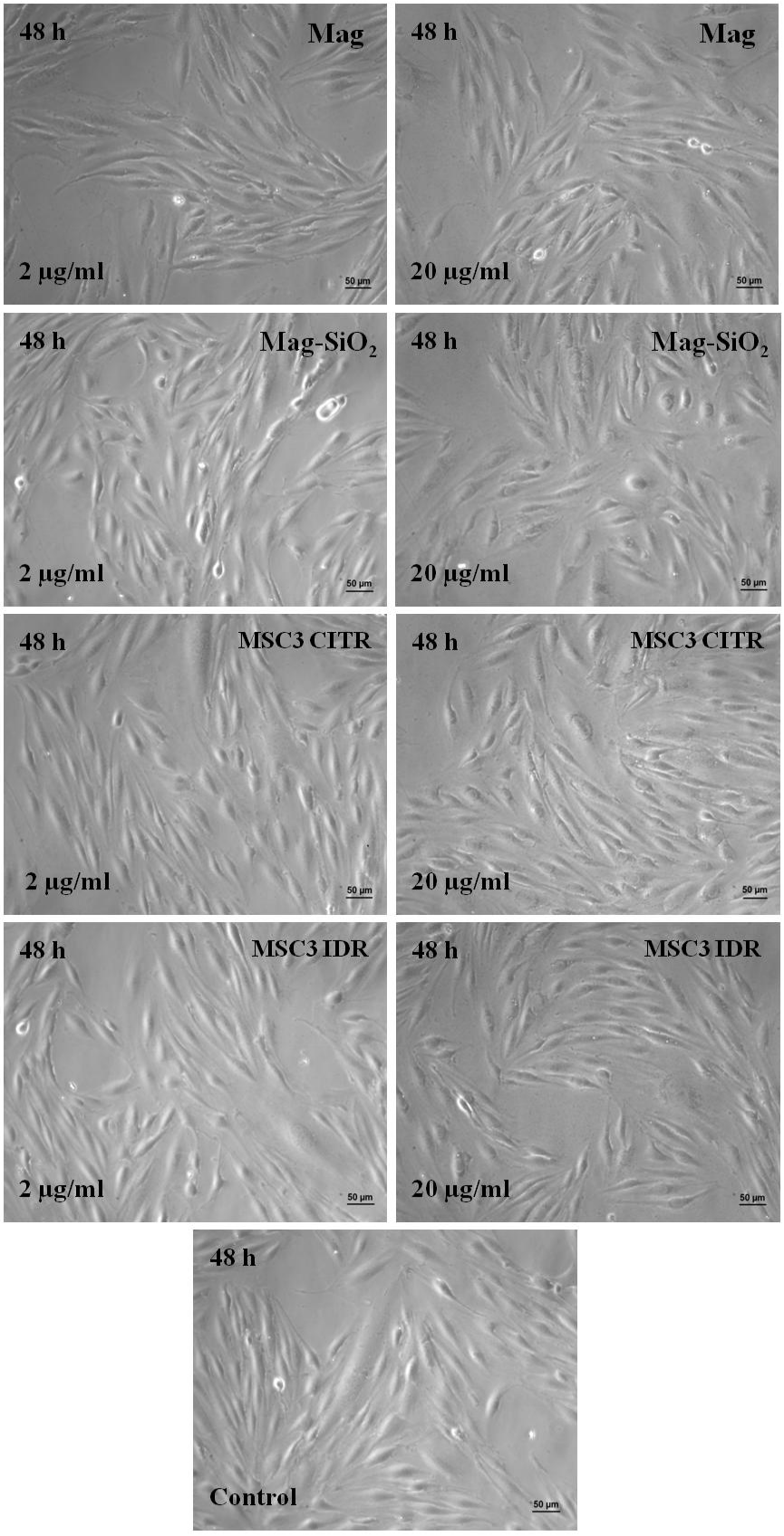

Figure 55. Optical microscopic images of endothelial cells (MS1 cells) after direct contact with MNPs (2 and 20 µg/ml) for 48 hours. Magnification: 20x, bar scale = 50 µm. No effects are observed on cell morphological features.

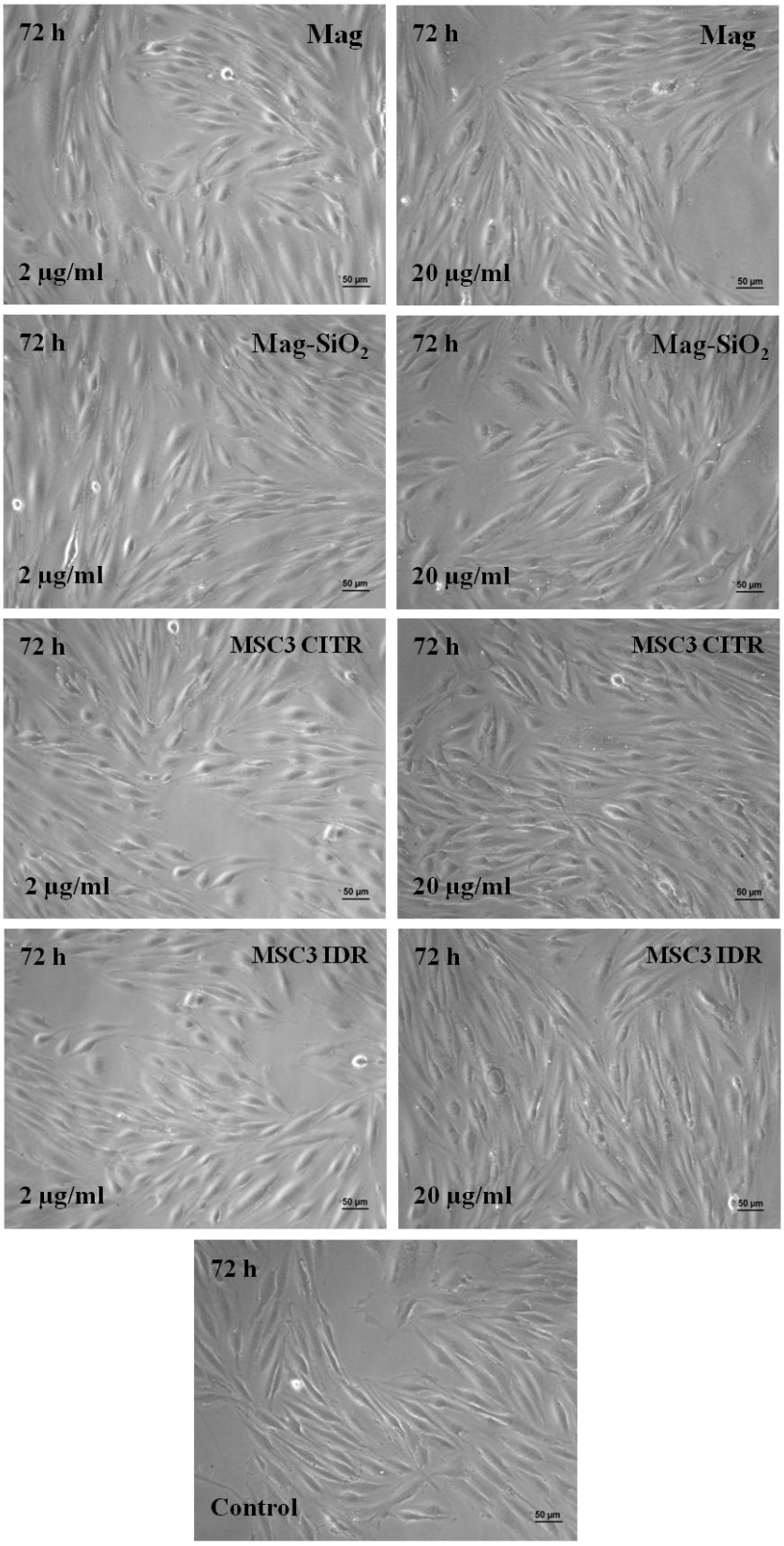

Figure 56. Optical microscopic images of endothelial cells (MS1 cells) after direct contact with MNPs (2 and 20 µg/ml) for 48 hours. Magnification: 20x, bar scale = 50 µm. No effects are observed on cell morphological features.

4.3.7 Cells morphology evaluation by fluorescent microscopy

No cellular morphological alterations were observed between cells in direct contact with MNPs and control using IF staining (**Figures 57-59**). These results confirmed that MNPs had not adverse effects on the cytoskeleton and cell morphology.

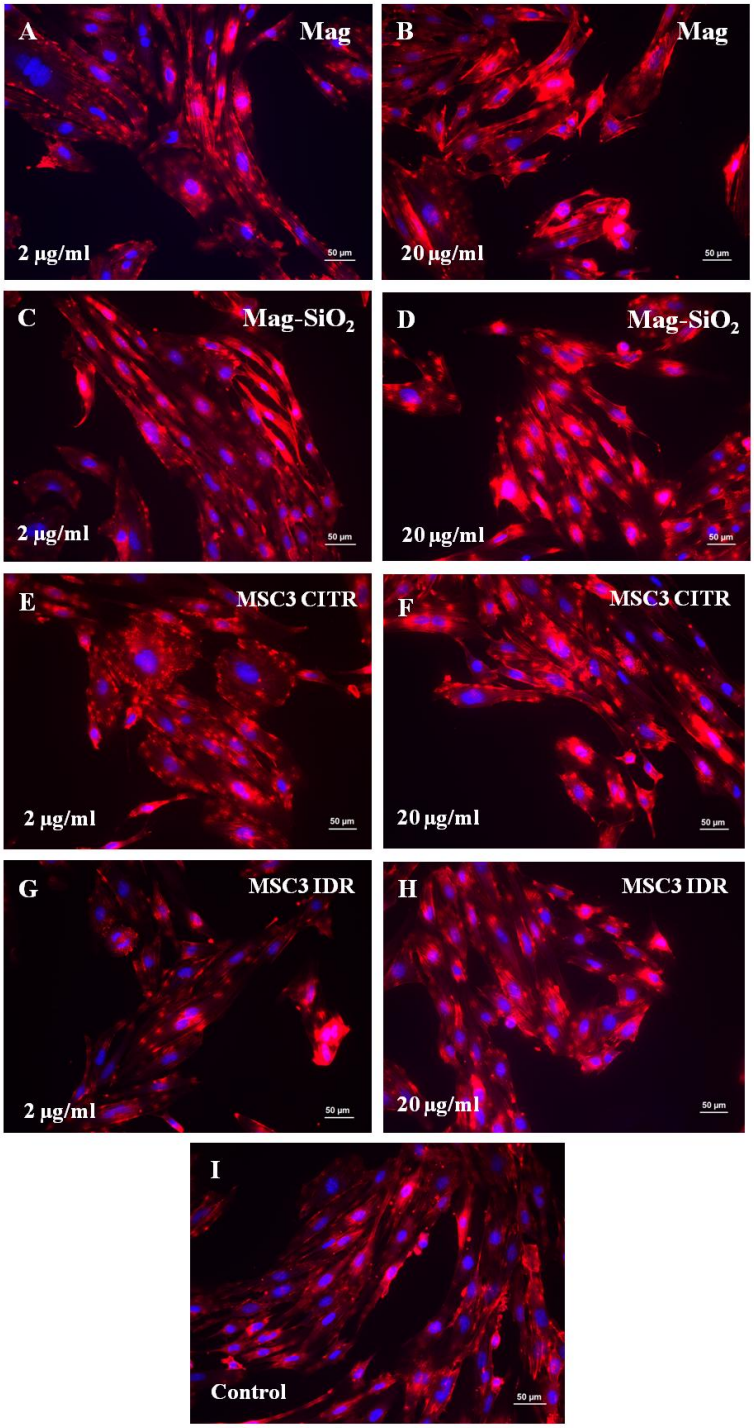

Figure 57. Cells seeded for 24 h in contact with magnetic nanoparticles (2 and 20 µg/ml). IF staining with DAPI (blue) and phalloidin (red). Magnification: 20x, bar scale = 50 µm.

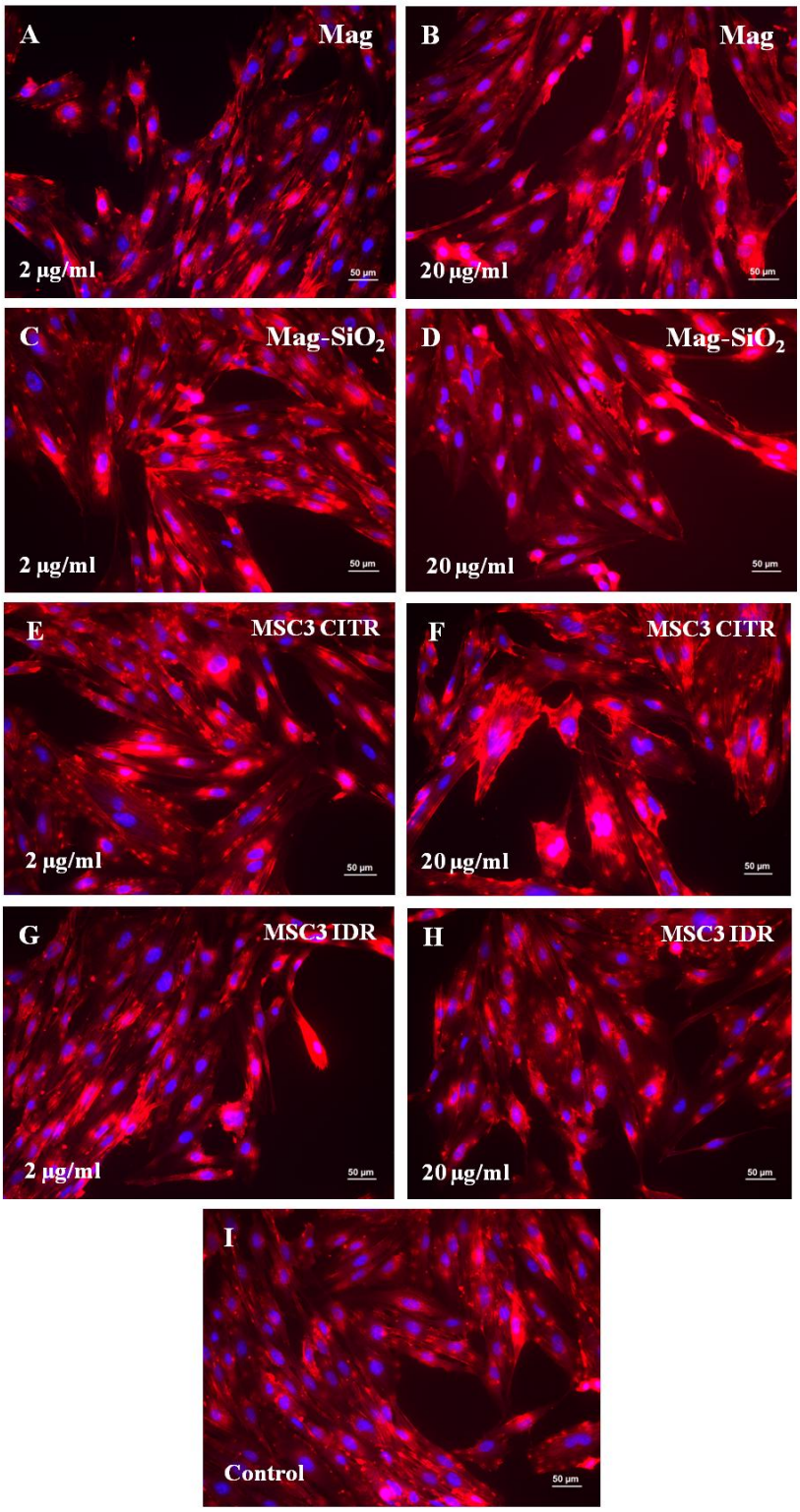

Figure 58. Cells seeded for 48 h in contact with magnetic nanoparticles (2 and 20 µg/ml). IF staining with DAPI (blue) and phalloidin (red). Magnification: 20x, bar scale = 50 µm.

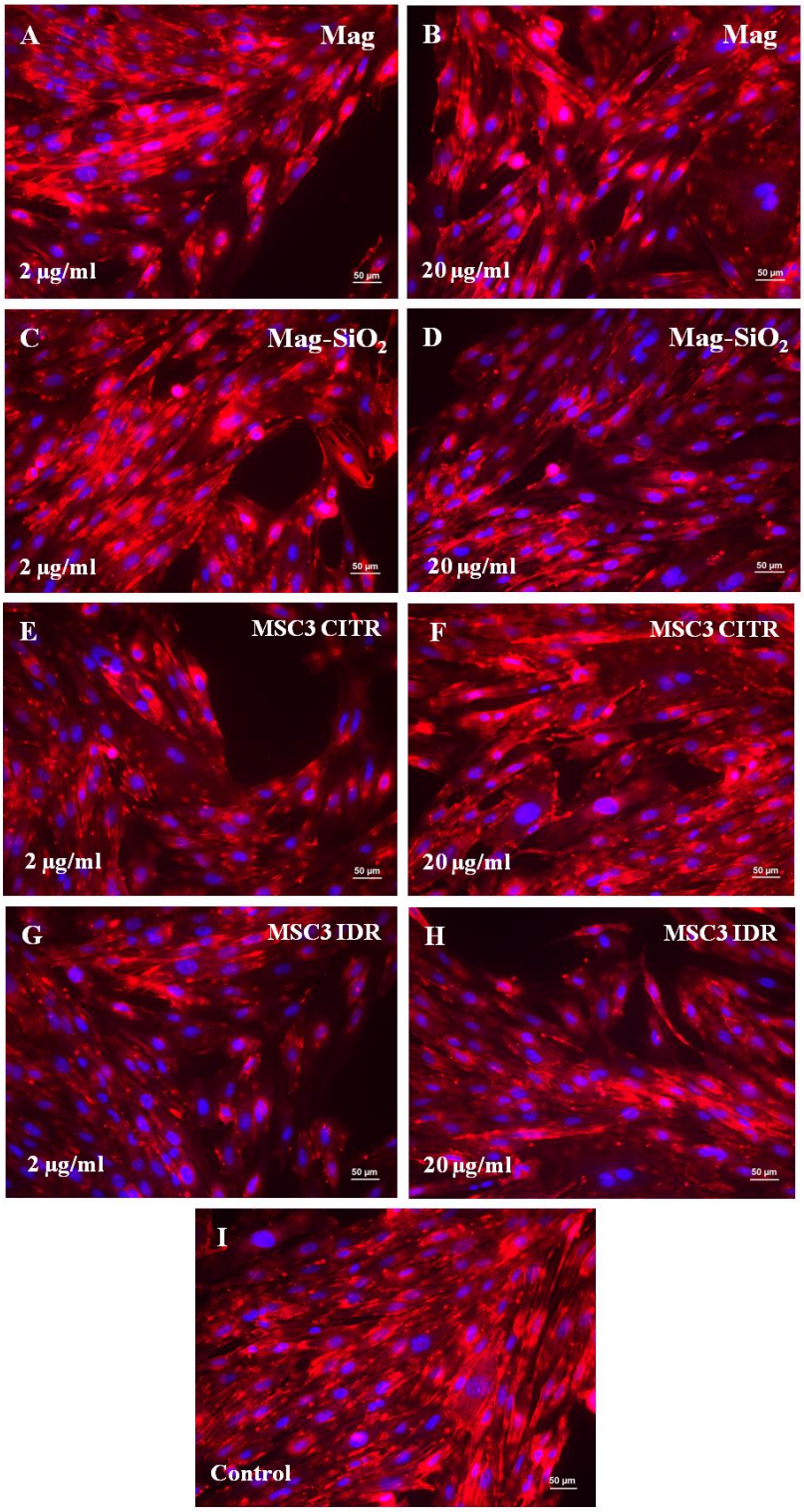

Figure 59. Cells seeded for 72 h in contact with magnetic nanoparticles (2 and 20 µg/ml). IF staining with DAPI (blue) and phalloidin (red). Magnification: 20x, bar scale = 50 µm.

4.3.8 ROS generation induced by MNPs

Naked and silica core-shell type iron oxide nanoparticles could induce the generation of intracellular reactive oxygen species (ROS) depending on the concentration of nanoparticles, and oxidative stress followed by ROS generation may cause damage to mitochondria and DNA. We investigated whether Mag and Mag-SiO_2, Mag-SiO_2-Ca(3) CITR and IDR NPs could induce the generation of intracellular ROS. CellROX Green Reagent was used to determine the generation of intracellular ROS induced by MNPs.

ROS generation was observed in MS1 cells exposed to Mag and Mag-SiO_2, Mag-SiO_2-Ca(3) CITR and Mag-SiO_2-Ca(3) IDR NPs at 2 and 20 µg/ml concentrations for 24 h (**Fig. 60**). An increase in ROS generation was observed in a concentration-dependent manner i.e., 3.75%, 20.04% of ROS expression following the exposure of 2 and 20 µg/ml of Mag NPs, respectively after 24 hours; 2.6%, 13.17% following the exposure of 2 and 20 µg/ml of Mag-SiO_2 NPs; 11.88%, 20.41% following the exposure of 2 and 20 µg/ml of Mag-SiO_2-Ca(3) CITR NPs and 1.01% and 9.52% following the exposure of 2 and 20 µg/ml of Mag-SiO_2-Ca(3) IDR NPs respectively after 24 hours. All data were considered statistically significant ($p < 0.05$).

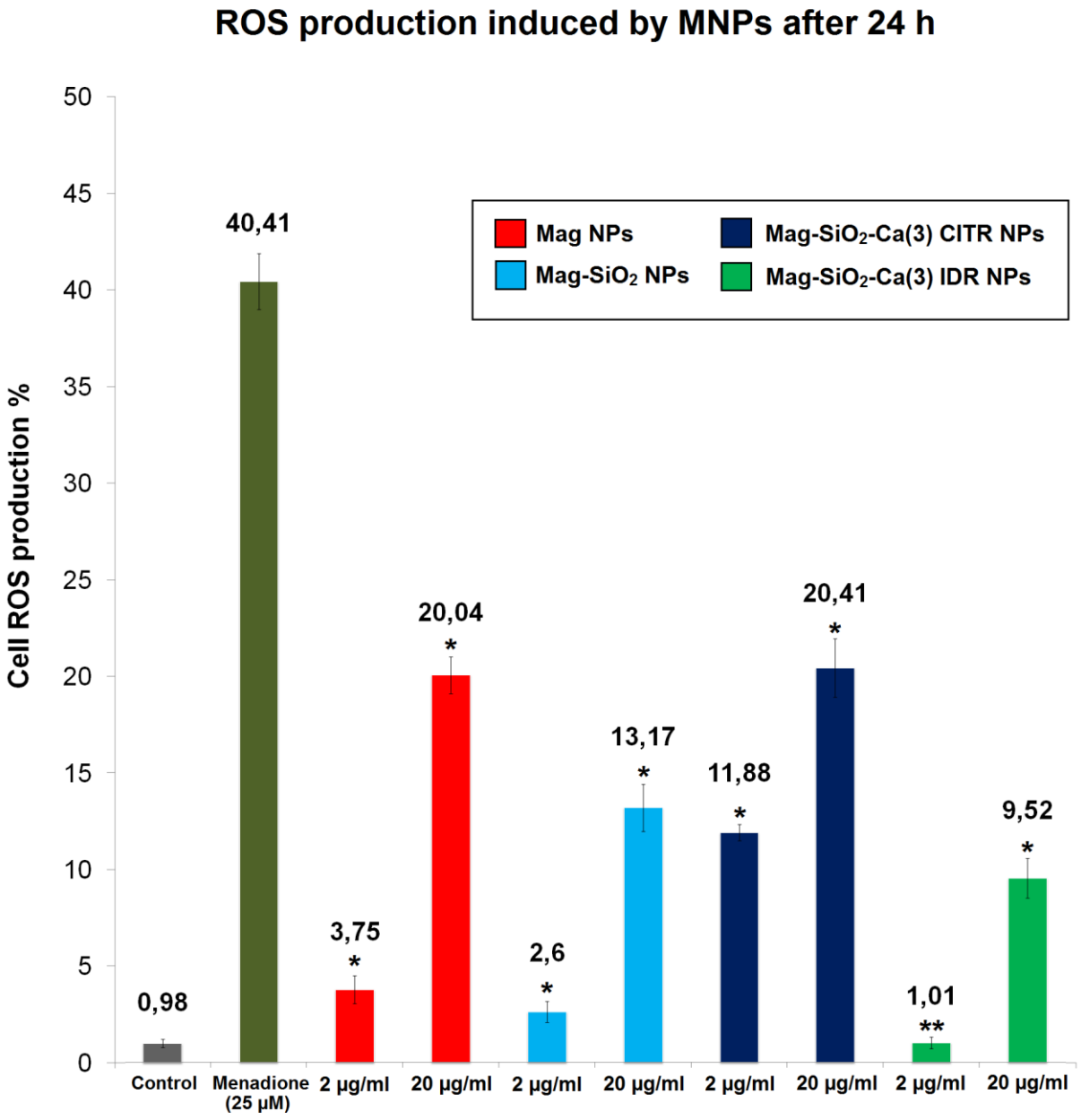

Figure 60. Effect of MNPs on the generation of ROS. Cells were treated with a designated concentration of MNPs for 24 hours. Results are expressed as mean ± SD. *P < 0.05 compared with control untreated and positive control (Menadione 25 µM). **P < 0.05 compared with positive control (Menadione 25 µM).

4.3.9 Apoptosis and necrosis

To further verify the apoptosis process induced by MNPs, Annexin-V/PI double staining was carried out. Annexin V (aV) which is easily reacted with phosphatidylserine (PS) was used as a marker of apoptosis. Propidium iodide (PI), which was utilized to detect plasma membrane integrity, was employed to detect necrotic cell death [103]. Statistical data were extracted from the

pseudo-color dot plot using CellQuest software, based on the percentage of aV−/PI− (viable cells), aV−/PI+ (necrotic cells), aV+/PI− (apoptotic cells), and aV+/PI+ (late apoptotic cells). The data on MS1 cells from the annexin-V staining experiment are summarized in **Fig. 61**. Compared to the negative control group, the percentage of viable cells is similar. MS1 cells did not undergo apoptosis following incubation with MNPs. Flow cytometry demonstrated that treatment with MNPs for 24, 48 and 72 h did not significantly increase the numbers of apoptotic cells compared to control cells. The lower left quadrant represents the living cells, and the upper right quadrant shows the late apoptotic cells, while the lower right quadrant shows the early apoptotic cells in the scatterplot of bivariate flow cytometry (**Figures 62-64**). The percentage of apoptotic cells after direct contact with MNPs was in a range between: 3.74% and 5.56% for 2 µg/ml and 3.31% and 6.3% for 20 µg/ml respectively after 24 hours; 1.29% and 5.7% for 2 µg/ml and 4.44% and 6.05% for 20 µg/ml respectively after 48 hours; 28.19% and 30.31% for 2 µg/ml and 31.29% and 36.4% for 20 µg/ml respectively after 72 hours, compared to 4.16% ± 0.45% at 24 h; 2.05% ± 0.24% at 48 h and 25.25% ± 1.86% for control cells ($P < 0.05$; **Figures 62-64**).

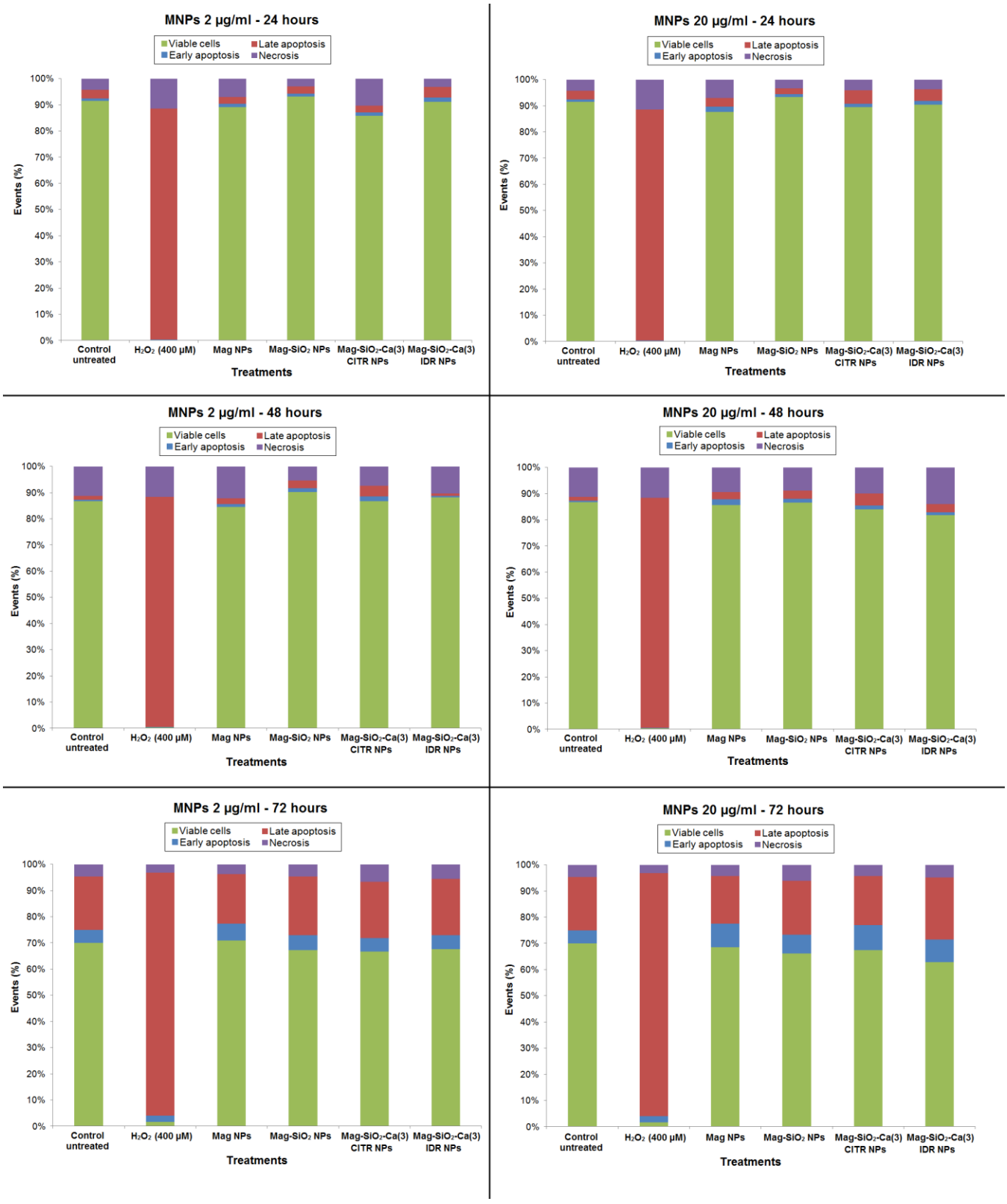

Figure 61. The percentages of apoptosis and necrosis of MS1 cells after the incubation with two concentrations of MNPs: 2 and 20 µg/ml for 24, 48 and 72 h at 37 °C. Values were the means ± SD. * P < 0.05 versus control cells.

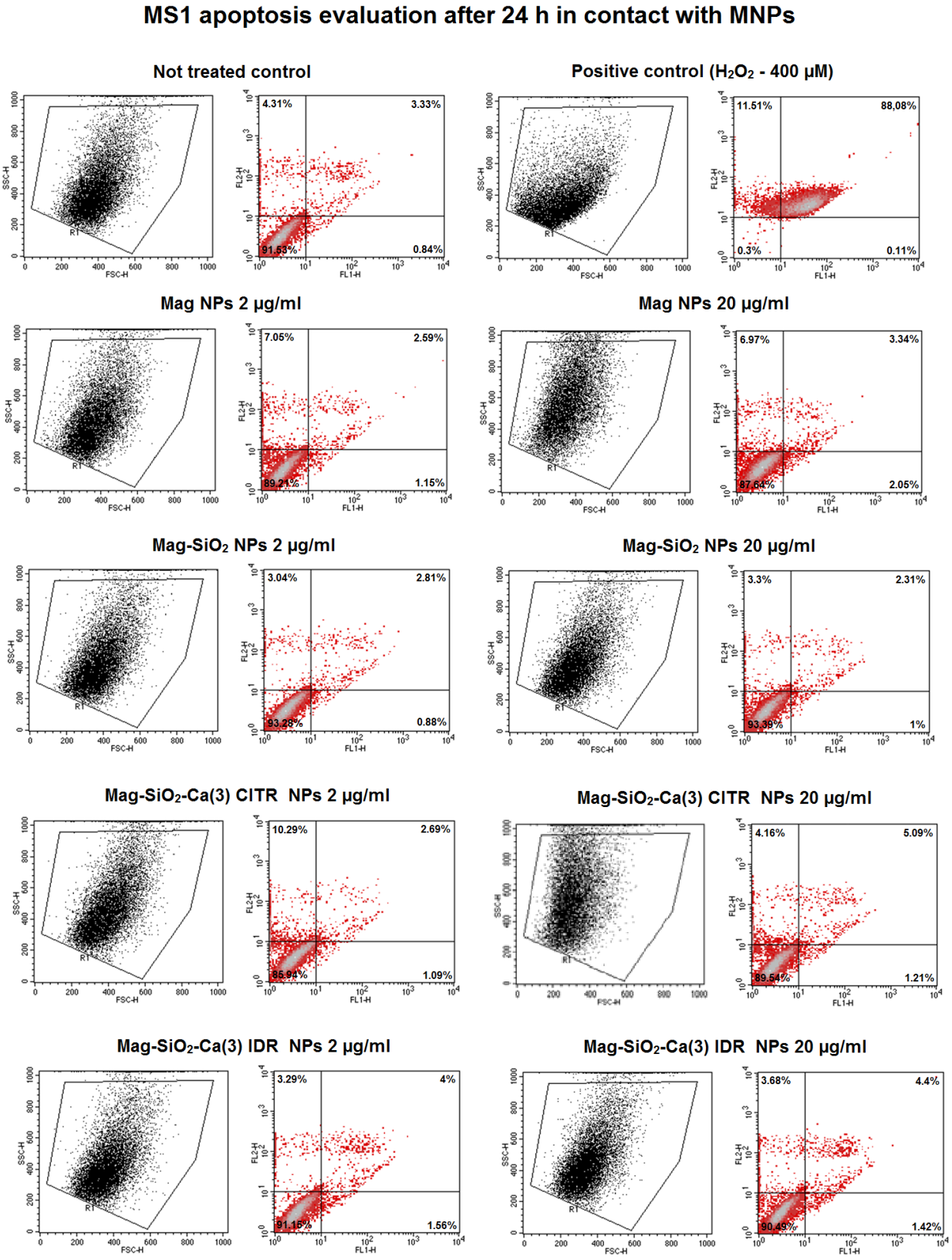

Figure 62. Representative graphs of apoptosis evaluation after 24 hours using Flow cytometry.

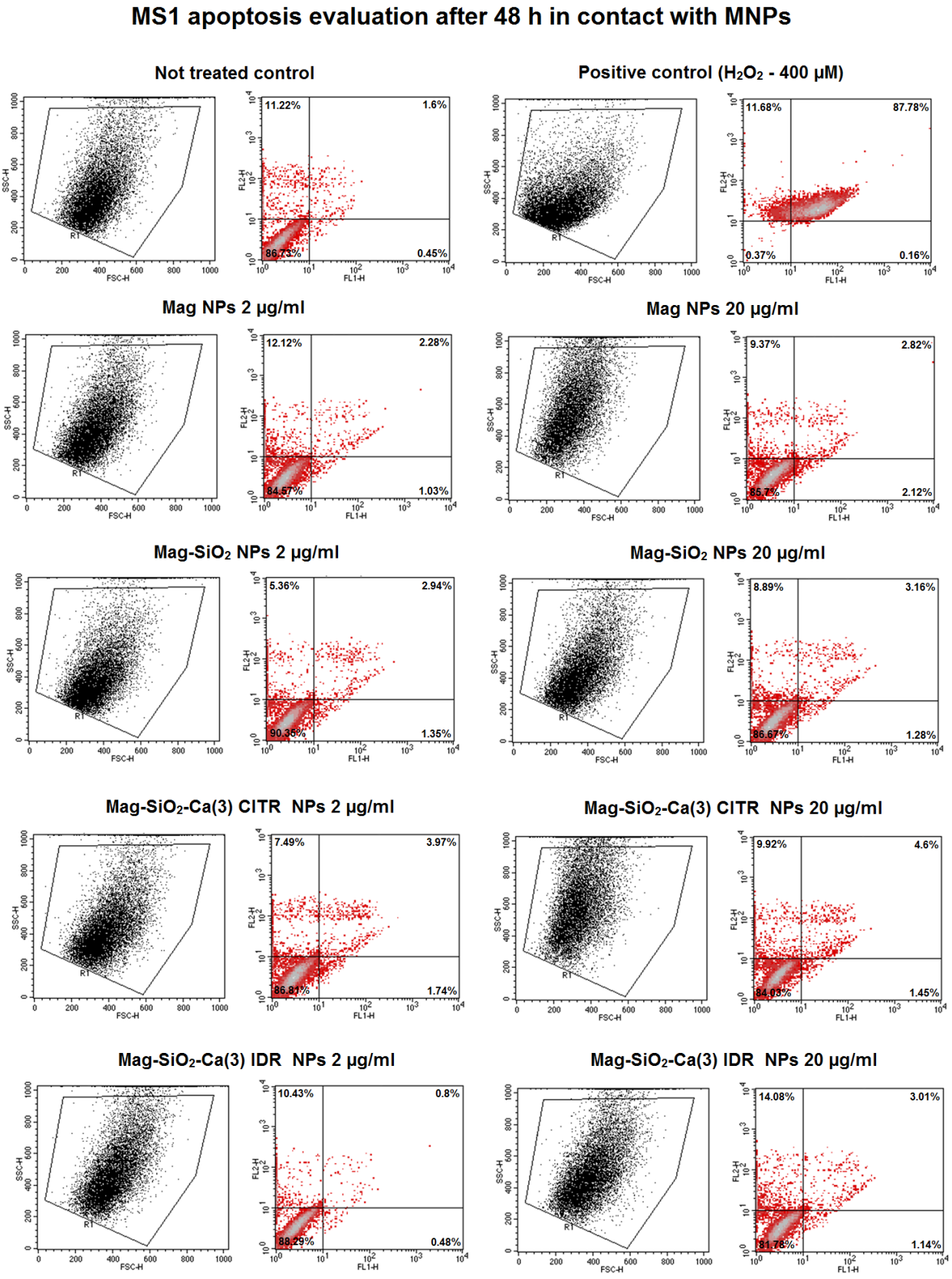

Figure 63. Representative graphs of apoptosis evaluation after 48 hours using Flow cytometry.

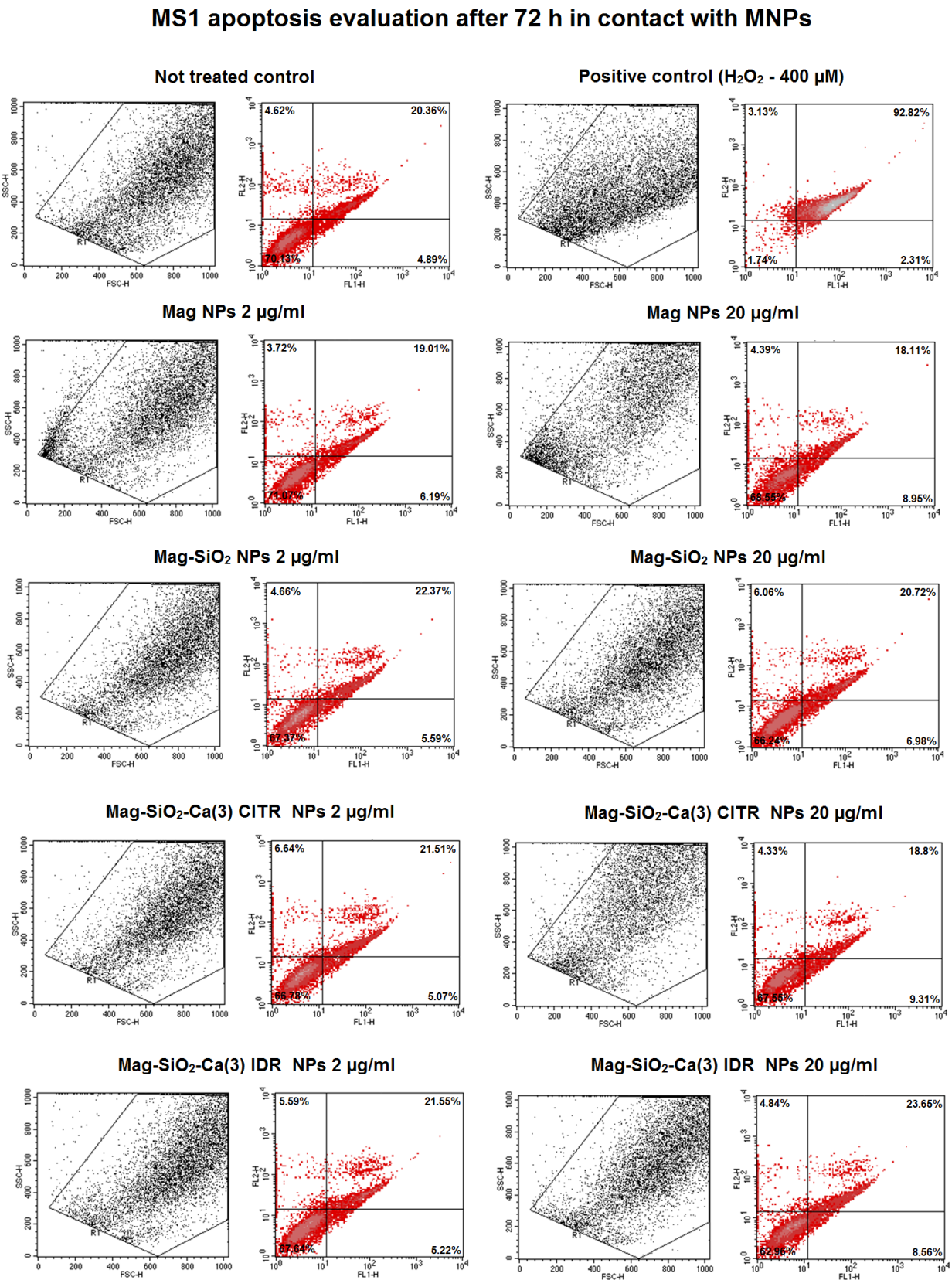

Figure 64. Representative graphs of apoptosis evaluation after 72 hours using Flow cytometry.

4.3.10 Direct contact cytotoxicity in dynamic conditions

The toxicity of MNPs in dynamic conditions was assessed using two different assays: LDH assay and XTT assay. In fact, a comparison between results of two independent assays should provide a higher level of confidence when quantifying toxic effects in dynamic conditions. As first result, it was assumed that the MNPs volumetric concentrations in static and dynamic conditions are comparable because we did not observe a significant decrease in MNPs media concentration after 2 h, 12 h and 24 h of circulation in the fluidic system. A recent report on gravitational sedimentation of MNPs in a cuvette by Alexander et al. (2013) [113] showed that small MNPs did not deposit in significant amounts over 24 h. The same experiment was reproduced with Mag and Mag-SiO_2 nanoparticles confirming this result (data not shown).

Using dynamic conditions of cell culture, the cells morphology appeared typically elongated. MS1 cells showed a cell viability in dynamic conditions comparable to control. Cell viability ranged between 86% and 97% in XTT assay for Mag and Mag-SiO_2 NPs. LDH release was in a range between 2.77 and 3.56% for Mag NPs and between 2.59 and 3.98% for Mag-SiO_2 NPs. LDH cytotoxicity assay confirmed the same trend of XTT assay (**Tables 22-23**). Data from XTT assay were considered statistically significant ($p < 0.05$). FESEM and EDS analyses showed Mag nanoparticles adsorbed onto the MS1 cell membrane. Instead Mag-SiO_2 NPs adsorption was not observed onto cells (**Fig. 65**).

LDH release (% of total)			
Stimulation	Mag NPs	Mag-SiO_2 NPs	Control
2 h	2.77 ± 0.39 %	2.59 ± 0.28%	2.24 ± 0.41%
12 h	3.19 ± 0.46%	3.04 ± 0.35%	2.48 ± 0.30%
24 h	3.56 ± 0.51%	3.98 ± 0.46%	2.74 ± 0.37%

Table 22. Effect on MS1 cell-membrane integrity following exposure to MNPs in dynamic conditions. Data are shown as the mean ± standard deviation.

XTT assay			
Stimulation	Mag NPs	Mag-SiO_2 NPs	Control
2 h	93.8 ± 4.2%	96.9 ± 3.7%	100%
12 h	89.5 ± 2.8%*	93.1 ± 3.3%	100%
24 h	86.8 ± 3.1%*	90.9 ± 2.7%	100%

Table 23. MS1 cell viability following exposure to MNPs in dynamic conditions; XTT assay. Data are shown as the mean ± standard deviation *P < 0.05 compared with control.

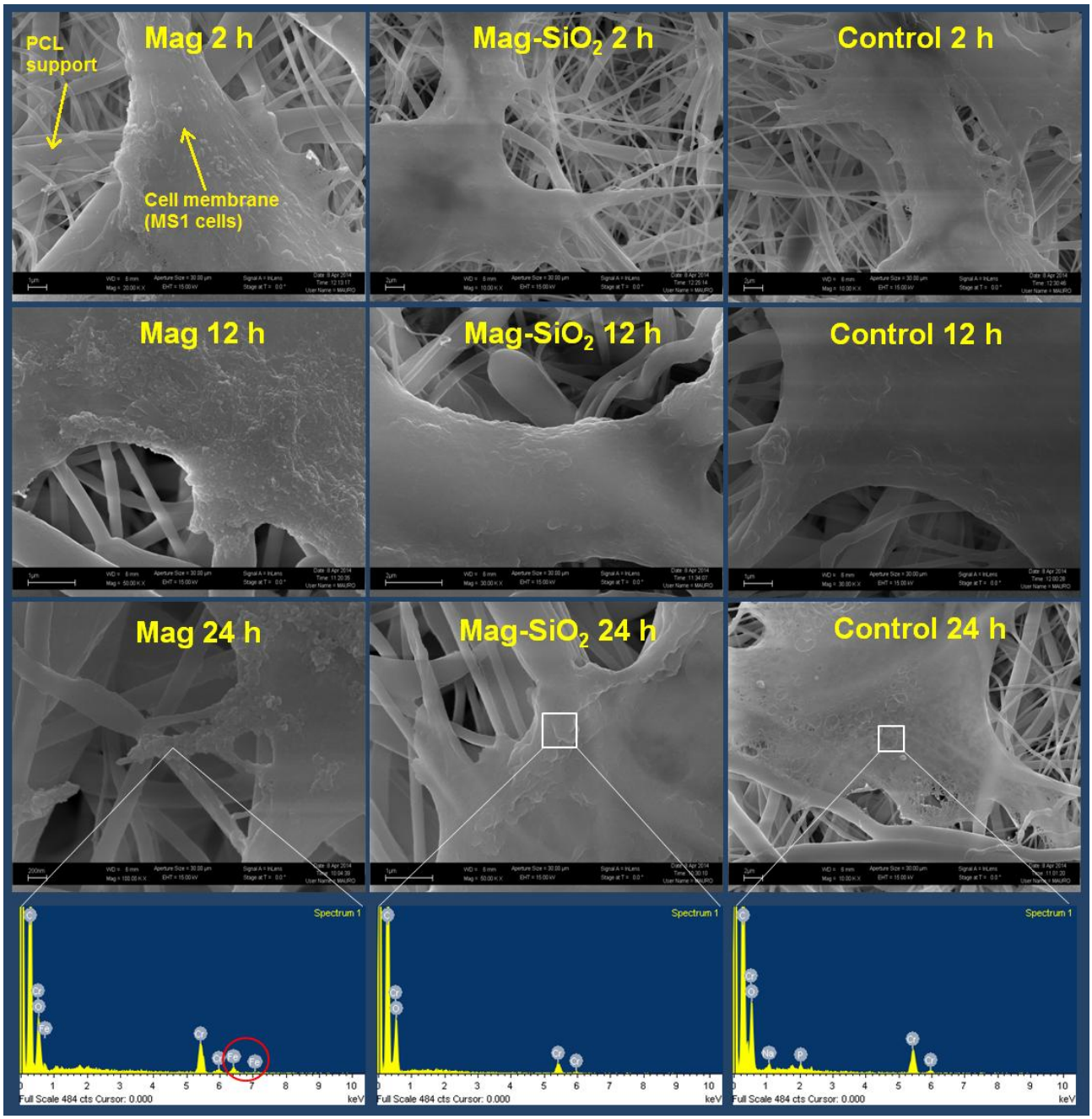

Figure 65. FESEM images and EDS spectrum of MS1 cells on polycaprolactone in dynamic conditions. Only Mag nanoparticles were adsorbed onto the MS1 cell membrane.

4.3.11 Macroscopic evaluation of organs

No death was after injection of either Mag or Mag-SiO_2 NPs either for doses of 2 and 20 mg Fe/kg. Mice showed no anorexia, lethargy, and lusterless skin symptoms. After 7 days, animals were euthanized and autopsied for both types and doses of MNPs and control. The autopsy revealed many organ alterations in animals injected with 20 mg Fe/kg Mag-SiO_2: splenomegaly, bleeding in lymph nodes and hepatomegaly (**Table 24**). No organ alterations were observed for 2 mg Fe/kg for both Mag and Mag-SiO_2 NPs in comparison with the control (**Table 25**).

Organ	Mag NPs	Mag-SiO2 NPs	Control
Liver	1,69 ± 0,07 g	1,79 ± 0,12 g	1,68 ± 0,08 g
Spleen	122,5 ± 12,4 mg	275,2 ± 38,7 mg	91,5 ± 18,7 mg
Left Kidney	136,5 ± 33,2 mg	144,5 ± 38,9 mg	126 ± 22,6 mg
Right Kidney	146,5 ± 36,5 mg	158 ± 39,9 mg	132,2 ± 19,7 mg
Brain	439,7 ± 9,1 mg	436,5 ± 16,3 mg	433,2 ± 12,1 mg
Lung	142,2 ± 12,5 mg	146,7 ± 18,1 mg	138,2 ± 14,3 mg
Heart	163 ± 45,5 mg	166,7 ± 41,8 mg	158 ± 51,6 mg

Table 24. Organ weights after MNPs injection at the dose of 20 mg Fe/kg. Data are shown as the mean ± standard deviation (n = 3). In red the most relevant alterations.

Organ	Mag NPs	Mag-SiO2 NPs	Control
Liver	1,37 ± 0,18 g	1,23 ± 0,22 g	1,46 ± 0,07 g
Spleen	94 ± 12,9 mg	102 ± 6,4 mg	100,3 ± 15,5 mg
Left Kidney	151,5 ± 20,8 mg	144,5 ± 22,2 mg	176,8 ± 8,3 mg
Right Kidney	165,2 ± 27,5 mg	164,5 ± 36,8 mg	177,5 ± 4,2 mg
Brain	421,5 ± 41,3 mg	415 ± 52,5 mg	441,5 ± 18,3 mg
Lung	157,5 ± 11,1 mg	166,8 ± 6,5 mg	170 ± 7,4 mg
Heart	167 ± 29,7 mg	157,8 ± 37,8 mg	173,8 ± 8,2 mg

Table 25. Organ weights after MNPs injection at the dose of 2 mg Fe/kg. Data are shown as the mean ± standard deviation (n = 3).

4.3.12 Hematological parameters evaluation

MNPs stabilized with silica coatings have been evaluated for safety following i.v. injection into mice using two doses: 2 and 20 mg Fe/kg. For the dose of 20 mg Fe/kg different alterations were observed for serum biomarkers and hematological parameters in particular for Mag-SiO_2 NPs respect to Mag NPs (Tables 26 and 27). In addition, these alterations for Mag-SiO_2 NPs (20 mg Fe/kg) were also reported in the histological sections and in ICP-AES measurement, as indicated below. However for both concentrations there was no death after injection of either Mag or Mag-SiO_2 at a dose of 20 mg/kg and all mice showed no anorexia, lethargy, and lusterless skin symptoms. Instead for the concentration of 2 mg Fe/kg although a bit of the injected nanoparticles accumulated in the liver and spleen at 7 days post injection, such accumulation did not result in any notable or long-term alteration of hematological parameters and serum biomarker levels such as alanine aminotransferase, aspartate aminotransferase, creatinine and lactic acid dehydrogenase, which are indicative of the liver functionality (Tables 28 and 29). Hematological parameters and serum biomarkers altered were considered statistically significant ($p < 0.05$).

	Control	**Mag NPs**	**Mag-SiO_2 NPs**
Red blood cell (10^6/µl) after 3 days	**8.77 ± 1.07**	**8.86 ± 0.91**	**8.52 ± 1.12**
Red blood cell (10^6/µl) after 7 days	**8.74 ± 1.13**	**8.93 ± 1.15**	**8.44 ± 1.31**
White blood cell (10^3/µl) after 3 days	**6.50 + 1.48**	**6.85 + 2.03**	**7.70 + 1.71***
White blood cell (10^3/µl) after 7 days	**6.47 ± 1.66**	**6.93 ± 1.48**	**7.81 ± 1.57***

Table 26. Hematological parameters in the mice groups injected with MNPs at concentrations of 20 mg Fe/kg in mice. Data are shown as the mean ± standard deviation. In red the most relevant alterations. *P < 0.05 compared with control.

	Control	Mag NPs	Mag-SiO_2 NPs
ALT (U/l)	**39.89 ± 3.63**	**41.78 ± 3.26**	**48.4 ± 2.04***
AST (U/l)	**128.54 ± 13.41**	**132.81 ± 8.11**	**147.58 ± 15.01***
CRE (µmol/l)	**19.6 ± 1.32**	**20.33 ± 1.52**	**25.96 ± 1.35***
LDH (U/l)	**837.67 ± 80.43**	**849.77 ± 88.91**	**908.07 ± 87.08***

Table 27. Serum biomarker levels in the mice groups injected with MNPs at concentrations of 20 mg Fe/kg in mice. Data are shown as the mean ± standard deviation. In red the most relevant alterations. *P < 0.05 compared with control.

	Control	Mag NPs	Mag-SiO_2 NPs
Red blood cell (10^6/µl) after 3 days	**9.83 ± 0.52**	**9.76 ± 0.93**	**9.71 ± 1.19**
Red blood cell (10^6/µl) after 7 days	**9.75 ± 0.83**	**9.69 ± 1.07**	**9.64 ± 0.71**
White blood cell (10^3/µl) after 3 days	**6.51 ± 0.73**	**6.63 ± 1.18**	**6.72 ± 1.26**
White blood cell (10^3/µl) after 7 days	**6.57 ± 1.14**	**6.73 ± 1.22**	**6.88 ± 1.61**

Table 28. Hematological parameters in the mice groups injected with MNPs at concentrations of 2 mg Fe/kg in mice. Data are shown as the mean ± standard deviation. In red the most relevant alterations.

	Control	Mag NPs	Mag-SiO_2 NPs
ALT (U/l)	**39.42 ± 2.69**	**43.15 ± 2.72**	**44.26 ± 2.06***
AST (U/l)	**127.35 ± 12.07**	**129.34 ± 7.12**	**134.81 ± 6.83**
CRE (µmol/l)	**19.21 ± 1.25**	**21.91 ± 1.03**	**23.48 ± 1.47***
LDH (U/l)	**833.75 ± 53.28**	**841.67 ± 57.91**	**843.46 ± 46.35**

Table 29. Serum biomarker levels in the mice groups injected with MNPs at concentrations of 2 mg Fe/kg in mice. Data are shown as the mean ± standard deviation. *P < 0.05 compared with control.

4.3.13 Iron uptake quantification

To quantify the nanoparticles uptaking in major organs, the iron content was measured by ICP-AES. Iron uptake was higher in liver in 2 mg Fe/kg Mag-SiO_2 group compared to Mag group and control. Iron uptake in 2 mg Fe/kg MNPs groups in other organs was comparable to that of control (**Fig. 66 and Table 30**). Data recorded in 20 mg Fe/kg MNPs presented high variability but generally the iron was mainly accumulated in liver and spleen ($p < 0.05$) (**Fig. 67 and Table 31**). No accumulation was observed in kidney, brain, lung and heart. Therefore in 20 mg Fe/kg group the organ were for iron accumulation as follows: 1) spleen, 2) liver, 3) heart, 4) lung, 5) kidney and 6) brain. In 20 mg Fe/kg Mag-SiO_2 group spleens accumulated more iron than those of Mag group ($p < 0.05$).

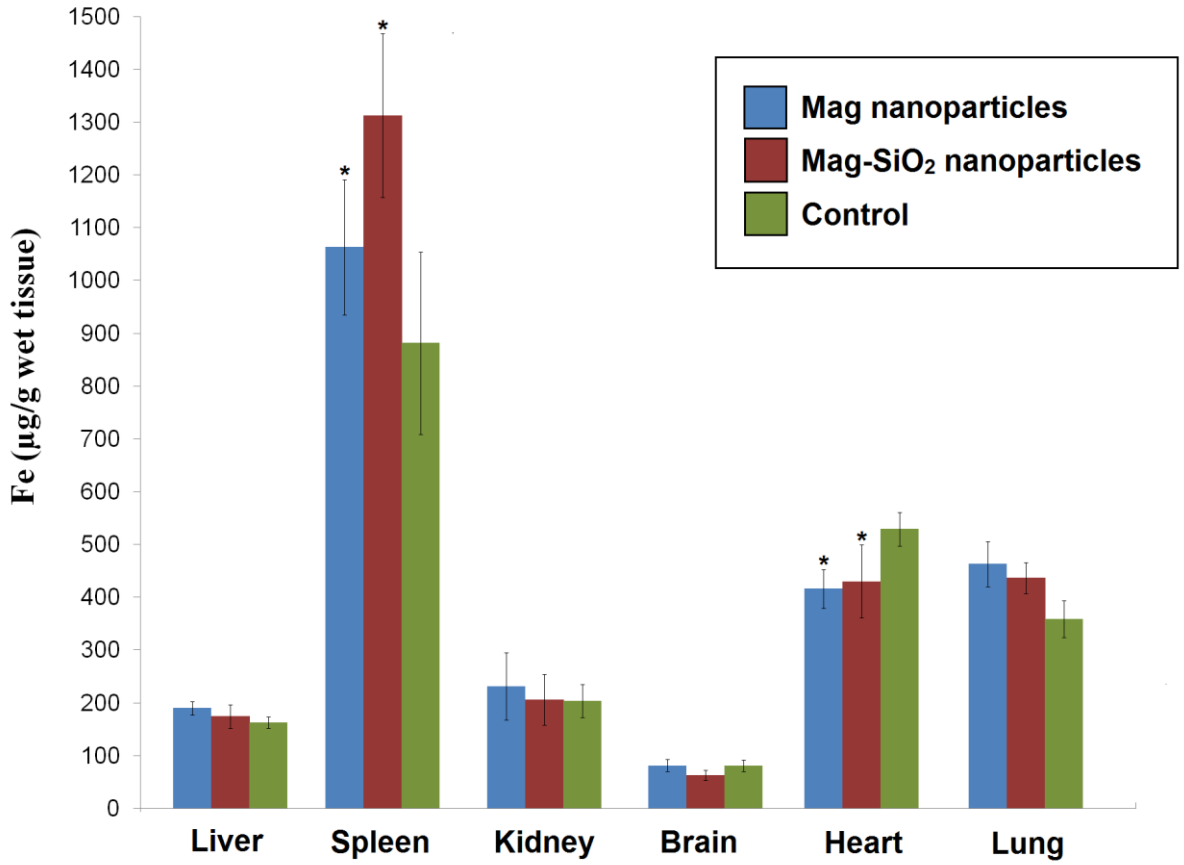

Figure 66. Iron uptake in different organs 7 days post-injection as measured by ICP-AES. The injection dose was 2 mg of Fe/kg in 300 µl of saline. Data are shown as the mean ± standard deviation (n = 3). *P < 0.05 compared with control.

	Mag NPs	Mag-SiO_2 NPs	Control
Liver	190,03 ± 12,45 µg Fe/g	174,47 ± 22,59 µg Fe/g	162,40 ± 10,70 µg Fe/g
Spleen	1042,54 ± 125,57 µg Fe/g*	1286,42 ± 152,08 µg Fe/g*	864,71 ± 169,24 µg Fe/g
Kidney	231,55 ± 63,93 µg Fe/g	206,13 ± 48,48 µg Fe/g	203,66 ± 31,08 µg Fe/g
Brain	79,68 ± 11,17 µg Fe/g	61,81 ± 9,81 µg Fe/g	79,69 ± 10,63 µg Fe/g
Heart	416,33 ± 36,40 µg Fe/g*	430,22 ± 69,10 µg Fe/g*	529,17 ± 32,02 µg Fe/g
Lung	463,04 ± 42,37 µg Fe/g	436,64 ± 29,53 µg Fe/g	359,11 ± 34,88 µg Fe/g

Table 30. Concentration of iron in different organs 7 days post-injection (2 mg Fe/kg) as measured by ICP-AES (the unit of measurement is expressed in µg g^{-1} wet tissue). Data are shown as the mean ± standard deviation (n = 3). *P < 0.05 compared with control.

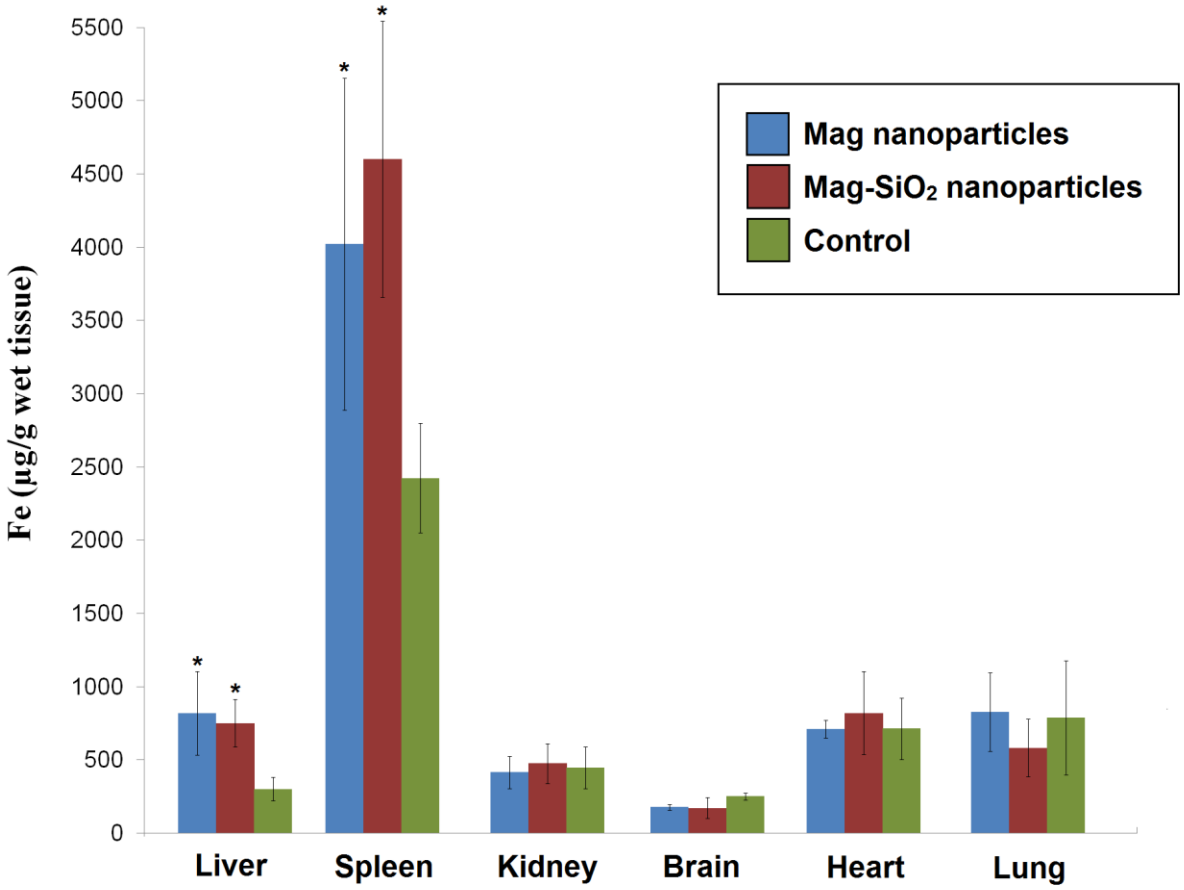

Figure 67. Iron uptake in different organs 7 days post-injection as measured by ICP-AES. The injection dose was 20 mg of Fe/kg in 300 µl of saline. Data are shown as the mean ± standard deviation (n = 3). *P < 0.05 compared with control.

	Mag NPs	Mag-SiO_2 NPs	Control
Liver	817,1 ± 285,25 µg Fe/g*	751,0 ± 161,89 µg Fe/g*	302,14 ± 81,88 µg Fe/g
Spleen	3990,6 ± 1123,52 µg Fe/g*	4563,9 ± 1233,98 µg Fe/g*	2404,4 ± 369,99 µg Fe/g
Kidney	412,7 ± 109,67 µg Fe/g	472,4 ± 134,19 µg Fe/g	443,8 ± 140,62 µg Fe/g
Brain	173,6 ± 18,23 µg Fe/g	166,9 ± 68,80 µg Fe/g	244,3 ± 24,10 µg Fe/g
Heart	706,3 ± 60,15 µg Fe/g	814,0 ± 282,52 µg Fe/g	707,9 ± 207,48 µg Fe/g
Lung	821,0 ± 267,6 µg Fe/g	577,80 ± 194,61 µg Fe/g	780,44 ± 385,95 µg Fe/g

Table 31. Concentration of iron in different organs 7 days post-injection (20 mg Fe/kg) as measured by ICP-AES (the unit of measurement is expressed in µg g^{-1} wet tissue). Data are shown as the mean ± standard deviation (n = 3). *P < 0.05 compared with control.

4.3.14 Histological evaluation of iron accumulation (20 mg Fe/kg)

To deeply investigate the iron accumulation in the tissues, the Perls' Prussian blue staining of major organs was performed using MNPs (Mag and Mag-SiO_2) at the concentrations of 2 and 20 mg Fe/kg. Iron (Fe^{2+} and Fe^{3+}) was observed as intense blue signals in liver and spleen and seldom in the kidney for both MNPs when injected at the concentration of 20 mg Fe/kg (**Figures 68 and 69**). No iron accumulation was observed in kidney, brain, lung and heart.

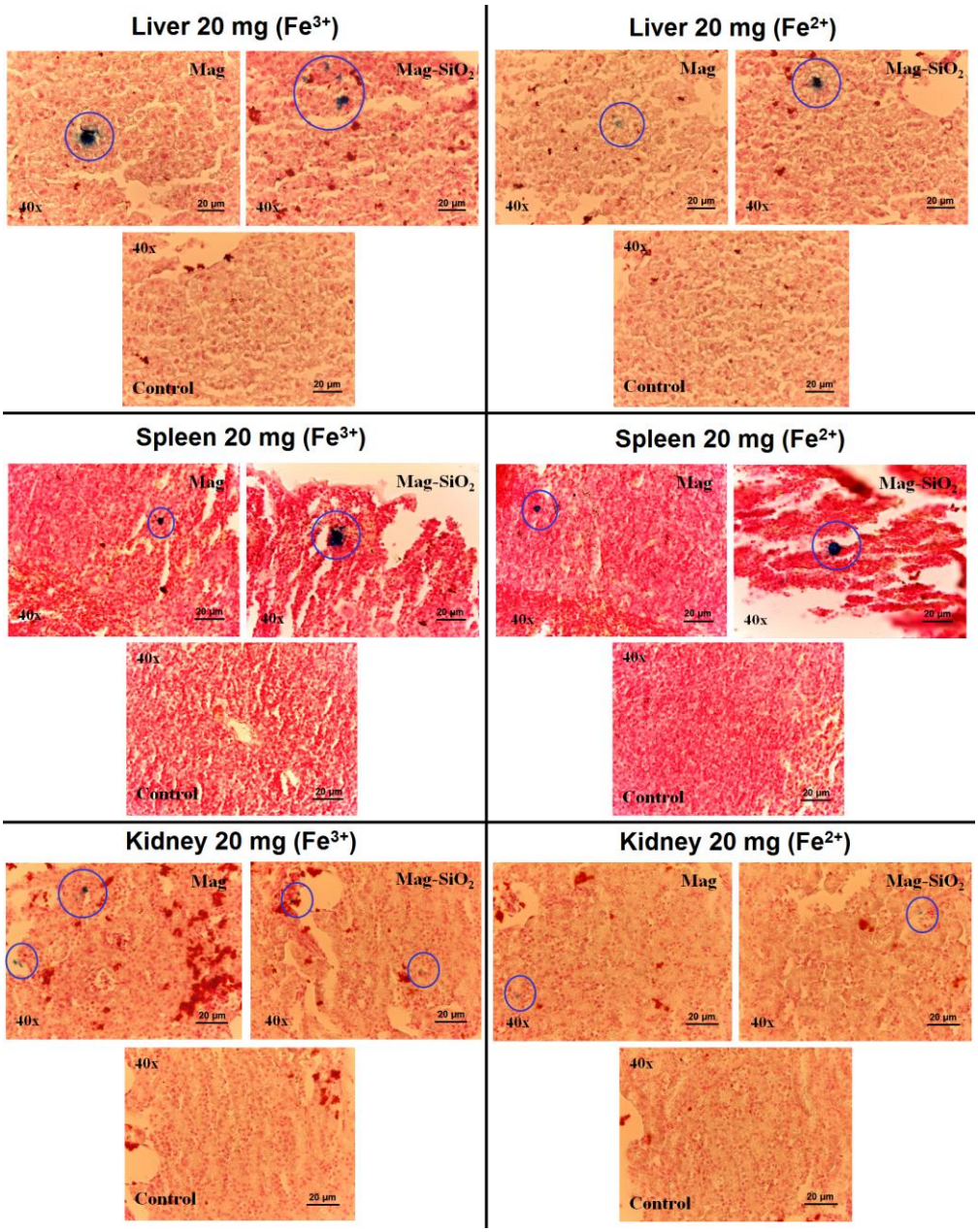

Figure 68. Representative images of Prussian blue stained histological tissue section of organs (liver, spleen and kidney) (MNPs 20 mg Fe/kg). The blue circles indicate iron deposits within tissue. Magnification: 40x, bar scale = 20 μm.

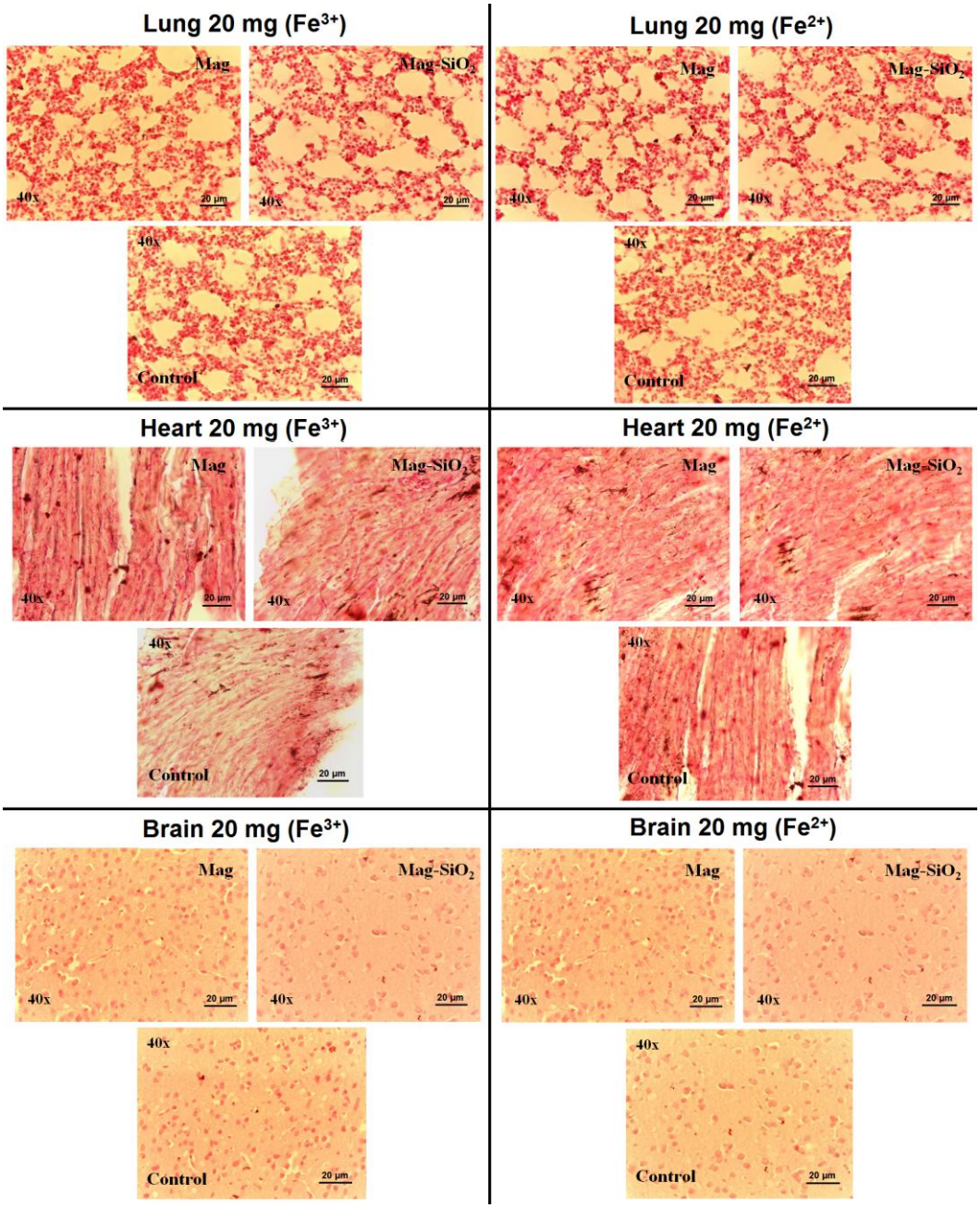

Figure 69. Representative images of Prussian blue stained histological tissue section of organs (lung, heart and brain) (MNPs 20 mg Fe/kg). Magnification: 40x, bar scale = 20 µm.

4.3.15 Histological evaluation of iron accumulation (2 mg Fe/kg)

In this group (2 mg Fe/kg) iron deposits were seldom observed in liver, spleen and kidney (**Figures 70 and 71**) and never in the brain, lung and heart.

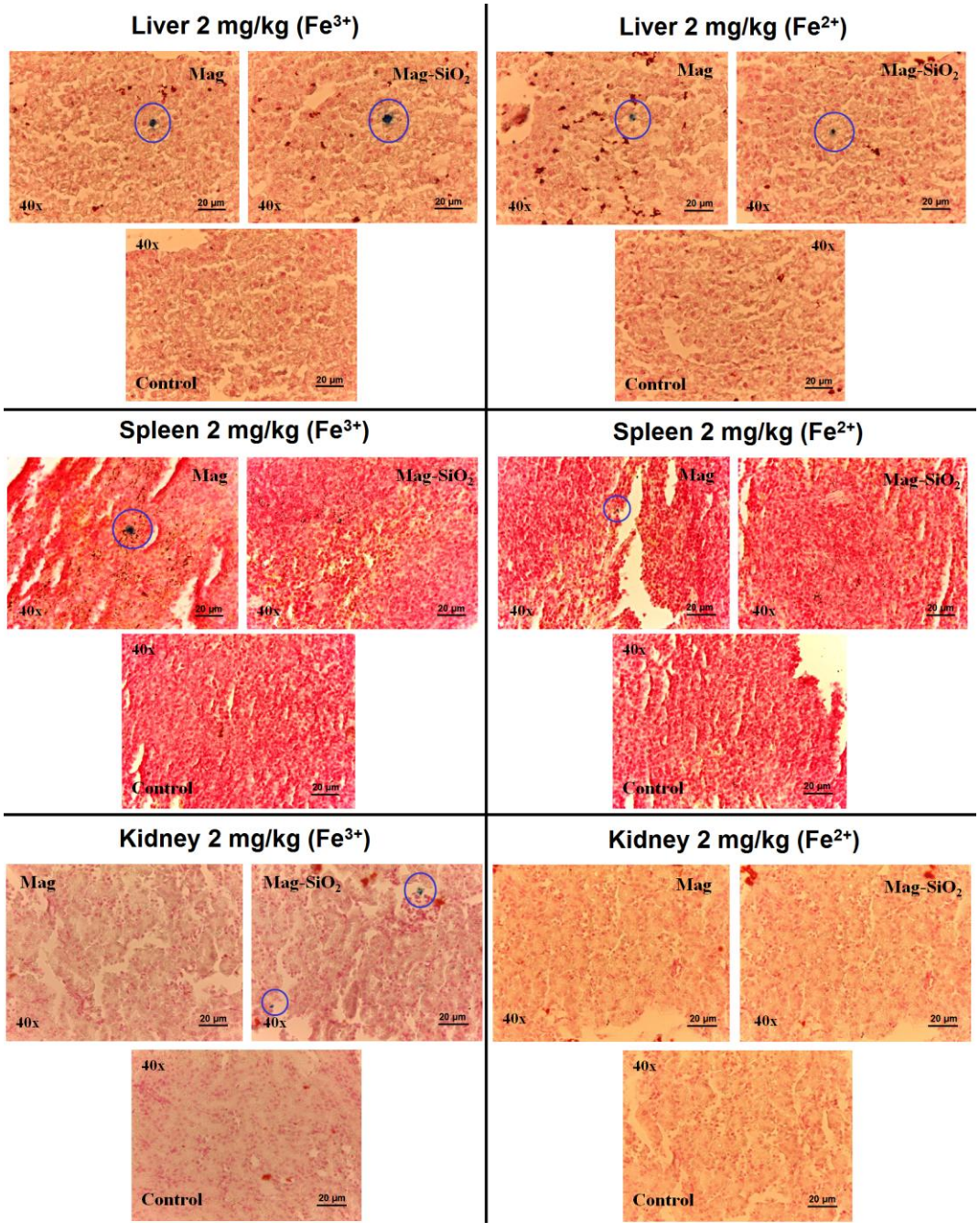

Figure 70. Representative images of Prussian blue stained histological tissue section of organs (liver, spleen and kidney) (MNPs 2 mg Fe/kg). The blue circles indicate iron deposits within tissue. Magnification: 40x, bar scale = 20 µm.

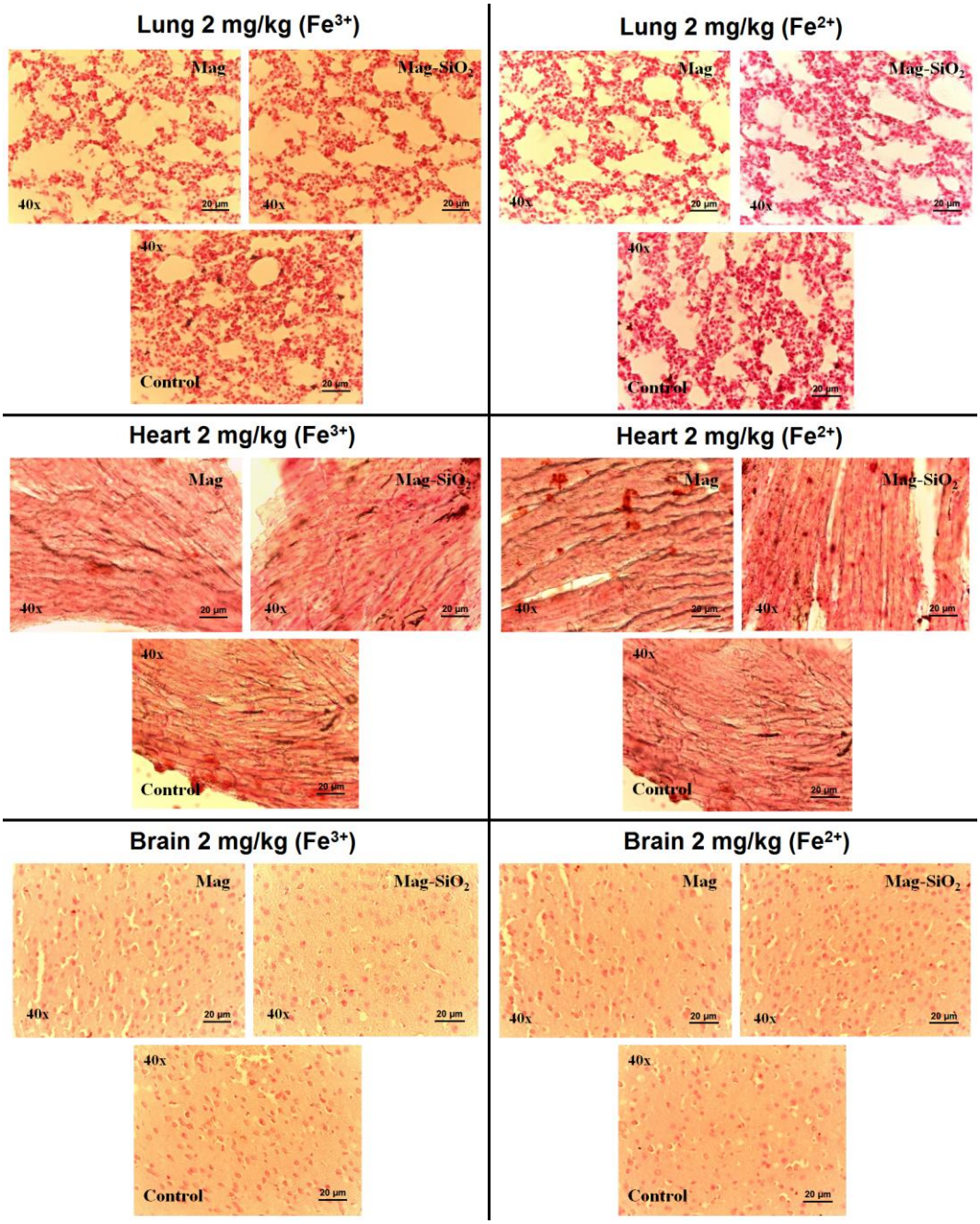

Figure 71. Representative images of Prussian blue stained histological tissue section of organs (lung, heart and brain) (MNPs 2 mg Fe/kg). Magnification: 40x, bar scale = 20 µm.

4.4 Discussion

The improvement of physicochemical properties of the third synthesis of MNPs was fundamental to produce stable magnetic nanoparticles as far as colloidal stability and dispersibility properties were concerned. The third synthesis of MNPs was produced using citric acid only for 3 hours as dispersant agent and washing extensively with water using an ultrafiltration device. Furthermore, the third synthesis of MNPs was produced to improve cytocompatibility of calcium-silica coated iron-oxide nanoparticles compared to the second synthesis.
The overall objective of this work was to screen MNPs within a set of standard assays commonly used by nanotoxicological evaluation and then determine the effect of flow on toxicity by exposing MS1 cells to MNPs in a bioreactor.

To reach this goal, we first characterised each MNP in DMEM cell culture medium, than we tested them in standard static conditions using a certain concentration. In static conditions apoptosis and ROS production by MS1 cells were also investigated. MS1 cells in contact with MNPs of last group showed a small percentage of apoptotic and necrotic cells. ROS are important intracellular mediators of the inflammatory response and cell death following uptake of nanoparticles. In fact cytotoxicity of MNPs can be triggered by ROS generation due to the release of metal ions and surface crystal defects [114-116]. Accumulation of ROS results in a loss of homeostatic mechanisms in cells, and then oxidative stress appears if the cell cannot sweep the generated ROS, and it may cause damage to mitochondria and DNA [117, 118].

For this reason, ROS generation induced by third synthesis of MNPs on MS1 cells was investigated. Naked and silica core-shell type iron-oxide nanoparticles could induce the generation of intracellular ROS depending on the concentration of nanoparticles. In fact, ROS generation induced by third synthesis of MNPs was in a concentration-dependent manner. The levels of ROS induced by third synthesis of MNPs on MS1 cells were not so high respect to untreated control. This effect could be due to a lower physiological production of ROS by MS1 murine endothelial cells because they are able to withstand to the particular conditions of oxygen pressure (pO_2) in the blood vessels [119].

Afterwards we compared the MNPs for testing in dynamic conditions demonstrating that even the application of gentle flow didn’t change the susceptibility of cells to toxic insult from nanoparticles. Moreover, cytocompatibility of third synthesis of MNPs in dynamic conditions by using a continuous flow bioreactor was carried out to simulate the flow of MNPs injected in a blood vessel

and reproduce the conditions more similar to an *in vivo* clinical situation. In the following, this experimental approach was further extended by evaluating the effects of in vivo toxicity of nanoparticles and by monitoring all vital, haematological and enzymatic parameters of mice used for the experiments of biodistribution of MNPs to have a complete view of possible toxic effects of MNPs.

The *in vivo* experiments showed that SiO_2 coated NPs, when injected at the dose of 20 mg Fe/kg, were toxic causing splenomegaly, bleeding in lymph nodes and hepatomegaly. Iron accumulation was mainly concentrated in liver and spleen in 20 mg Fe/kg Mag-SiO_2 NPs group. In contrast no macroscopic organ alteration was observed for 20 mg Fe/kg Mag NPs even if iron accumulation was observed in liver and spleen. Using doses ten-fold less (2 mg Fe/kg), no clinical signs of toxicity were observed for both Mag and Mag-SiO_2 NPs. Isolated sporadic iron accumulation were observed histologically only in liver, spleen and kidney.

4.5 Conclusions

The cytocompatibility of MNPs is multifactorial and depends upon their composition, physicochemical properties, dose and cellular model used for characterization. The dynamic *in vitro* tests were carried out like a first step aimed at mimicking the *in vivo* situation, in which MNPs interact with cells under a tangential flow. The MNPs described in this chapter were demonstrated to be cytocompatible in not direct contact cell model and in both static and dynamic cell models suggesting a promising feasibility for applications in biomedicine. However, the *in vivo* experiments showed that SiO_2 coated NPs, when injected at 20 mg Fe/kg, were toxic. All together these data suggest that magnetic nanoparticles are promising tools for biomedicine, especially if used at the appropriate dose and chemical composition. The *in vivo* data confirmed a good performance of the nanoparticles using a concentration of 2 mg Fe/kg body weight. This new synthesis of core-shell calcium doped MNPs was important to reduce their toxic effects respect to the previous synthesis and give the possibility of surface functionalization.

5. Concluding remarks

In this PhD project three sequential syntheses of magnetic nanoparticles were prepared by improving their physical-chemical, colloidal properties and cytocompatibility with the aim to reach the best preparation of stable MNPs to be used in biomedicine.

The first synthesis of MNPs were flawed by rapid precipitation and consequent clusters formation affecting cytocompatibility. For this reason, a colloidal stabilizer in the synthesis procedure of nanoparticles, the citric acid, was then introduced.

Calcium-silica core-shell type iron-oxide nanoparticles were developed with the aim to offer a positively charged surface available for functionalization. These MNPs were characterized to investigate their cytocompatibility. Colloidal stability but unsuitable cytocompatibility in particular as far as of Mag-SiO_2-Ca(3) NPs and Mag-SiO_2-Ca(17) NPs were regarded.

Finally improving the inclusion method and stabilization of Ca^{2+} ions in the silica shell, the cytocompatibility was enhanced and the materials were addressable to in-vivo application.

The tools developed in this thesis spanned a range of physical-chemical, biological and magnetic aspects and incorporate innovations on a nanometric range of scales. MNP-based technologies appear to hold a significant potential for a myriad of biomedical applications and the toxic potential of MNPs cannot be overlooked. For this reason we carried out different physical-chemical and biological characterization of MNPs to identify a safe dose and formulation of MNPs. Understanding the relationship between the physicochemical properties of MNP constructs and their behavior will induce full translational potential of these nanoparticles. The magnetic nanoparticles could be in future one of the field with higher perspectives of development for different scientific applications, especially such as a smart targeted drug delivery platform for in vivo disease therapies.

Acknowledgments

I would like to express my gratitude to my supervisor Prof. ssa Lia Rimondini. Her constant support, stimulating suggestions and encouragement helped me in research work. It was a great pleasure for me to conduct this thesis under her supervision.

I want to thank Prof.ssa Antonia Follenzi and Associazione Italiana Ricerca Cancro (AIRC) to support my fellowship during these three years of PhD.

Moreover, I would like to thank COST Action MP1005 (NAMABIO) and Prof. Saša Novak for support for STSM program at Jožef Stefan Institute, Ljubljana, Slovenia.

I would like to express my honest and sincere regards to Dr. Andrea Cochis for his kind help. Finally, I would like to thank Prof.ssa Enrica Vernè and Dr. Marta Miola for synthesis and physicochemical characterization of magnetic nanoparticles.

References

1. Zoraida PA. Nanomaterials for medical applications. Springdale, Elsevier 2013; 1-32.
2. Poon W, Zhang X, Nadeau J. Nanoparticle drug formulations for cancer diagnosis and treatment. Crit Rev Oncog 2014; 19:223-45.
3. Kreuter J. Nanoparticles-based drug delivery system. J Cont Rel 1991; 16:169-176.
4. Bozzuto G, Molinari A. Liposomes as nanomedical devices. Int J Nanomedicine 2015; 10:975-999.
5. Euliss LE, DuPont JA, Gratton S, DeSimone J. Imparting size, shape, and composition control of materials for nanomedicine. Chem Soc Rev 2006; 35:1095-1104.
6. Wennerstrom H, Linman B. Micelles. Physical chemistry of surfactant association. Rev Sec Phys Lett 1979; 52:1-86.
7. Nelson PH, Rutledge GC, Hatton TA. On the size and shape of self-assembled micelles. J Chem Phys 1997; 107:10777-10781.
8. Duncan R, Vicent MJ, Greco F, Nicholson RI. Polymer-drug conjugates: towards a novel approach for the treatment of endocrine-related cancer. Endocr Relat Cancer 2005; 12:S189-S199.
9. Vicent MJ, Duncan R. Polymer conjugates: nanosized medicines for targeting cancer. Trends Biotechnol 2006; 24:39-47.

10. Klajnert B, Bryszewska M. Dendrimers: properties and applications. Acta Biochim Pol 2001; 48: 199-208.
11. Sigh P. Dendrimers and their applications in immunoassays and clinical diagnosis. Biotechnol Appl Biochem 2007; 48:1-9.
12. Kobayashi H, Kawamoto S, Jo SK, Bryant HL, Brechbiel MW, Star RA. Macromolecular MRI contrast agents with small dendrimers: pharmacokinetic differences between sizes and cores. Bioconjug Chem 2003; 14:388-394.
13. Gillies ER, Fréchet JM. Dendrimers and dendritic polymers in drug delivery. Drug Discov Today 2005; 10:35-43.
14. Wu G, Barth RF, Yang W, Chatterjee M, Tjarks W, Ciesielski MJ, et al. Site-specific conjugation of boron-containing dendrimers to anti-EGF receptor monoclonal antibody cetuximab (IMC-C225) and its evaluation as potential delivery agent for neutron capture therapy. Bioconjug Chem 2004; 15:185-194.
15. Dufès C, Uchegbu IF, Schatzlein AG. Dendrimers in gene delivery. Adv Drug Deliv Rev 2005; 57:2177-2202.
16. Oliveira JM, Salgado AJ, Sousa N, Mano JF, Reis RL. Dendrimers and derivatives as potential therapeutic tool in regenerative medicine strategies-a review. Prog Polym Sci 2010; 35:1163-1194.
17. Reis CP, Neufeld RJ, Ribeiro AJ, Veiga F. Nanoencapsulation I. Methods for preparation of drug-loaded polymeric nanoparticles. Nanomedicine 2006; 2:8-21.
18. Pecher J, Mecking S. Nanoparticles from step-growth coordination polymerization. Macromolecules 2007; 40:7733-7735.
19. Hittinger E, Kokil A, Weder C. Synthesis and characterization of cross-linked conjugated polymer milli-, micro-, and nanoparticles. Angew Chem Int Ed 2004; 43:1808-1811.
20. Stoeva S, Klabunde KJ, SorensenCM, Dragieva I. Gram-scale synthesis of monodisperse gold colloids by the solvated metal atom dispersion method and digestive ripening and their organization into two- and three-dimensional structures. J Am Chem Soc 2002; 124:2305-2311.
21. Uccello-Barretta G, Evangelisti C, Balzano F, Vanni L, Aiello F, Jicsinszky L. Water soluble heptakis(6-deoxy-6-thio)cyclomaltoheptaose capped gold nanoparticles via metal vapour synthesis: NMR structural characterization and complexation properties. Carbohydr Res 2011; 346:753-758.

22. Špringer T, Ermini ML, Špačková B, Jabloňků J, Homola J. Enhancing sensitivity of surface plasmon resonance biosensors by functionalized gold nanoparticles: size matters. Anal Chem 2014; 86:10350-10356.
23. Bedford EE, Spadavecchia J, Pradier CM, Gu FX. Surface plasmon resonance biosensors incorporating gold nanoparticles. Macromol Biosci 2012; 12:724-739.
24. Alivisatos AP. Semiconductor clusters, nanocrystals, and quantum dots. Science 1996; 271: 933-937.
25. Murray CB, Kagan CR, Bawendi MG. Synthesis and characterization of monodisperse nanocrystals and close-packed nanocrystal assemblies. Annual Review of Materials Research 2000; 30:545-610.
26. Bruchez M, Moronne M, Gin P, Weiss S, Alivisatos AP. Semiconductor nanocrystals as fluorescent biological labels. Science 1988; 281:2013-2016.
27. Michalet X, Pinaud F, Lacoste TD, Dahan M, Bruchez M. Properties of fluorescent semiconductor nanocrystals and their applications to biological labelling. Single Mol 2001; 2:261-276.
28. Rosenthal SJ, Tomlinson I, Adkins EM, Schroeter S, Adams S, Swafford L, et al. Targeting cell surface receptors with ligand-conjugated nanocrystals. J Am Chem Soc 2002; 124: 4586-4594.
29. Wu X, Liu H, Liu J, Haley KN, Treadway JA, Larson JP, et al. Immunofluorescent labeling of cancer marker Her2 and other cellular targets with semiconductor quantum dots. Nat Biotechnol 2003; 21:41-46.
30. Gupta AK, Gupta M. Synthesis and surface engineering of iron oxide nanoparticles for biomedical applications. Biomaterials 2005; 26:3995-4021.
31. Hofmann-Amtenbrink M, von Rechenberg B, Hofmann H. Nanostructured Materials for Biomedical Applications. Transworld Research Network 2009; 5:119-149
32. Huber DL. Synthesis, properties, and applications of iron nanoparticles. Small Weinh Bergstr Ger 2005; 1:482-501.

33. Lu CW, Hung Y, Hsiao JK, Yao M, Chung TH, Lin YS, Wu SH, Hsu SC, Liu HM, Mou CY, et al. Bifunctional magnetic silica nanoparticles for highly efficient human stem cell labeling. Nano Lett 2007; 7:149-154.

34. Balakrishnan S, Bonder M. Particle size effect on phase and magnetic properties of polymer-coated magnetic nanoparticles. J Magn Magn Mater 2009; 321:117-122.
35. Peng S, Xie J, Sun S. Synthesis of Co/MFe(2)O(4) (M = Fe, Mn) Core/Shell nanocomposite particles. J Solid State Chem 2008; 181:1560-1564.
36. Emad G, Mohamed W, Atef O, Lokeshwar B. Synthesis, magnetic and optical properties of core/shell $Co_{1-x}Zn_xFe_2O_4/SiO_2$ nanoparticles. Nanoscale Res Lett 2011; 6:460-468.
37. Rohilla S, Kumar S, Aghamkar P, Sunder S. Investigations on structural and magnetic properties of cobalt ferrite/silica nanocomposites prepared by the coprecipitation method. J Mag Magn Mater 2011; 323:897-902.
38. Baldi G, Bonacchi D, Innocenti C, Lorenzi G, Sangregorio C. Cobalt ferrite nanoparticles: The control of the particle size and surface state and their effects on magnetic properties. J Magn Magn Mater 2007; 311:10-16.
39. Soleimani R, Soleimani M, Godarzi MG. Investigation of the thermal stability of Mn ferrite particles synthesized by a modified co-precipitation method. J Fusion Energ 2011; 30:338-341.
40. Kim DH, Nikles DE, Brazel CS. Synthesis and characterization of multifunctional chitosan - $MnFe_2O_4$ nanoparticles for magnetic hyperthermia and drug delivery. Materials 2010; 3:4051-4065.
41. Kim DH, Zeng H, Ng TC, Brazel CS. T_1 and T_2 relaxivities of succimer-coated $MFe_2^{3+}O_4$ ($M=Mn^{2+}$, Fe^{2+} and Co^{2+}) inverse spinel ferrites for potential use as phase-contrast agents in medical MRI. J Magn Magn Mater 2009; 321:3899-3904.
42. Batoo KM. Study of dielectric and impedance properties of Mn ferrites. Physica B 2011; 406:382-387.
43. Vaidyanathan G, Sendhilnathan S, Arulmurugan R. Structural and magnetic properties of $CoZnFe_2O_4$ nanoparticles by co-precipitation method. J Magn Magn Mater 2007; 313:293-299.
44. Rath C, Anand S, Das RP, Sahu KK, Kulkarni SD, Date SK, et al. Dependence on cation distribution of particle size, lattice parameter, and magnetic properties in nanosize Mn-Zn ferrite. J Appl Phys 2002; 91:2211-2215.

45. Sharifi I, Shokrollahi H, Amiri S. Ferrite-based magnetic nanofluids used in hyperthermia applications. J Magn Magn Mater 2012; 324:903-915.

46. Itoh H, Sugimoto T. Systematic control of size, shape, structure, and magnetic properties of uniform magnetite and maghemite particles. J Colloid Interface Sci 2003; 265:283-295.

47. Wu JH, Ko SP, Liu HL, Kim S, Ju JS, Kim YK. Sub 5 nm magnetite nanoparticles: Synthesis, microstructure, and magnetic properties. Mater Lett 2007, 61, 3124-3129.

48. Eckert CA, Knutson BL, Debenedetti PG. Supercritical fluids as solvents for chemical and materials processing. Nature 1996; 383:313-318.

49. Lee CS, Lee H, Westervelt RM. Microelectromagnets for the control of magnetic nanoparticles. Appl Phys Lett 2001; 79:3308-3310.

50. Mathur S, Barth S, Werner U, Hernandez-Ramirez F, Romano-Rodriguez A. Chemical vapor growth of one-dimensional magnetite nanostructures. Adv Mater 2008; 20:1550-1554.

51. Narayanan KB, Sakthivel N. Biological synthesis of metal nanoparticles by microbes. Adv Colloid Interface Sci 2010; 156:1-13.

52. Hulkoti NI, Taranath TC. Biosynthesis of nanoparticles using microbes - a review. Colloids Surf B Biointerfaces 2014; 121:474-483.

53. Mohanraj S, Kodhaiyolii S, Rengasamy M, Pugalenthi V. Green synthesized iron oxide nanoparticles effect on fermentative hydrogen production by Clostridium acetobutylicum. Appl Biochem Biotechnol 2014; 173:318-331.

54. Reddy LH, Arias JL, Nicolas J, Couvreur P. Magnetic nanoparticles: design and characterization, toxicity and biocompatibility, pharmaceutical and biomedical applications. Chem Rev 2012; 112:5818-5878.

55. Weissleder R, Moore A, Mahmood U, et al. In vivo magnetic resonance imaging of transgene expression. Nat Med 2000; 6:351-355.

56. Bulte JW, Douglas T, Witwer B, Zhang SC, et al. Magnetodendrimers allow endosomal magnetic labeling and in vivo tracking of stem cells. Nat. Biotechnol 2001; 19:1141-1147.

57. Kircher MF, Allport JR, Graves EE, Love V, Josephson L, Lichtman AH, Weissleder R. In vivo high resolution three-dimensional imaging of antigenspecific cytotoxic T-lymphocyte trafficking to tumors. Cancer Res 2003; 63:6838-6846.

58. Farokhzad OC, Langer R. Impact of nanotechnology on drug delivery. ACS Nano 2009; 3:16-20.

59. Pankhurst QA, Connolly J, Jones SK, Dobson J. Applications of magnetic nanoparticles in biomedicine. J Phys Appl Phys 2003; 36:r167-r181.

60. Duguet E, Vasseur S, Mornet S, et al. Magnetic nanoparticles and their applications in medicine. Nanomed 2006; 1:157-168.

61. Soenen SJ, De Cuyper M. Assessing iron oxide nanoparticle toxicity in vitro: current status and future prospects. Nanomedicine (Lond) 2010; 5:1261-1275.

62. Clift MJD, Boyles MSP, Brown DM, Stone V. An investigation into the potential for different surface-coated quantum dots to cause oxidative stress and affect macrophage cell signalling in vitro. Nanotoxicology 2010; 4:139-149.

63. Thanh NTK, Green LAW. Functionalisation of nanoparticles for biomedical applications. Nano Today 2010; 5:213-230.

64. Verma A, Stellacci F. Effect of surface properties on nanoparticle-cell interactions. Small 2010; 6:12-21.

65. Mironava T, Hadjiargyrou M, Simon M, Jurukovski V, Rafailovich MH. Gold nanoparticles cellular toxicity and recovery: effect of size, concentration and exposure time. Nanotoxicology 2010; 4:120-137.

66. Lanone S, Rogerieux F, Geys J, Dupont A, Maillot-Marechal E, Boczkowski J, Lacroix G, Hoet P. Comparative toxicity of 24 manufactured nanoparticles in human alveolar epithelial and macrophage cell lines. Part Fibre Toxicol 2009; 6:14-26.

67. Monteiro-Riviere NA, Inman AO, Zhang LW. Limitations and relative utility of screening assays to assess engineered nanoparticle toxicity in a human cell line. Toxicol Appl Pharmacol 2009; 234:222-235.

68. Pfaller T, Colognato R, Nelissen I, Favilli F, Casals E, Ooms D, et al. The suitability of different cellular in vitro immunotoxicity and genotoxicity methods for the analysis of nanoparticle-induced events. Nanotoxicology 2010; 4:52-72.

69. Carlson C, Hussain SM, Schrand AM, Braydich-Stolle LK, Hess KL, Jones RL, Schlager JJ. Unique cellular interaction of silver nanoparticles: Size-dependent generation of reactive oxygen species. J Phys Chem B 2008; 112:13608-13619.
70. Gurr J-R, Wang ASS, Chen C-H, Jan K-Y. Ultrafine titanium dioxide particles in the absence of photoactivation can induce oxidative damage to human bronchial epithelial cells. Toxicology 2005; 213:66-73.
71. Karlsson HL, Cronholm P, Gustafsson J, Möller L. Copper oxide nanoparticles are highly toxic: A comparison between metal oxide nanoparticles and carbon nanotubes. Chem Res Toxicol 2008; 21:1726-1732.
72. Nel A, Xia T, Mädler L, Li N. Toxic potential of materials at the nanolevel. Science 2006; 311:622-627.
73. Ahamed M, Alhadlaq HA, Alam J, Khan MA, Ali D, Alarafi S. Iron oxide nanoparticle-induced oxidative stress and genotoxicity in human skin epithelial and lung epithelial cell lines. Curr Pharm Des 2013; 19:6681-6690.
74. Kreuter J. Nanoparticulate systems for brain delivery of drugs. Adv Drug Deliv Rev 2001; 47:65-81.
75. Schroeder U, Sommerfeld P, Ulrich S, Sabel BA. Nanoparticle technology for delivery of drugs across the blood-brain barrier. J Pharm Sci 1998; 87:1305-1307.
76. Ferrari M. Cancer Nanotechnology: Opportunities and Challenges. Nat Rev Cancer 2005; 5:161-171.
77. Liong M, Lu J, Kovochich M, Xia T, Ruehm SG, Nel AE, Tamanoi F, Zink JI. Multifunctional inorganic nanoparticles for imaging, targeting, and drug delivery. ACS Nano 2008; 2:889-896.
78. Bamrungsap S, Zhao Z, Chen T, Wang L, Li C, Fu T, Tan W. Nanotechnology in therapeutics: a focus on nanoparticles as a drug delivery system. Nanomedicine (Lond) 2012; 7:1253-71.
79. Torchilin VP. Passive and active drug targeting: drug delivery to tumors as an example. Handb Exp Pharmacol 2010; 197:3-53.
80. Maeda H, Wu J, Sawa T, Matsumura Y, Hori K. Tumor vascular permeability and the EPR effect in macromolecular therapeutics: a review. J Control Release 2000; 65:271-284.

81. Maxwell DJ, Bonde J, Hess DA, Hohm SA, et al. Fluorophore-conjugated iron oxide nanoparticle labeling and analysis of engrafting human hematopoietic stem cells. Stem Cells 2008; 26:517-524.

82. Tucker BA, Rahimtula M, Mearow KM. A procedure for selecting and culturing subpopulations of neurons from rat dorsal root ganglia using magnetic beads. Brain Res Brain Res Protoc 2005; 16:50-57.

83. McCarthy JR, Kelly KA, Sun EY, Weissleder R, et al. Targeted delivery of multifunctional magnetic nanoparticles. Nanomed 2007; 2:153-167.

84. Weber C, Falkenhagen D. Specific blood purification by means of antibody-conjugated magnetic microspheres. in: U. Hafeli, et al., (Eds.), Scientific and Clinical Applications of Magnetic Carriers, Plenum Press, New York, 1997; 371-378.

85. Nam JM, Thaxton CS, Mirkin CA. Nanoparticle-based bio-bar codes for the ultrasensitive detection of proteins. Science 2003; 301:1884-1886.

86. López-López MT, Durán JDG, Delgado AV, González-Caballero F. Stability and magnetic characterization of oleate-covered magnetite ferrofluids in different nonpolar carriers. J Colloid Interface Sci 2005; 291:144-151.

87. Fuller KJ, Issels RD, Slosman DO, Guillet JG, Soussi T, Polla BS. Cancer and the heat-shock response. Eur J Cancer 1994; 30A:1884-1891.

88. Harmon BV, Takano YS, Winterford CM, Gobe GC. The role of apoptosis in the response of cells and tumours to mild hyperthermia. Int J Radiat Biol 1991; 59:489-501.

89. Chatterjee DK, Diagaradjane P, Krishnan S. Nanoparticle-mediated hyperthermia in cancer therapy. Ther Deliv 2011; 2:1001-1014.

90. Jordan A, Scholz R, Wust P, et al. Endocytosis of dextran and silan-coated magnetite nanoparticles and the effect of intracellular hyperthermia on human mammary carcinoma cells in vitro. J Magn Magn Mater 1999; 194:185-196.

91. Ito A, Shinkai M, Honda H, Kobayashi T. Medical application of functionalized magnetic nanoparticles. J Biosci Bioeng 2005; 100:1-11.

92. Krotz F, Sohn HY, Gloe T, Plank C, Pohl U. Magnetofection potentiates gene delivery to cultured endothelial cells. J Vas Res 2003; 40:425-434.

93. Scherer F, Anton M, Schillinger U, Henke J, Bergemann C, Kruger A, Gansbacher B, Plank C. Magnetofection: enhancing and targeting gene delivery by magnetic force in vitro and in vivo. Gene Ther 2002; 9:102-109.

94. Griffith LG, Naughton G. Tissue engineering-current challenges and expanding opportunities. Science 2002; 295:1009-1014.

95. Santo VE, Rodrigues MT, Gomes ME. Contributions and future perspectives on the use of magnetic nanoparticles as diagnostic and therapeutic tools in the field of regenerative medicine. Expert Rev Mol Diagn 2013; 13:553-566.

96. Ito H, Kato R, Ino K, Honda H. Magnetic manipulation device for the optimization of cell processing conditions. J Biosci Bioeng 2010; 109:182-188.

97. Yamamoto Y, Ito A, Fujita H, Nagamori E, Kawabe Y, Kamihira M. Functional evaluation of artificial skeletal muscle tissue constructs fabricated by a magnetic force-based tissue engineering technique. Tissue Eng Part A 2011; 17:107-114.

98. Gould P. Nanomagnetism shows in vivo potential. Nano Today 2006; 1:34-39.

99. Qiao RR, Yang CH, Gao MY. Superparamagnetic iron oxide nanoparticles: from preparations to in vivo MRI applications. J Mater Chem 2009; 19:6274-6293.

100. Schwarz S, Wong JE, Bornemann J, Hodenius M, Himmelreich U, Richtering W, Hoehn M, Zenke M, Hieronymus T. Polyelectrolyte coating of iron oxide nanoparticles for MRI-based cell tracking. Nanomed Nanotechnol 2012; 8:682-691.

101. Li Z, Kawashita M, Araki N, Mitsumori M, Hiraoka M, Doi M. Magnetite nanoparticles with high heating efficiencies for application in the hyperthermia of cancer. Mater Sci Eng C 2010; 30:990-996.

102. Stöber W, Fink A. Controlled growth of monodisperse silica spheres in the micron size range. J Colloid Interface Sci 1968; 26:62-69.

103. Yu C, Zhou Z, Wang J, Sun J, Liu W, Sun Y, Kong B, Yang H, Yang S. In depth analysis of apoptosis induced by silica coated manganese oxide nanoparticles in vitro. J Hazard Mater 2015; 283:519-528.

104. Park EJ, Choi DH, Kim Y, Lee EW, Song J, Cho MH, Kim JH, Kim SW. Magnetic iron oxide nanoparticles induce autophagy preceding apoptosis through mitochondrial damage and ER stress in RAW264.7 cells. Toxicol In Vitro 2014; 28:1402-1412.

105. Deng YH, Wang CC, Hu JH, Yang WL, Fu SK. Investigation of formation of silica-coated magnetite nanoparticles via sol-gel approach. Colloids and Surfaces A: Physiochem Eng Aspects 2005; 262:87-93

106. Men HF, Liu HQ, Zhang ZL, et al. Synthesis, properties and application research of atrazine Fe_3O_4-SiO_2 magnetic molecularly imprinted polymer. Environ Sci Pollut Res Int 2012; 19:2271-2280.

107. Singh RK, Kim TH, Patel KD, Knowles JC, Kim HW. Biocompatible magnetite nanoparticles with varying silica-coating layer for use in biomedicine: physicochemical and magnetic properties, and cellular compatibility. J Biomed Mater Res A 2012; 100:1734-1742.

108. Shubayev VI, Pisanic TR, Jin S. Magnetic nanoparticles for theragnostics. Adv Drug Deliv Rev 2009; 61:467-477.

109. Robert JH. Zeta Potential in Colloid Science: Principles and Applications. Colloid Sciences Series, Sydney. Academic Press 1989; 1-38.

110. Jasper R, Locatelli GO, Pilati C, Locatelli C. Evaluation of biochemical, hematological and oxidative parameters in mice exposed to the herbicide glyphosate-Roundup. Interdiscip Toxicol 2012; 5:133-40.

111. Stefánsson A, Gunnarsson I, Giroud N. New methods for the direct determination of dissolved inorganic, organic and total carbon in natural waters by reagent-free ion chromatography and inductively coupled plasma atomic emission spectrometry. Anal Chi Acta 2007; 582:69-74.

112. Mermet JM. Is it still possible, necessary and beneficial to perform research in ICP-atomic emission spectrometry? J Ana At Spectrom 2005; 20:11-16.

113. Alexander CM, Dabrowiak JC, Goodisman J. Gravitational sedimentation of gold nanoparticles. J Colloid Interface Sci 2013; 396:53-62.

114. Lovric J, Cho SJ, Winnik FM, Maysinger D. Unmodified cadmium telluride quantum dots induce reactive oxygen species formation leading to multiple organelle damage and cell death. Chem Bio 2005; 12:1227-1234.

115. Karlsson HL, Cronholm P, Gustafsson J, Moller L. Copper oxide nanoparticles are highly toxic: a comparison between metal oxide nanoparticles and carbon nanotubes. Chem Res Toxicol 2008; 21:1726-1732.

116. Yan DH, Yin GF, Huang ZB, Li L, Liao XM, Chen XC, Yao YD, Hao BQ. Cellular compatibility of biomineralized ZnO nanoparticles based on prokaryotic and eukaryotic systems. Langmuir 2011; 27:13206-13211.

117. Nel A, Xia T, Madler L, Li N. Toxic potential of materials at the nanolevel. Science 2006; 311:622-627.

118. Zhu MT, Feng WY, Wang Y, Wang B, Wang M, Ouyang H, Zhao YL, Chai ZF. Particokinetics and extrapulmonary translocation of intratracheally instilled ferric oxide nanoparticles in rats and the potential health risk assessment. Toxicol Sci 2009; 107:342-351.

119. Kapitulnik J, Benaim C, Sasson S. Endothelial cells derived from the blood-brain barrier and islets of Langerhans differ in their response to the effects of bilirubin on oxidative stress under hyperglycemic conditions. Front Pharmacol 2012; 3:131-136.